Robustness of Shear Plate Connections under Quasi-Dynamic Loading

by

Jacklyn E. Lesser

A Report Submitted to the Faculty of the

Milwaukee School of Engineering

in Partial Fulfillment of the

Requirements for the Degree of

Master of Science in Structural Engineering

Milwaukee, Wisconsin

May 2016

Abstract

Simple shear connections have been commonly used in steel-frame construction because they are quick to erect and relatively cost effective. The connections are used for shear resistance, but studies have shown that these connections are capable of sustaining measurable rotational demands and axial load. This enables the connection to help resist collapse in the event of a column failure.

The purpose of this research is to evaluate the robustness of single plate "shear tab" connections when subjected to quasi-dynamic loading scenarios. The research outlines the shear tab's capacity, its ability to utilize catenary action as a source of secondary load transfer, and the connection's innate ability to sustain rotational demands and axial forces in both statically and dynamically loaded conditions.

Eleven full-scale tests were conducted, consisting of two wide flange beams connected to a wide flange column stub with single plate connections of three-, four-, and five-bolt configurations. Two of the 11 tests used galvanized bolts. The column stub was pulled vertically downward simulating the compromise of a central column in a building. Axial forces and moments in the connection were calculated from measured strains. Beam rotations were calculated from displacement measurements. Applied load was measured by means of a force transducer.

The shear tab connection resists the applied quasi-dynamic load by means of flexural resistance and catenary action, similar to what was seen in prior static tests. Systems that undergo quasi-dynamic loading achieve failure at a lesser rotation than do those subjected to static loading. An analysis of the work done showed that both statically and quasi-dynamically loaded systems dissipate similar amounts of energy.

Acknowledgments

Without the continual support and assistance of numerous people and organizations, this research would not have achieved the success that it has. I would first like to thank Germantown Iron and Steel for their donation of materials and fabrication as well as allowing us to tour your facilities. I would also like to thank Marquette University and David Newman, the Director of Operations at Marquette University, for the use of their lab equipment. I would also like the thank Mr. Newman for his endless generosity of not only the equipment but his time as well.

I would like to thank H. Peter Huttelmaier, Ph.D., Richard Devries, Ph.D, and Christopher Foley, Ph.D. for their continual efforts to aid in the development of this research. A special thanks to my advisor Christopher Raebel, Ph.D.; he has been so gracious as to give his time and motivation throughout the past two years.

I would like to also thank Megan Hayes. I am eternally grateful to have had worked with her on both of our research. Not only did she prove her devotion and knowledge in this endeavor, but she also became a closer friend than we had already been.

I would also like to express my gratitude for my family. My parents, Jo Ann and Chuck, as well as my brother, Jake, have given me their endless support. They would and have done everything that they could to help me succeed my entire life and without them, this research would not have been possible. I would also like to thank my friends for their encouragement and friendship throughout this entire process.

Table of Contents

List of Figures

List of Tables

Nomenclature

Symbols

a = horizontal distance from the bolt line to the weld line, in.

d = nominal bolt diameter, in.

d_b = bolt diameter, in.

d_{max} = maximum distance from the bolt group centroid to the beam flange, in.

e = bolt design eccentricity, in.

l = length of weld, in.

n = number of bolts.

t = thickness of the connected material, in.

$t_{fl,min}$ = minimum flange thickness, in.

t_{max} = maximum plate thickness, in.

t_{min} = minimum weld thickness, in.

t_p = thickness of the plate, in.

t_w = thickness of the weld, in.

x_b = horizontal distance from the true pin connection to the bolt line, in.

x_f = horizontal distance from the true pin connection to the supporting column flange, in.

x_{sg} = horizontal distance from the true pin connection to the strain gage, in.

y_b = distance to the bottom location of strain gage from the neutral axis, in.

y_t = distance to the top location of strain gage from the neutral axis, in.

A = cross sectional area, in.^{2}.

A_b = bolt area, in.^{2}.

A_e = effective net area, in.^{2}.

A_g = gross area, in.^{2}.

A_{gv} = gross shear area, in.^{2}.

A_{nv} = net shear area, in.^{2}.

A_{nt} = net tension area, in.^{2}.

A_w = area of weld, in.^{2}.

E = Modulus of elasticity of steel, 29,000 ksi.

F_{exx} = weld strength, ksi.

F_n = yield strength of bolts, ksi.

F_u = specified minimum tensile strength of the connected material, ksi.

$F_{x,n}$ = horizontal bolt force component at specified rotation, kips.

$F_{y,n}$ = vertical bolt force component at specified rotation, kips.

$H_{mx,n}$ = horizontal bolt force component due to measured moment ICOR analysis, kips.

$H_{my,n}$ = vertical bolt force component due to measured moment ICOR analysis, kips.

I_x = strong axis moment of inertia, in.^{4}.

L = framing bay width, in.

L_c = clear edge distance in the direction of force between the edge of the hole and the edge of the adjacent hole or the edge of the connected material, in.

L_{eh} = horizontal distance from the center of bolt to plate edge, in.

L_{ev} = vertical distance from the center of bolt to plate edge, in.

L_{sg} = horizontal distance from the true pin connection to the strain gages, in.

M = moment at the strain gauge, kip-in.

M_c = moment at the connection, kip-in.

M_M = calculated moment, kip-in.

$M_{M,\,n}$ = moment at time step ‘n’, kip-in.

P = applied axial force, kips.

$P_{m,n}$ = applied axial force at time step ‘n’, kips.

P_x = horizontal axial force component at each bolt, kips.

P_y = vertical axial force component at each bolt, kips.

R_A = axial load in beam, kips.

R_T = transverse reaction in beam, kips.

R_n = calculated capacity, kips.

U_{bs} = factor of 1.0 for uniform tension stress.

V_{app} = applied load of actuator, kips.

$V_{b\ max,n}$ = resultant bolt shear force at the point of the maximum measured moment, kips.

V_{norm} = normalized unit shear.

$V_{m.n}$ = applied load at time step ‘n’, kips.

$V_{mx,n}$ = horizontal bolt force component due to the eccentric shear ICOR analysis, kips.

$V_{my,n}$ = vertical bolt force component due to the eccentric shear ICOR analysis, kips.

W = work, in-kips.

δ = actuator deflection, in.

Δ = beam elongation, in.

Δ_n = vertical deflection measured by DWT at time step ‘n’, in.

θ = rotation of beam, radians.

θ_n = beam end rotation at time step ‘n’, radians.

μ^{-6} = experimentally measured microstrain.

σ_n = stress at strain gage ‘n’, ksi.

Abbreviations

in	Inch
ksi	Kips per square in.
AISC	American Institute of Steel Construction
ASTM	American Society of Testing and Material
DWT	Draw Wire Transducer
EMSTL	Engineering Materials and Structural Testing Laboratory
HFC	High Fidelity Connection
ICOR	Instantaneous Center of Rotation
NIST	National Institute of Standards and Technology
RCC	Reduced Component Connection
RCSC	Reduced Coarse Shell Connection

Chapter 1

INTRODUCTION

1.1 Background

Building collapse has been a topic of interest in structural engineering. In order to prevent it, it is important to determine the level of robustness in a structural system that is required in design. “Building connections potentially represent the most vulnerable structural elements in steel framed buildings and their failure can lead to progressive collapses” [1]. The connection is an important aspect into the performance of a structural system to prevent structural failure.

Structural steel framework utilizes simply supported framing in typical design. The design of connections is simplified, and they are assumed to resist only vertical shear loading. The members are not considered to contribute to the robustness of the system, but are likely to contribute some robustness which is inherent in their connections. Current research has shown that simple connections can resist more than vertical force and possess innate robustness to overcome axial, shear, and moment present in the connection.

The single plate “shear tab” connection is a simple connection which is common in research as well as construction for the simplicity alone. The single plate connection consists of one plate welded to a primary framing member such as a column or girder which is then bolted to a secondary member. The “Conventional Configuration” presented in the AISC [2] manual presents the shear tab with one row of vertical bolts at the supporting beam’s web. AISC also presents the “Extended Configuration” which

allows an unlimited number of vertical rows of bolts. Typical single plate connections can be seen in Figure 1.1.

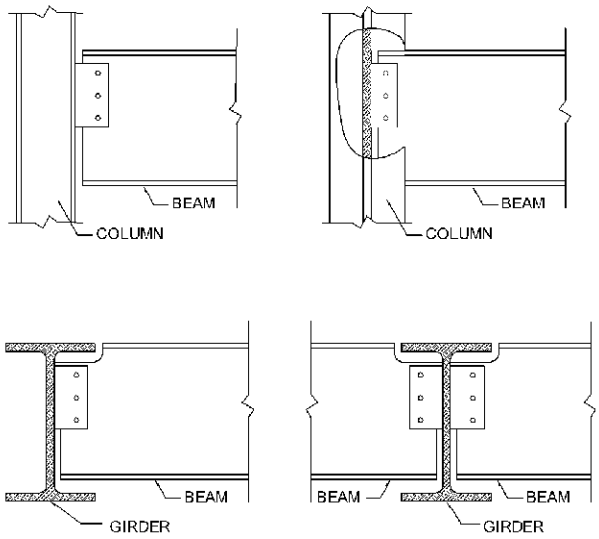

Figure 1.1: Typical Single Plate Connections [2].

1.2 Scope of Research

1.2.1 Research Objective

Two purposes in this research exist. The first is to expand upon the tests presented in the research done by Thompson [3] in 2009. The static tests performed in each configuration in the current research were used to compare to the testing program by Thompson.

Thompson investigated the shear tab connection's ability to handle extreme loading circumstances and whether catenary action could be used as an effective load path. It was found that the shear tab connection had the ability to withstand unexpected forces when designed per AISC specifications, concluding that there was inherent robustness in the system that transfers flexural and axial forces that was not expected during the connection design.

The second purpose is that the research presented by Thompson [3] lacked insight into the speed of the extreme load case due to the fact that dynamic loading was not an option at the time of testing. A column failure would happen instantaneously. Thompson's tests were considered static as the loading on the connection was gradually applied, and at times loaded intermittently. The scope of this research is to emulate the testing performed in 2009 and use quasi-dynamic loading, thus determining if a shear tab connection has the ability to sustain flexural capacity and continue to use catenary action as a secondary load path in a quasi-dynamic loading scenario.

1.2.2 Overview of Experimental Program

This research is an expansion on the work performed by Thompson [3]. The current research is meant to simulate the removal of a central column. The "quasi-dynamic" loading rates are faster than those of statically loaded tests, one inch per minute, but do not reach the strain rates expected by instantaneous column removal.

To emulate the testing performed by Thompson, three- , four- , and five-bolt configurations are utilized. A total of 11 tests are performed, four tests per configuration with the exception of the three-bolt configuration. Each test configuration consists of one statically loaded test and two or three quasi-dynamically loaded tests. Strain, load, and displacements are measured in each of the tests to determine the set of forces present in the system.

Chapter 2

LITERATURE REVIEW

2.1 Overview

Shear tab behavior has been researched with respect to gravity loading as well as with extreme loading circumstances. Research has been done to simulate extreme loading circumstances to understand how shear and tension combine with flexural capacity in a connection at low loading rates, but currently available research is limited to quasi-static loading rates as opposed to high speed load application.

The literature review provides a summary of information that is currently available in understanding the behavior of the shear tab connection. A review of past research is included to provide insight as to how a shear tab behaves when subjected to gravity loads. Research pertaining to progressive collapse, as applicable to the current research initiative, is included as well.

2.2 Connection Behavior

The "Conventional Configuration" provisions in the AISC design specifications do not account for incidental tension or a combination of shear and tension in the connection. Due to this exclusion, experimental research has been conducted to provide knowledge and design limitations for connections.

2.2.1 Axial, Shear and Moment Interaction of Single Plate "Shear Tab" Connections

Thompson [3], showed that there is an innate robustness in single plate connections when subjected to combined axial, shear and moment as a result of significant rotational demands. Thompson tested three configurations of shear tabs: three- , four- , and five-bolt configurations. Each configuration was used to connect a central

column stub to a pair of test beams, and the column stub was pulled downward with an actuator. Figure 2.1 shows Thompson's experimental test setup. The strain was measured at approximately mid-span in each beam and used to calculate axial force and moment in the system. Vertical displacement and applied load was also measured.

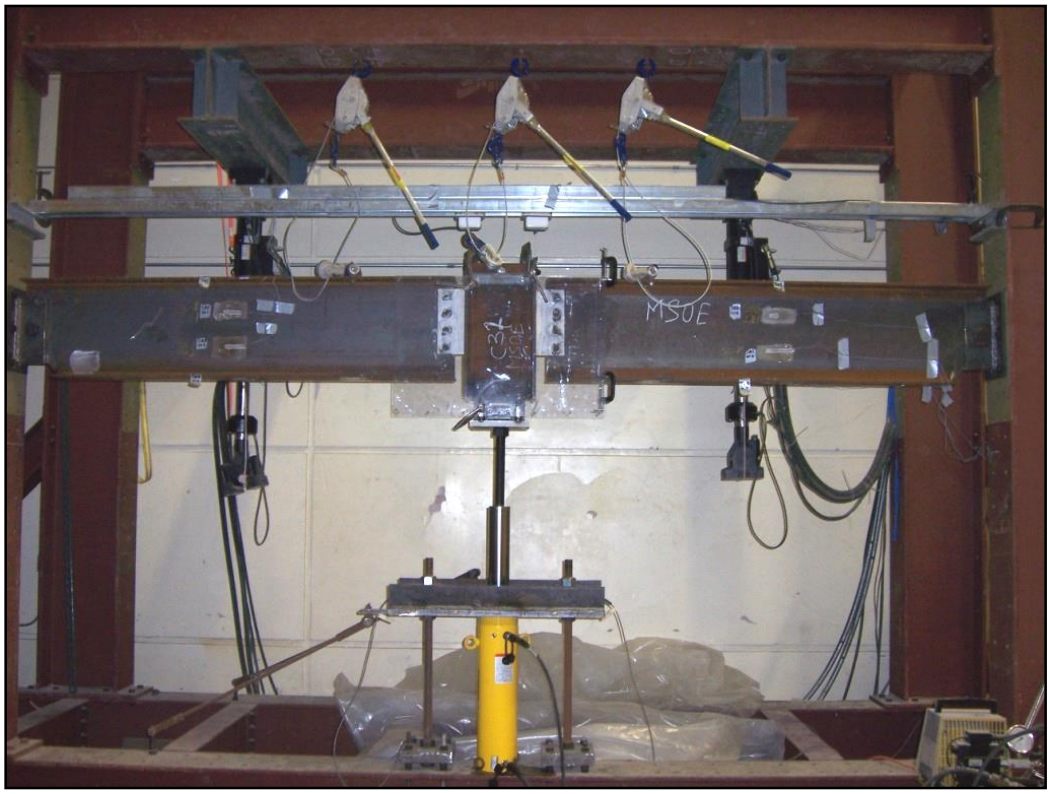

Figure 2.1: Typical Test System Configuration Prior to Testing [3].

Thompson found that there were three distinct phases in the force-rotation behavior of the test specimens' response. The first being minimal force-rotation for approximately 0.03 radians of beam rotation (as measured from the pin-connected end opposite the shear tab connection). The next phase was a relatively linear increase in moment followed by a range of rotation where the moment plateaus. The following phase was the transition from flexural to catenary response, when catenary action became the

primary load path for applied shear. A plot of force and moment versus rotation can be seen in Figure 2.2. This plot outlines the three phases of each test in graphical format.

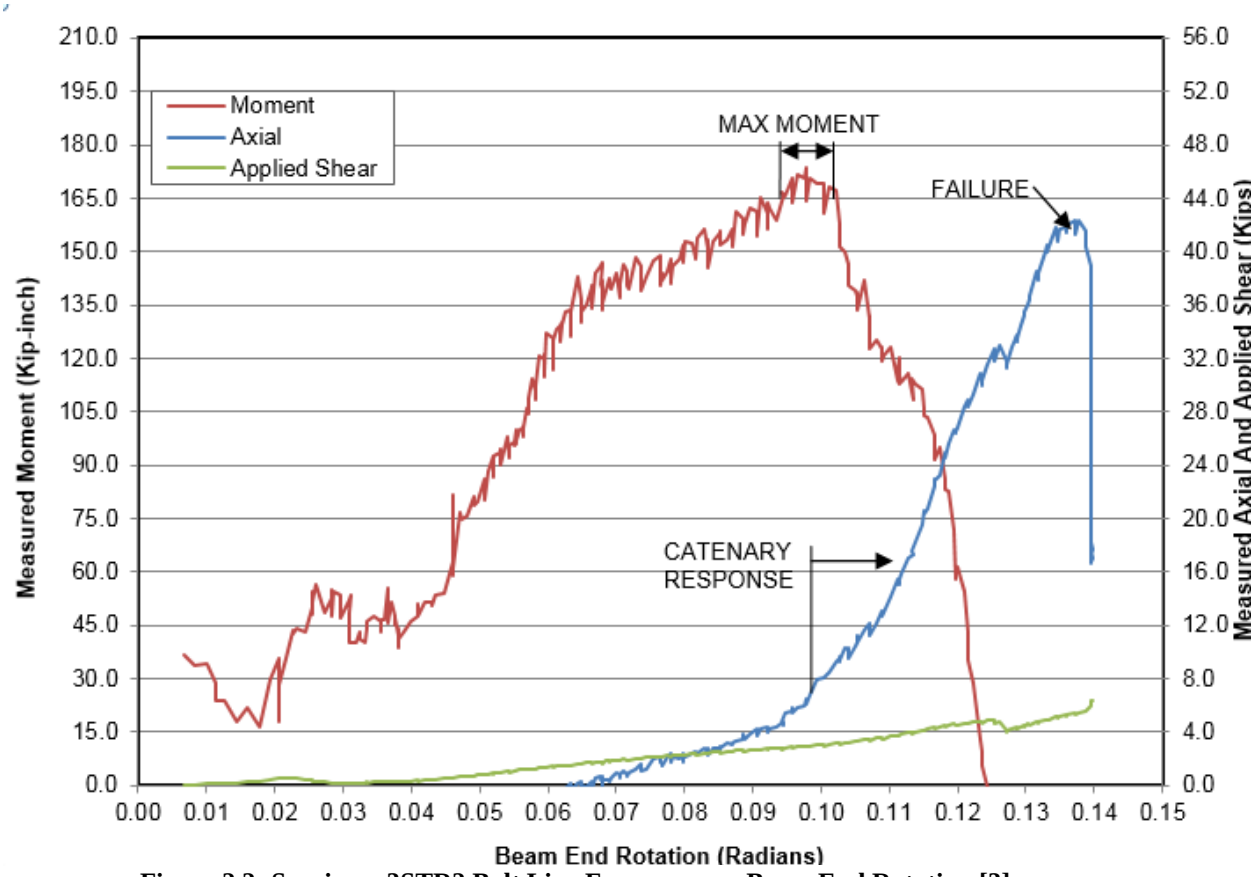

Figure 2.2: Specimen 3STR2 Bolt Line Forces versus Beam End Rotation [3].

Thompson found that the shear tabs failed through both bolt shear rupture as well as "localized" block shear and net tension rupture. It was determined that the bolt shear forces were in the range of 30-40 kips.

According to Thompson [3], the shear tab connections were able to resist significant axial tensile forces in combination with significant flexural resistance. The connection was able to resist applied shear loadings from 7.5 to 9 percent of the un-factored connection design strength. It was suggested that five-bolt configurations may have the ability to recover from initial failure and support around one percent increase of applied shear.

2.2.2 Robustness of Steel Gravity Frame Systems with Single-Plate Shear Connections

Computational assessments of the performance of steel gravity framing systems are used to analyze the influence of factors such as bay spacing, slab continuity, and the mode of connection failure on the collapse resistance of gravity frame systems. Main and Sadek [4] used the data from Thompson's [3] five-bolt test configuration and performed numerical analyses on the same setup. Figure 2.3 shows the computational reduced model used in their research.

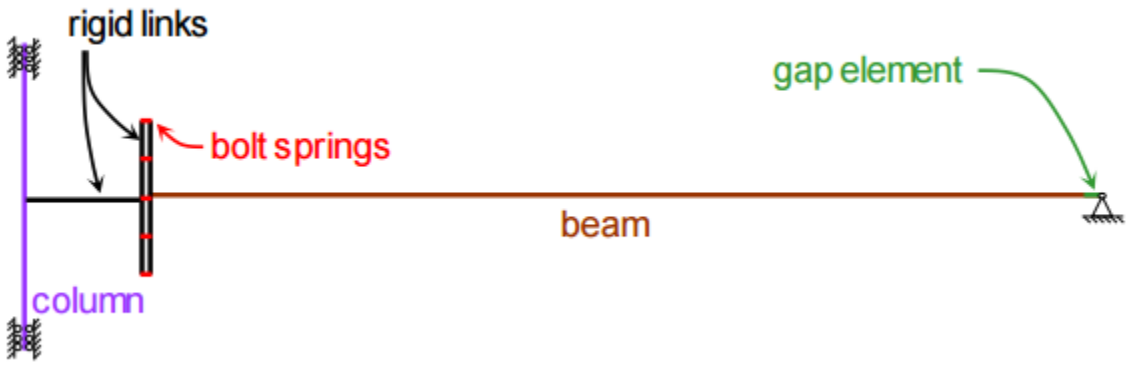

Figure 2.3: Reduced Model of Two-Span Beam Assembly Tested by Thompson [4].

Main and Sadek's numerical model [4] resulted in values within 15% to 21% of the ultimate vertical load as measured in Thompson's [3] tests. The measured rotation in the computational model showed a 5% difference. Figure 2.4 shows the difference between the computational model results and Thompson's experimental results.

The same three-phase phenomena that Thompson [3] observed were also found in Main and Sadek's [4] computational results. The first phase was connection slippage before bolt bearing engaged. Then the second phase began, flexural action increasing until plateauing. Lastly, catenary action occurred until initial failure.

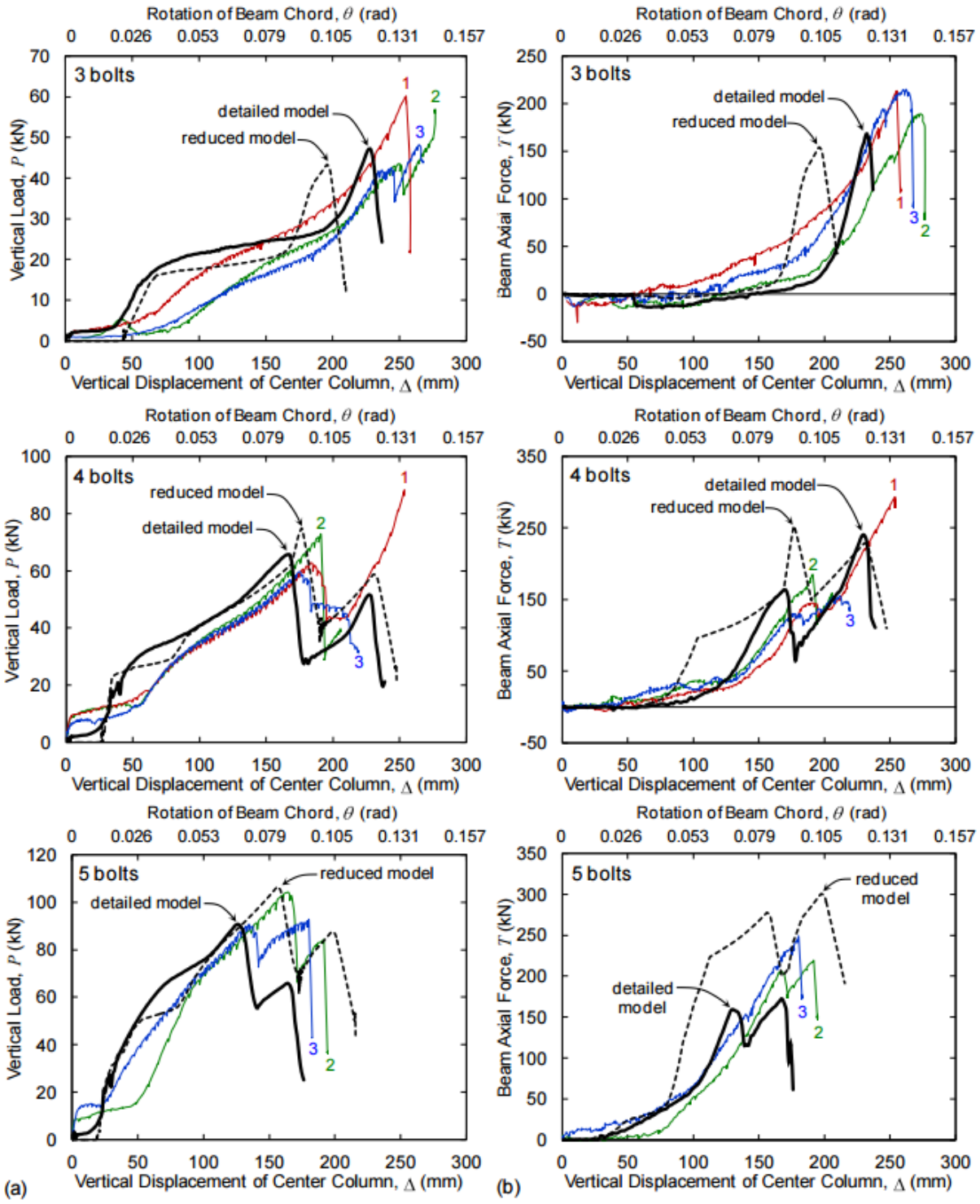

Figure 2.4: Comparison of Detailed and Reduced Model Results with Experimental Measurements (Thompson) for Two-Span Beam Assemblies [4].

2.2.3 Experimental and Analytical Studies of the Cyclic Behavior of Simple Connections in Steel Frame Buildings

Liu [5] investigated when simple connections can be used to resist seismic loads using cyclic behavior. A series of sixteen full-scale cyclic tests with and without floor slabs were conducted. Four, six, and eight bolt shear tab configurations were utilized in the research. Series A, including four- and six-bolt tests and Series B utilizing the eight-bolt configuration. Series A tests were tested without the floor slab while Series B compared the use of normal-weight and light-weight concrete.

It was concluded that the connections had significant moment capacity as well as ductile behavior and large drift rotations. It was found that with the addition of the slabs the connections acted as semi-rigid with moment capacities that were 30% to 60% of the plastic moment capacities of the beams and girders. After 0.04 radians, the contribution was lost as the slab began to incur damage. Table 2.1 shows the test values for each test specimen.

Table 2.1: Test Values [5].

	Average Initial Stiffness		Average Maximum Positive Moment		Average Maximum Negative Moment		Ultimate Drift
	(in-kip)	($Ki/L_{beam}/EI_{beam}$)	(in-kip)	(%M_{pbeam})	(in-kip)	(%M_{pbeam})	(radians)
1A	55100	1.12	583	18%	525	16%	0.14
2A	167000	1.28	1310	20%	1700	25%	0.09
3A	101000	2.05	1590	43%	850	23%	0.15
4A	136000	2.76	1320	38%	1120	32%	0.13
5A	217000	4.39	2310	63%	1300	36%	0.06
6A	233000	1.79	4130	59%	4170	60%	0.11
7A	250000	1.91	2920	40%	3370	91%	0.11
8A	441000	3.38	3930	53%	5710	78%	0.09
1B	17500	0.36	440	13%	420	12%	0.14
2B	29900	0.23	550	8%	2310	33%	0.11
3B	110000	2.24	2070	57%	719	20%	0.15
4B	354000	2.71	3560	51%	4500	65%	0.11
5B	121000	0.93	2900	41%	5650	81%	0.12
6B	250000	1.91	3640	49%	4410	60%	0.11
7B	349000	0.61	5360	24%	6140	28%	0.08
8B	487000	3.73	3620	52%	6060	87%	0.06

2.2.4 Simple Beam Connections in Combined Shear and Tension

Guravich and Dawe [6] tested shear tab connections behavior when subjected to combined shear and tension forces. Eleven shear tab connection tests using 3/4 in. ASTM A325 diameter bolts with 3/8 in. ASTM A36 shear plates were conducted. The tests were set up to ensure additional moment was not added after initial rotation, 0.03 radians.

To ensure a constant and verifiable angle of the beam rotation, shear was applied as close to the connection as practical. Tension load was collinear with the axis of the beam and applied through the center of the beam. The testing specifically looked at the capacity of the connection by eliminating potential test beam failure modes through the use of stiffeners and doubler plates on the beam web. Load was applied using four

different level: pure shear, fifty percent of the factored shear strength, one hundred percent of the factored shear strength, and pure tension.

The results showed that during two pure shear tests, out-of-plane buckling occurred in the connecting plate. The connections did not meet the AISC specification requirement which states that the connection's overall length to be greater than one-half the supported beam's clear web depth, T, to reduce the likelihood of an out-of-plane buckling failure mode.

The research found that the shear tab specimen deformed in bearing in the direction of the resultant force opposite the bolt. An average ratio of 0.94 was found comparing the applied resultant force to the plate bearing capacity. This showed the bolt bearing limit state due to combined shear and tension was a good predictor of the shear tab connection capacity.

Guravich and Dawe [6] concluded that tension resistance in shear tabs subjected to tension or combined shear and tension can be predicted from the bearing resistance of the plate. The dimension was found to be greater than the minimum specified in code.

2.2.5 Behavior of Bolted Beam-Column Connections under Catenary Action in Damaged Steel Structures

Girhammar [7] experimentally tested bolted end plates and bolted heel connections with respect to catenary action. Girhammar examined the statics of catenary action, investigated the capacities of the tested connections, and presented a design theory and design procedure for bolted end plates and bolted heel connections.

The bolted heel plate is a Swiss version of an un-stiffened seat connection, where a supported beam rests on a plate which is bolted to the supporting member. The bolted

end plate tested was a semi-rigid connection with a designed moment capacity. Girhammar's test setup and the statics for a simply supported member subject to catenary forces were important concepts when relating to the research presented in this thesis.

The test setup utilized in the research is an important aspect in understanding the behavior of catenary action and a connections ability to bridge over a removed column. Girhammar's test setup shown in Figure 2.5 utilized two equally spaced bays with simply supported connections at both exterior columns as well as at each side of the interior column. The test arrangement was laid parallel to the ground to prevent the collapse of the structure upon failure. The exterior columns were idealized to have fully restrained connections preventing both axial and rotational movements. The interior column simulated the compromised column and served as the point of load application, F, for the testing.

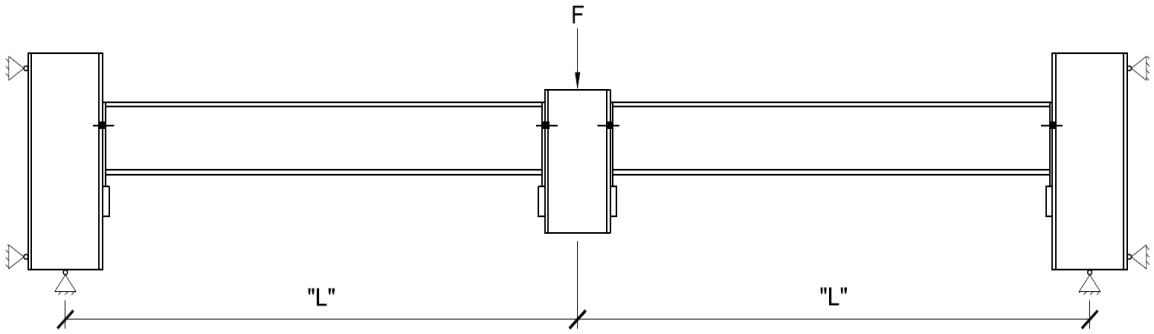

Figure 2.5: Test Arrangement for Simple Supports Subject to Catenary Action [7].

The bay length, L, was approximately 16 ft. Large deflections at the interior column were generated which exceeded the stroke of the hydraulic ram due to the large bay length causing the ram assembly to be adjusted multiple times during testing.

Testing measurements included deflection of the interior column, strain gage readings of the beam flanges near the connections to determine moment distribution in

the beam, strain gage readings of the bolts to determine the normal load on the bolts, and applied force from the hydraulic ram.

Girhammar [7] provided a breakdown of the static force distribution of the system in Figure 2.6 assuming a symmetric test system about the applied load.

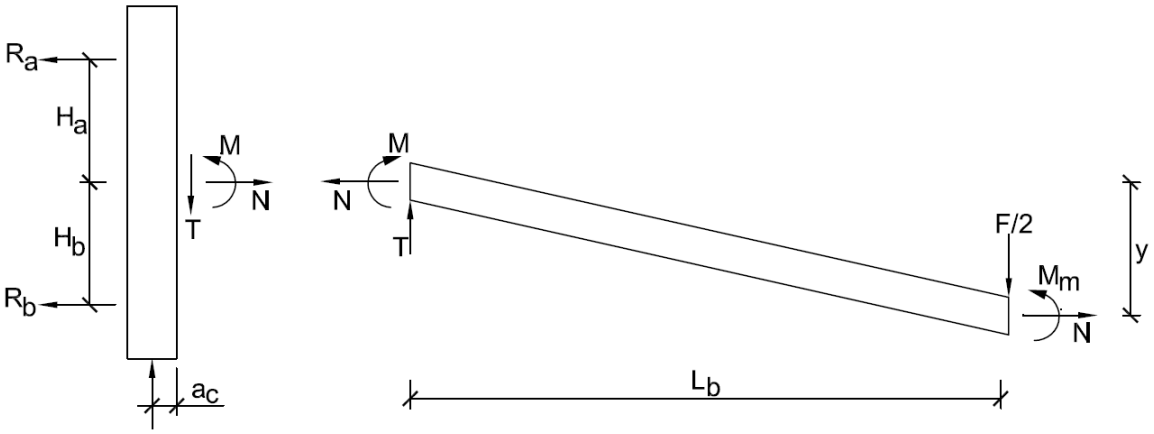

Figure 2.6: Static Free Body Diagram for Beam and Supporting Column [7].

A static equilibrium equation was derived [7] for one-half of the tested system to provide the normal force, N, caused by the applied force, F, shown as

$$N = \frac{\left(\frac{FL_b}{2} + M - M_m\right)}{y} \quad . \tag{1}$$

Assuming a true catenary state where no moment is present, Equation (1) can be simplified to

$$N = \frac{FL_b}{2y} \quad . \tag{2}$$

In pure catenary, the shear force, T, can be taken as,

$$T = \frac{F}{2} . \tag{3}$$

Summing the horizontal forces to zero, the supporting column reaction at support A is equal to.

$$R_A = \frac{\left(Nh_B + R_C a_C - M\right)}{(h_A + h_B)} \quad . \tag{4}$$

Similarly, the supporting column reaction at B is equal to

$$R_B = \frac{\left(Nh_B - R_C a_C + M\right)\cdot}{(h_A + h_B)} \tag{5}$$

Assuming that during catenary action the moment capacity within the beam to column connection has been released and h_A is equal to h_B, the reactions at A and B can be simplified to

$$R_A = R_B = \frac{N}{2}\ . \tag{6}$$

The statics model can be used to predict the normal forces present when catenary action occurs as a result of an applied vertical load. This process can also be used to ensure load measurement devices provide accurate data during elastic stages of load application by maintaining equilibrium in the test system where the sum-of-forces is equal to zero. Additionally, the pure catenary response can be used to determine the maximum tensile force occurring at the connections. This allows maximum forces to be developed for the initial design of the tested connections and for the verification of testing apparatuses.

2.3 Progressive Collapse Research

Progressive collapse research is important in understanding how a system reacts when extreme loading circumstances are present. The robustness of a system allows for the system to resist the unanticipated forces generated from such an event. The ability of a connection to “bridge-over” a column that has been damaged in an extreme event has been shown to introduce catenary action as a primary mechanism for the transfer of the forces in the system.

2.3.1 Robustness of Composite Floor Systems with Shear Connections: Modeling, Simulation, and Evaluation

Sadek *et al.* [8] studied the robustness of composite floors with shear connections. This research provides insight through two simulation models, the first being a beam-column subassembly which was modeled without the contribution of a floor deck, and the second including beams and connections, columns, floor slab, and metal deck.

The prototype floor system used in the research was designed by the National Institute of Standards and Technology (NIST). The prototype was considered in two different seismic design categories, Seismic Design Category C and D. This ensured that two different types of moment frames would need to be considered during research, intermediate and special moment frames. The frame itself consisted of bays built with W16×26 and W14×22 ASTM A992 beams and columns. The connections between these beams and columns are shown in Figure 2.7.

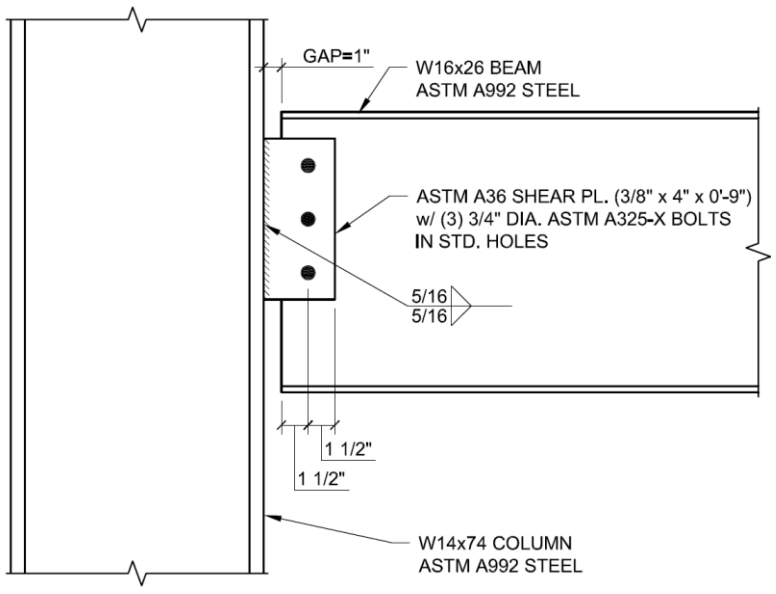

Figure 2.7: NIST Theoretical Test Assembly for Shear Tab Connections [8].

Numerical models were used to analyze the behavior of the connections. The analysis utilized a slow loading rate to ensure static response. The first model used to simulate the connection was a high fidelity connection (HFC) model. This model consisted of half of the sub-assembly due to its symmetrical nature. The shear tab is modeled as rigidly connected to the column flange because the fillet weld stresses are low compared to their strength. The beams, columns and connection components are modeled using a piecewise linear plasticity model. The system begins responding in flexural mode before switching to "cable-like" (i.e., catenary) behavior. The failure mode in this model is tear-out failure of the beam web.

A reduced component connection (RCC) model was created to simulate the connection strength using non-linear springs at the bolts to represent the connection behavior. When determining limit states, it was found that tear-out of the beam web was the governing failure mode.

A reduced coarse shell connection (RCSC) model was utilized to compare the data found by the RCC. In this model, a coarse shell element mesh was used to emulate the beam, column, and connection. An elastic-perfectly plastic spring was supplemented into the system to ensure shear rigidity and strength. The failure in the model is due to sequential failure/erosion of the shell elements representing the connection. A comparison of these three models can be seen in Figure 2.8.

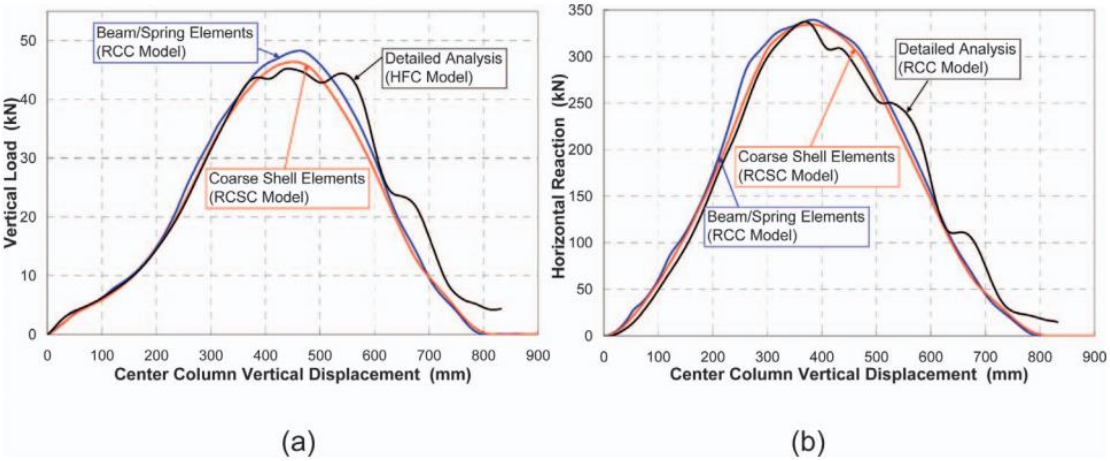

Figure 2.8: (a) Applied Vertical Load versus Center Column Vertical Displacement; (b) Horizontal Reaction versus Center Column Vertical Displacement [8].

When modeled with a floor, significant capacity increase occurred. Figure 2.9 shows a plot comparing floor models with framing only models. It was concluded that in simple shear connections loads are initially resisted by flexural behavior and then cable action in the beam. The connection failure may occur from various different methods including fillet weld failure, bolt failure, block shear, and tear-out failure. Lastly, it was concluded that floor assemblies contribute significantly to floor response because the floor acts as a rigid diaphram preventing the exterior columns being pulled inward, and the floor behaves like a membrane providing two-way membrane action through the reinforment mesh and one-way membrane action through the metal deck.

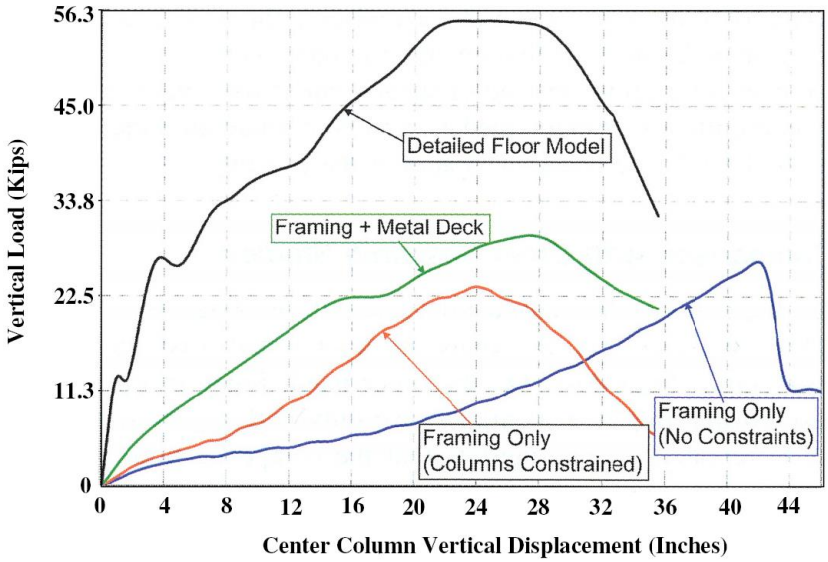

Figure 2.9: Analytical Floor Model Analysis Comparisons [8].

2.3.2 Application of Seismic Steel Connection Experiments to Column Removal Scenario

Daneshvar and Driver [9] presented research on "column removal" scenarios. They found that in progressive collapse scenarios catenary action is important which is different than seismic scenarios. Catenary action is a primary mechanism of load resistance after column removal. It was also found that tension and moment interaction plays a key role in the resistance of progressive collapse.

The authors concluded that connections in progressive collapse do not always behave more ductile than in seismic applications. Realizing the presence of the axial tensile capacity after inelastic rotation plays a significant role in the understanding of how connections react after column removal.

2.3.3 Progressive Collapse Resistance of Steel-Concrete Composite Floors

Research performed by Alashker *et al.* [10] provides insight into progressive collapse resistance for steel-concrete composite floors with the use of shear tabs. Finite

element modeling was used to model each part of the composite system including the concrete slab, steel deck, shear studs, mesh reinforcement, beams, and columns. The software, LS-DYNA, was used to validate the models of tests performed by Hallquist [11] and Sadek [8] through studies and comparison of independent results for composite connections and single bolt responses.

It was found that when an interior column was removed, the concentrated load simulations produced failures of the floor system that progressed through failures of shear tab connections. Extra bolts were added to the simulation to investigate the effect of bolt number. Three- , four- , and five-bolt configurations were used utilizing A325 bolts. The results showed that as the number of bolts increased, greater strength occurred. It was found that when utilizing five bolts instead of three, the capacity increased by 40%. The uniform load model did not agree with these results due to the fact that the connection fails much sooner than the full capacity of the floor is reached, increasing the capacity of three to five bolts by 17%. Figure 2.10 shows the load versus displacement plots between the concentrated load and uniform load models with respect to the number of bolts used.

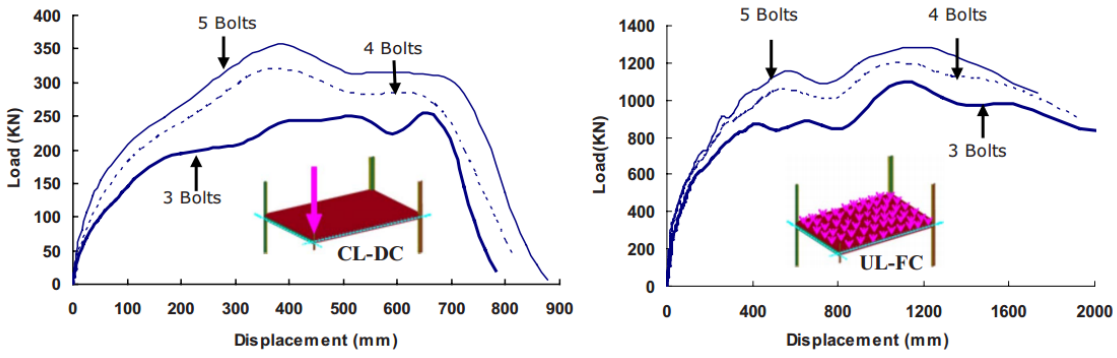

(a) Concentrated load (b) Uniform load

Figure 2.10: Effect of Number of Bolts in Shear Tab Connection on Floor Load-Deflection Response [10].

Dynamic effects were included in this research by magnifying the statically computed design forces. The prototype floor system was uniformly loaded, and a center column stub was supported vertically. The center column was then removed suddenly. Once the system recovered from the initial column removal, it was subjected to incremental loading until the system collapsed. The floor system collapsed at 850 kN when the load was applied dynamically, while the static capacity was approximately 1,100 kN. This resulted in a dynamic impact factor of 1.29, less than U.S. General Service Administration guidelines typically used, 2.0.

It was concluded that composite floor capacity is mainly from the steel deck. It was also concluded that increasing the number of bolts present in the system has little effect on the floor collapse capacity because the connection fails before the floor's full capacity is reached. If collapse resistance through the connection is to be achieved, the connection itself must carry the capacity. It was found that the dynamic impact factor depends on the ductility and amount of inelastic action within a structure when subjected to the column removal scenario. Lastly, it was found that the uniform load model allows a more accurate representation of collapse when compared to concentrated load models. This is because it mobilizes all sources of collapse resistance.

2.3.4 Quantifying and Enhancing the Robustness in Steel Structures Part 1- Moment-Resisting Frames

Foley *et al.* [12] examined disproportionate collapse in structural steel framing in an effort to improve the understanding of secondary load paths in structural framing when localized failure occurs and to understand the distribution of tensile forces within steel floor framing.

The SAC-FEMA suite of buildings was used. The framing plans consisted of framing modeled with flexible connections throughout the interior and some along the exterior, as well as moment-resisting connections along the perimeter of the building. All columns were connected at the base utilizing idealized pinned supports.

A superimposed dead load of 83 pounds per square foot and live load of 50 pounds per square foot were used throughout the main floor areas. A superimposed dead load of 96 pounds per square foot and live load of 50 pounds per square foot were used at the location of the penthouse. The roof outside of the penthouse location had a dead load of 63 pounds per square foot and live load of 50 pounds per square foot. Cladding was assumed to be 25 pounds per square foot.

After determining the loading on the structure, analysis was conducted using SAP2000 [13]. A perimeter column was instantaneously removed. It was found through time-history analysis that a three-story frame included the floor system as a transfer mechanism. As the number of floors decrease, the number of floors damaged increases. It was found that full moment reversal at plastic moment capacity is likely in the beam and girders, meaning that all moment-resisting connections should be designed for fully plastic moment capacity in both directions.

The research showed that when only a few floors exist, an inelastic flexural mechanism forms due to column removal. The tension forces in a three story building was 1.9% of the nominal tension capacity while a ten-story and twenty-story building are 2% and 1.6%, respectively.

2.3.5 Quantifying and Enhancing the Robustness in Steel Structures Part 2- Floor Framing Systems

Part two of the work performed by Foley *et al.* [14] presents insight into the methodologies proposed and validated for quantifying catenary and membrane mechanisms in concrete floor systems, as well as to outline a methodology for quantifying the membrane and catenary capacity of a structure.

It was found that when an interior column was rendered ineffective, a static nonlinear analysis indicated that the system will be able to support the self-weight, partitions, and expected point-in-time live loading. The double angle connections used should be a higher thickness and the number of bolts used in the connection should be at the maximum allowed for the beam or girder to enhance the inherent robustness in the system when an interior column is removed.

It was also found that it is better to have small moment capacity and flexural stiffness in the connections. When low moment capacity is present, a smoother transition between flexural mechanism and catenary tension occurs after the initial flexural mechanism forms. If the moment capacity is too large, snap-through can occur.

2.3.6 Collapse Behavior of Steel Special Moment Resisting Frame Connections

Khandelwal and El-Tawil [15] performed computational structural simulation to investigate variables that influence catenary action in special moment frames. A two-bay steel sub-assemblage with seismic detailing was utilized in the computational simulation.

It was found that every sub-assemblage deformed in a ductile manner and developed catenary forces. The inelasticity was concentrated in the plastic hinge regions. Some sub-assemblages underwent local bucking as well as lateral torsional buckling

when loads transferred due to flexure in the beam to catenary forces. The instabilities were stopped when catenary action began.

It was concluded that out-of-plane pulling action induced by transverse beams did not affect the behavior of the system negatively. It was found that what did affect ductility and strength negatively was beam depth and increase in yield and ultimate strength ratios.

2.3.7 Parametric Analysis of Progressive Collapse in High-Rise Buildings

Gamaniouk [16] conducted research into the performance of high-rise buildings under the loss of a column. The use of nonlinear dynamic alternate path method was used to perform parametric analysis for progressive collapse due to its accuracy for the behavior of a structure. SAP2000 was used as structural analysis program. The analysis was conducted on a moment frame, a braced frame with outriggers, and a truss tube system.

Nonlinear static analysis was used to establish equilibrium conditions. The dynamic analysis was performed using nonlinear direct integration time history. Parameters presented in the analysis included a damping ratio of 2%, a time step of 0.01 seconds, a total duration of five seconds or until failure, and a column removal duration of one fifteenth of the period.

A comparison of the linear dynamic and nonlinear dynamic response shows that the nonlinear dynamic achieves higher deflection and stabilizes at about 0.05 m more of deflection than the linear dynamic. Figure 2.11 shows the plots of the responses as deflection versus time.

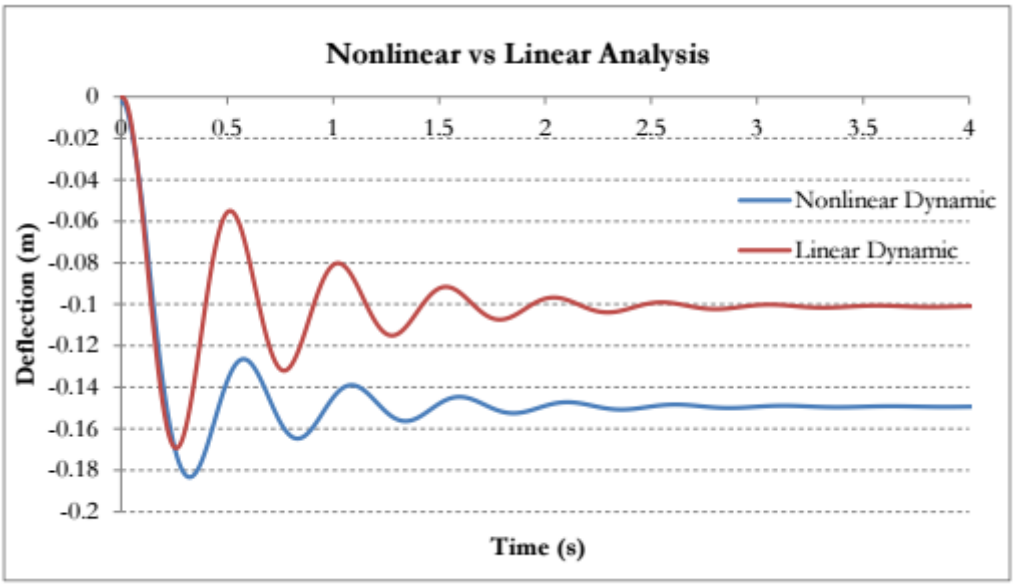

Figure 2.11: Comparison of Linear and Nonlinear Vertical Deflection of Joint at Column Removal [16].

With the increase of stories it was found that the building's ability to deal with local failure improved. The deflection at joint where the column was removed is greatly affected by how many stories are present for the first 25 stories, as shown in Figure 2.12.

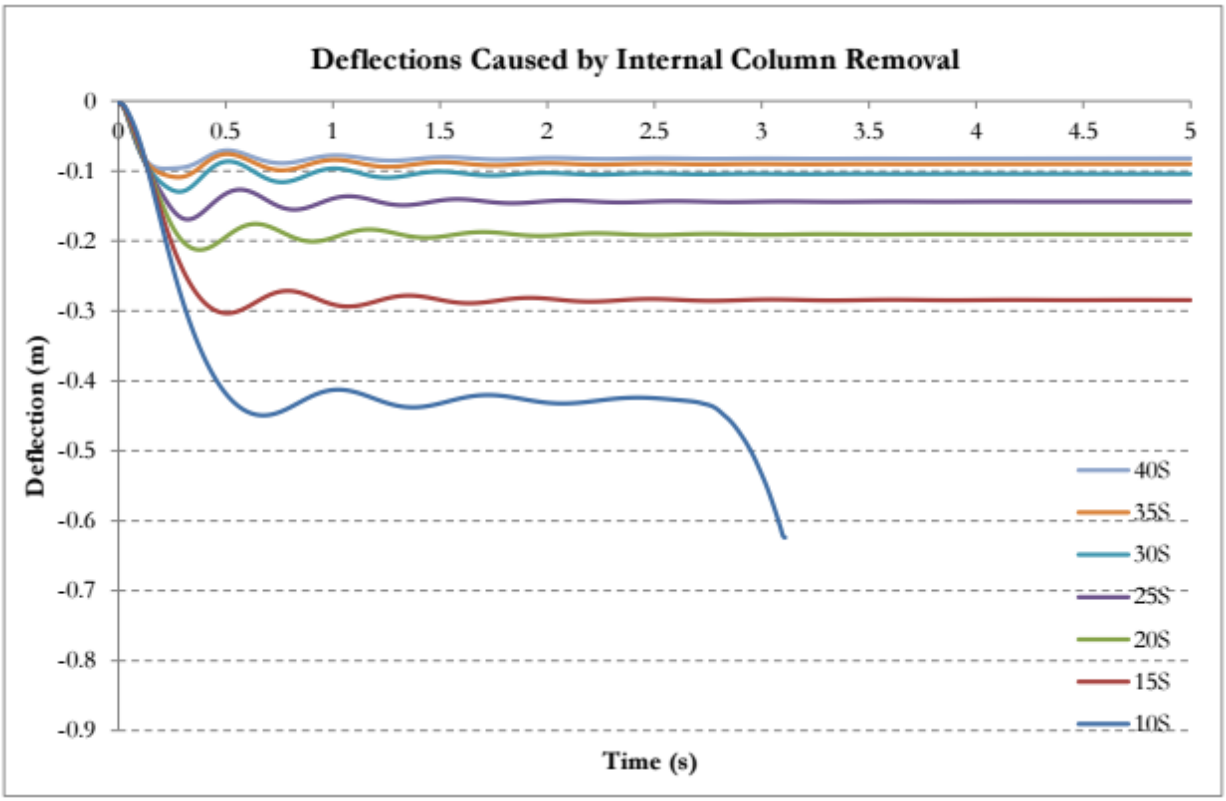

Figure 2.12: Moment Frame Deflections for Internal Column Removal [16].

It was concluded that as the number of floors increase, the ability for the structure to redistribute the load and diminish to a level within the structure's capacity increases. It was noted that there was a correlation between the number of stories and the number of plastic hinges that occur in the building, as increasing in height decreases the number of hinges.

2.3.8 Experimental and Analytical Assessment on Progressive Collapse Potential of Two Actual Steel Frame Buildings

Song *et al.* [17] performed an investigation into the progressive collapse performance of two existing buildings through experimental testing and computational analysis. Each building was tested by removing four first story perimeter columns.

SAP2000 was used to create models to analyze through linear static and nonlinear dynamic procedures.

It was found through computational analysis that the building's top story columns were the most significantly influenced by the column loss. It was found that beams were less impacted by the removal than columns.

In order to simulate column removal for the nonlinear dynamic analysis, equivalent reactions were used to replace the columns. A time history function was used to simulate the loss. Smaller displacements were seen in nonlinear dynamic analysis than in linear static analysis. The time for stabilization increased as columns were removed, becoming more vulnerable to dynamic loads causing progressive collapse.

2.3.9 An Approach to Testing the Performance of Steel Connections Subjected to Extreme Loading Scenarios

Oosterhof and Driver [18] provided research into shear connection performance under extreme loading. The research outlines proportions for moment, shear, and tension that can be expected following column failure.

The test setup was used to allow independent control of moment, shear, and tension allowing the same demands as what would be present in a double-span column removal test. Figure 2.13 shows the test setup utilized in Oosterhof and Driver's [18] research.

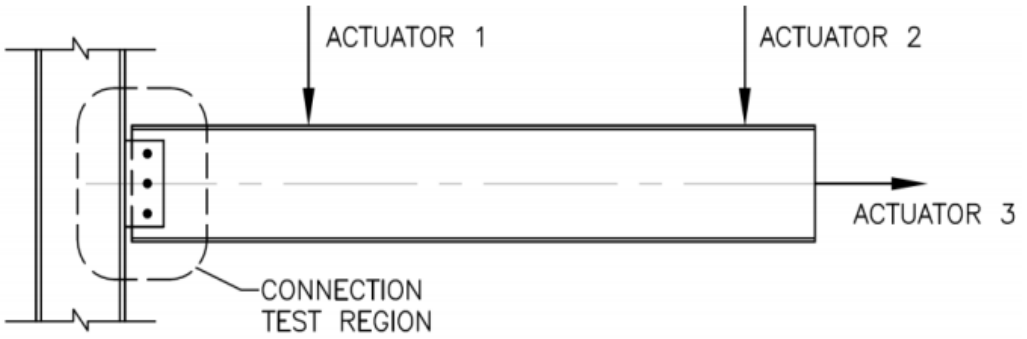

Figure 2.13: Schematic of Test Setup [18].

Oosterhof and Driver [18] examined a symmetric three-hinged beam with a central point load which was solved by Timoshenko in 1955, shown in Figure 2.14 and Figure 2.15. The shear force and tensile force were used as vertical and horizontal reactions, respectively. This was opposed to perpendicular and parallel to the axis of beam rotation. The contribution of the moment resistance of certain types of shear connection through large rotation is expected to be significant. Timoshenko's three-hinged model was then modified to consider rotational and axial stiffness of the connections. The rotational and axial stiffness was modeled as rotational springs shown in Figure 2.16. These springs were included to account for elongation of the flexible connections. From this were derived the following equilibrium equations,

$$V_4 = \frac{P}{2} = T \tan\theta_c + \frac{2M}{L}, \tag{7}$$

and for uniform loading,

$$V_5 = \omega L = 2\left[T \tan\theta_c + \frac{2M}{L}\right]. \tag{8}$$

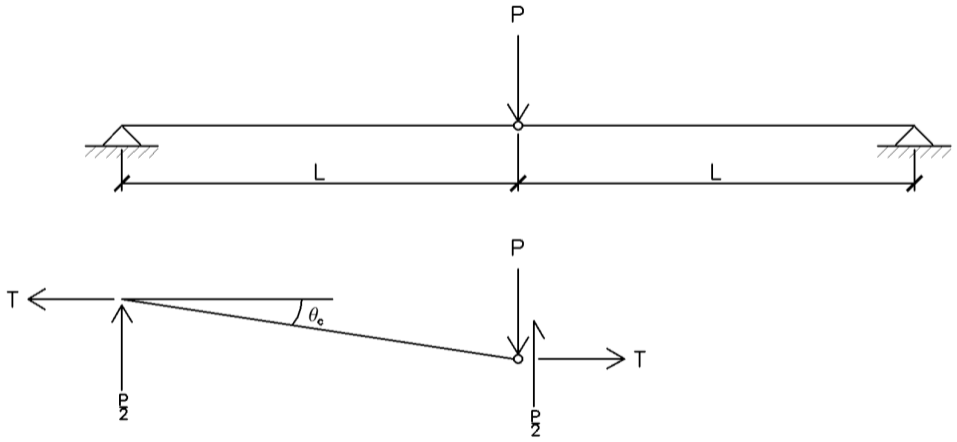

Figure 2.14: Three-Hinged Beam (after Timoshenko) [18].

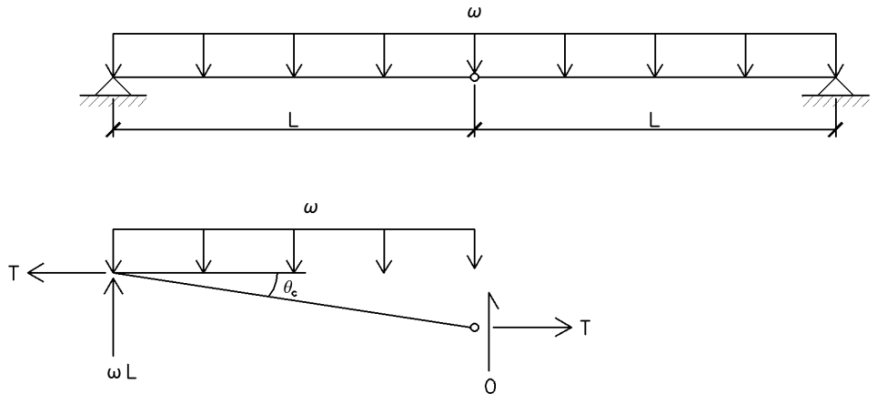

Figure 2.15: Three-Hinged Beam under Uniformly Distributed load [18].

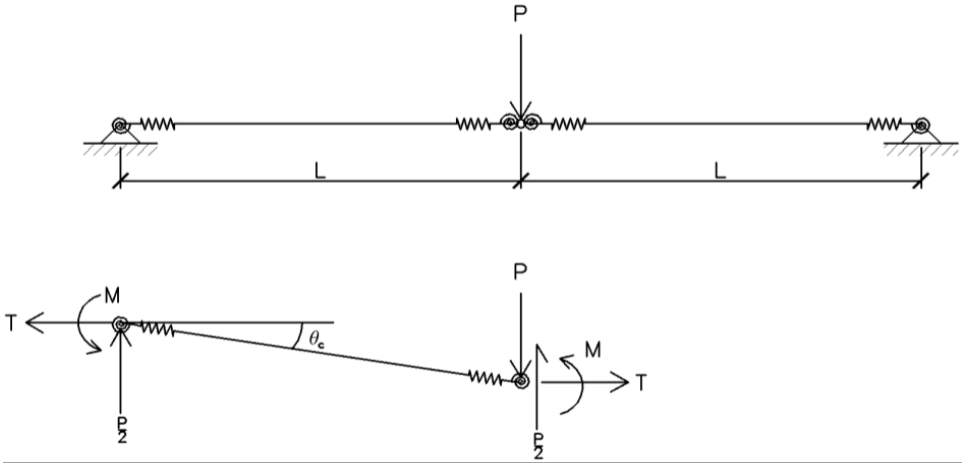

Figure 2.16: Modified Three-Hinged Beam with Connections Represented by Springs [18].

Oosterhof and Driver discussed that three histories represent the cases of a central point load, a uniformly distributed load for the connection at the removed column, and a uniformly distributed load for the connection at the remaining column. These load histories test the realistic combination of strength with ductility demands.

Actuator 2 needed to be displacement-controlled, applying an incremental rotation to the system at each finite load step. Actuator 3 needed to be displacement-controlled as well. The axial displacement that was applied was calculated using the measured rotation at the current load step. The forces in the actuators were measured by controlling the applied displacement. By using Actuator 1 with force control, equilibrium state was achieved.

Oosterhor and Driver predicted how the load history would compare with physical tests, shown in Figure 2.17. Due to the difference in the response of the system, it was concluded that physical testing and research need to be performed.

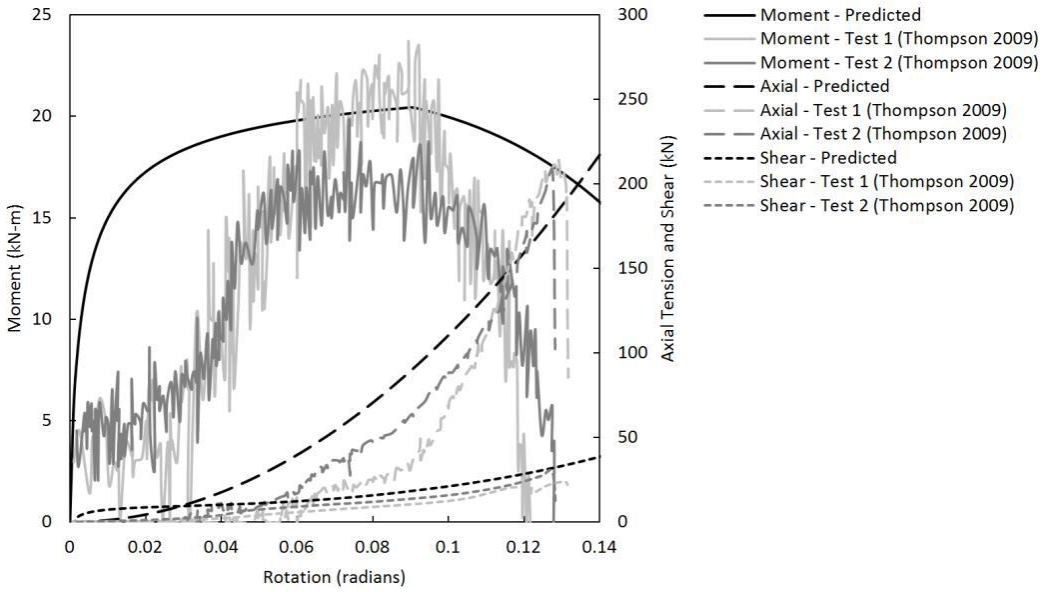

Figure 2.17: Predicted Load History and Physical Test Results for Shear Tab Connection [18].

Chapter 3

EXPERIMENTAL TESTING

3.1 Experimental Testing Overview

The purpose of this research initiative is to expand upon research conducted by Thompson [3]. The previous testing was performed to understand how a shear tab connection's behavior changed when subjected to unexpected forces caused by failures in supporting columns. The present study provides insight into how shear tab connections react when subjected to quasi-dynamic forces.

A total of eleven tests were performed at the Marquette University Engineering Materials and Structural Testing Laboratory (EMSTL). The tests were performed on specimens with three-, four-, and five-bolt connections. These connections were designed per the "Conventional Configuration" by Thompson [3]. The design performed by Thompson was used as a comparison as the codes have changed.

As stated previously, this experimentation was an expansion on Thompson's work; it is important to note that this experimentation was designed to exact specifications prescribed in his work in 2009. This was to ensure the results were comparable. The shear tab experimental testing was also performed in conjunction with WT simple shear connections conducted by Hayes in 2016 [19], an expansion on the work of Friedman in 2009 [20].

3.2 Experimental Setup

3.2.1 Test Assembly Overview

The test frame shown in Figure 3.1 illustrates the typical test configuration. The test frame consists of two existing W12×87 outer columns, and one W12×79 supporting

beam spanning between them. This supporting beam consists of the beam itself with a 1 in. thick plate welded at each end. Each test frame column is attached at the bottom to a W10×88 floor beam. The W10×88 was bolted to the strong floor by threaded rods at 3 feet increments. The W18×35 test beams were connected to each existing column with a true pin connection. At the other end of the test beam was the specimen. A hydraulic actuator was attached in the center of the test setup to the strong floor and was connected to the column stub assembly. Refer to Appendix C for design calculations of the test apparatus sub-assemblies. Figure 3.2 shows the overall test frame setup built in the EMSTL at Marquette.

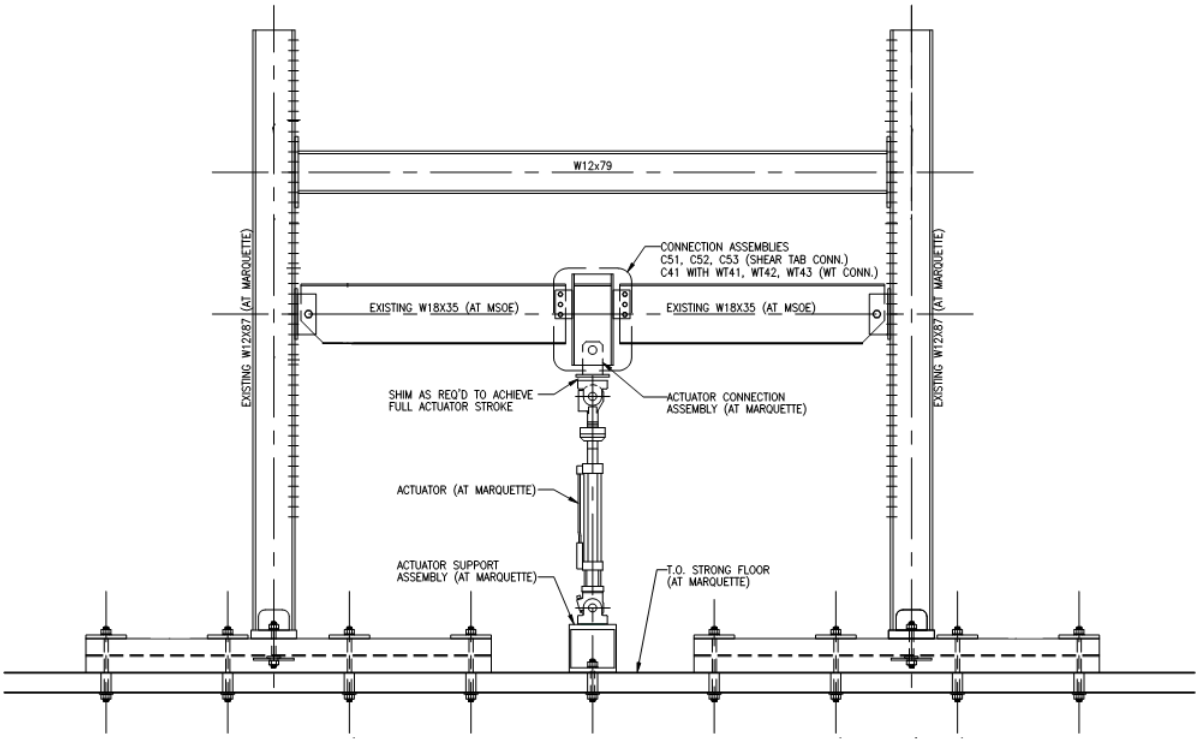

Figure 3.1: Experimental Test Frame.

Figure 3.2: Overall Test Setup.

3.2.2 Test Beams

The test beams selected were ASTM A992 W18×35 sections. The beams used in this experimental testing were the exact beams used by Thompson [3]. An illustration can be seen in Figure 3.3. The web depth of these sections were sufficient to provide clearance for a five-bolt connection without violating the one-half depth rule for the three-bolt configurations per specifications in AISC [2]. The beams were designed to be reused for multiple tests. As such, a 3/8 in. ASTM A36 web doubler plate was welded with 5/16 in. E70XX fillet welds at three sides, attaching to the beam at the bolt hole location at the outer column connection. The size of the bolt hole was a 1-5/16 in. diameter. A doubler plate was also located at the side where the connection to each test specimen would be attached. The plate was welded with 1/4 in. E70XX fillet welds. These plates were added to strengthen the bolt hole and limit deformation due to repeated tests. The bottom flange of the beam was chamfered for rotational purposes as not to have any issue with beam-column interference as the test beam rotated in plane. The dark

bolded lines down the center of the test beam show the representative location of each strain gauge.

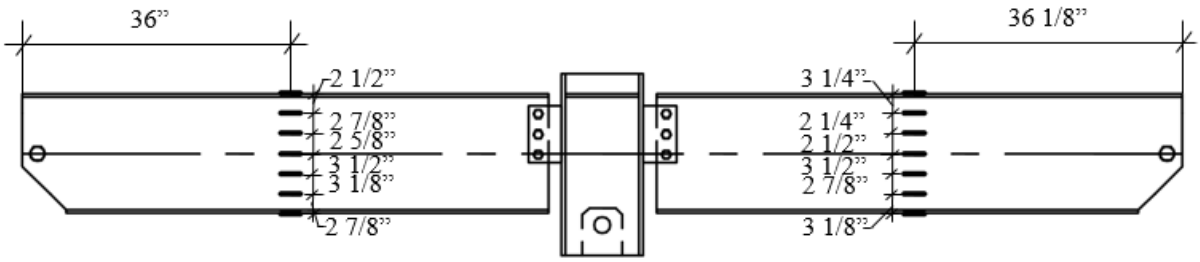

Figure 3.3: Test Beam Configuration and Strain Gauge Locations.

3.2.3 True Pin Connection

The true pin connections of the test beams were used to ensure minimal load transfer at the beam end to a unidirectional tensile force in line with the test frame. This pin connection was designed as a welded plate assembly which was to be connected to the tests beams with a 1-1/4 in. diameter ASTM A490 bolt with threads excluded from the shear plane. The assembly was then connected to the W12×87 columns with (10) 5/8 in. ASTM A490 bolts. The true pin connection assembly can be seen in Figure 3.4.

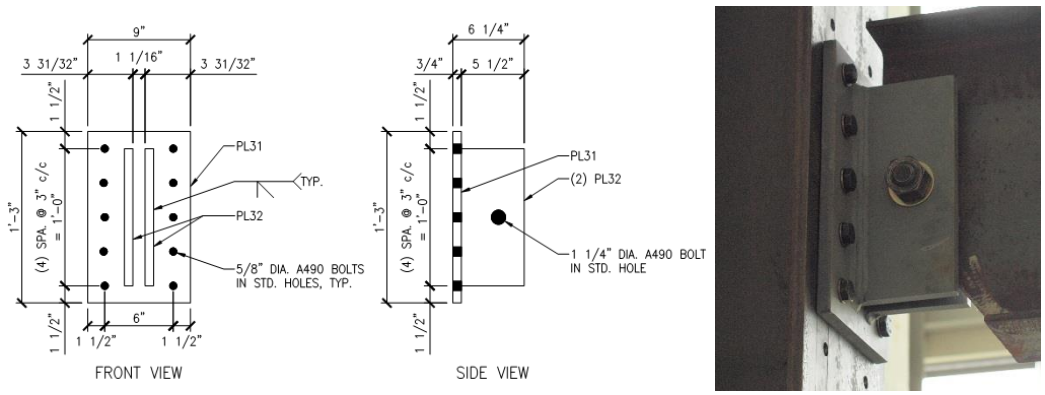

Figure 3.4: Beam End True Pin Connection.

3.2.4 Test Specimen

The column stub test specimens are shown in Figure 3.5. Three, four, and five bolt shear tab specimens were fabricated, and the details are similar to those used by

Thompson [3]. The specimens were designed with the maximum allowable bolt offset of 3-1/2 in. from the column flange to ensure binding of the test beam and the test columns did not occur due to beam end rotation. The shear plates were made of 3/8 in. ASTM A36 material with 3/4 in. diameter A325 bolts designed with threads included in the shear plane. Per AISC specifications, edge distance did not exceed 1-1/2 in. The spacing of the bolt holes is 3 in. center to center as is industry standard. Design capacity calculations can be seen in Appendix A and Appendix B. Further detailing of the shear tab specimen can be found in Appendix C.

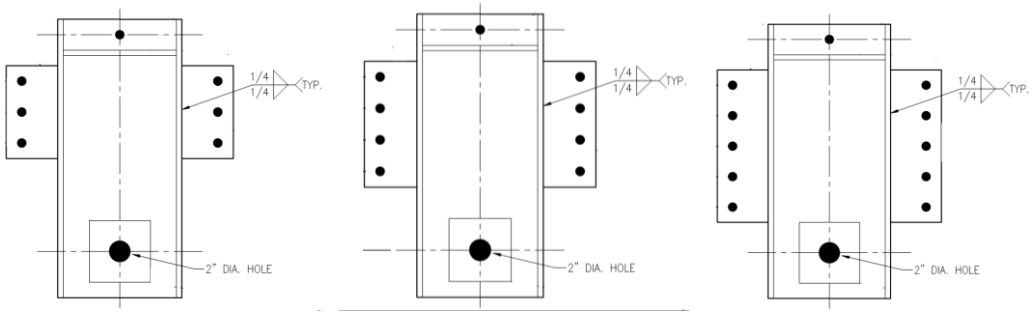

(a) (b) (c)

Figure 3.5: Shear Tab Specimen. a) Three-Bolt Configuration. b) Four-Bolt Configuration. c) Five-Bolt Configuration.

When determining limiting design capacities, two different sets of limits states were evaluated. The first set was determined considering the connection's vertical shear capacities as prescribed in the AISC 14th Edition Specification [2] using the "conventional configuration" guidelines.

A second set of limit states was found by calculating the connection's capacity as a "hanger" (i.e., tension only) connection as determined using Chapter J of the AISC 14th Edition Specification. Calculations of the limit states can be found in Appendix A and Appendix B. A summary of the connection capacities for the three- , four- , and five-bolt configurations are shown in Tables 3.1 and 3.2.

Table 3.1: "Conventional Configuration" Single Plate Un-Factored Shear Capacities per AISC 14th Edition Limit States.

Single Plate "Conventional Configuration" Ultimate Shear Capacity				
Connection Limit State	AISC 14th Equation	3-Bolt	4-Bolt	5-Bolt
Single Bolt Shear Rupture [kips/bolt]	J3-1	23.9	23.9	23.9
Shear Plate Single Bolt Tearout [kips/bolt]	J3-6b	35.7	35.7	35.7
Shear Plate Single Bolt Bearing [kips/bolt]	J3-6b	48.9	48.9	48.9
Beam Web Single Bolt Tearout [kips/bolt]	J3-6b	-	-	-
Beam Web Single Bolt Bearing [kips/bolt]	J3-6b	43.8	43.8	43.8
Bolt Shear Rupture [kips]	J3-1	71.6	95.4	119.3
Shear Plate Bolt Bearing [kips]	J3-6b	133.6	182.4	231.4
Beam Web Bolt Bearing [kips]	J3-6b	131.6	175.6	219.5
Weld Shear Rupture [kips]	J4-4	129.9	174.4	219.0
Base Metal Shear Rupture [kips]	J2-4	114.2	153.3	192.5
Shear Plate Shear Yield [kips]	J4-3	72.9	97.2	121.5
Shear Plate Shear Rupture [kips]	J4-4	83.2	110.9	138.7
Shear Plate Block Shear Rupture [kips]	J4-5	83.9	108.2	132.4
Beam Shear Yield [kips]	G2-1	159.3	159.3	159.3

Table 3.2: Single Plate Un-Factored Tensile Capacities per AISC 14th Edition Limit States.

Single Plate Ultimate Tensile Capacity				
Connection Limit State	AISC 14th Equation	3-Bolt	4-Bolt	5-Bolt
Single Bolt Shear Rupture [kips/bolt]	J3-1	23.9	23.9	23.9
Shear Plate Single Bolt Tearout [kips/bolt]	J3-6b	35.7	35.7	35.7
Shear Plate Single Bolt Bearing [kips/bolt]	J3-6b	48.9	48.9	48.9
Beam Web Single Bolt Tearout [kips/bolt]	J3-6b	32.0	32.0	32.0
Beam Web Single Bolt Bearing [kips/bolt]	J3-6b	43.9	43.9	43.9
Bolt Shear Rupture [kips]	J3-1	71.6	95.4	119.3
Shear Plate Bolt Bearing [kips]	J3-6b	107.1	142.8	132.5
Beam Web Bolt Bearing [kips]	J3-6b	96.0	128.0	160.0
Weld Shear Rupture [kips]	J2-4	194.9	261.7	328.5
Base Metal Tensile Rupture [kips]	J4-4	190.3	255.6	320.8
Shear Plate Tensile Yield [kips]	J4-3	121.5	162.0	202.5
Shear Plate Tensile Rupture [kips]	J4-4	138.7	184.9	231.1
Shear Plate Block Shear Rupture [kips]	J4-5	116.5	163.1	209.3
Beam Web Block Shear Rupture [kips]	J4-5	107.8	149.3	190.7

Each test specimen was given a unique name using a standard naming convention. The first letter of the name indicated whether the test was static or dynamic, S or D. The next number indicated the number of bolts per test, 3, 4, or 5. The next two letters indicated the type of connection, ST for shear tab. The number located at the end indicated which number test was occurring in that bolt group, 1 through 3 or 4. Figure 3.6 shows a standard naming convention. This is the second dynamic four bolt shear tab test.

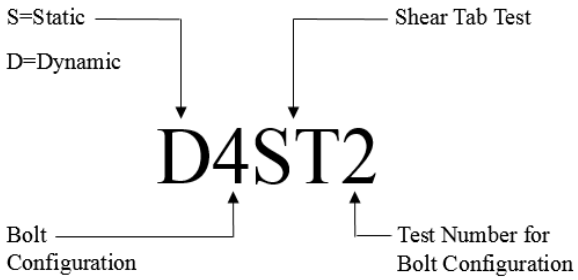

Figure 3.6: Specimen Naming Convention.

3.2.5 Experimental Instrumentation

The experimental data acquisition consisted of three main components: strain gauges, displacement transducers and force transducers. These three components provided information regarding deflection, applied load, and strain in the system.

A MTS 201.30T single ended hydraulic actuator with integral force and displacement instrumentation was used during the testing. The actuator was connected to the column stub through a clevis, where two plates slide on each side of the column stub. A pin was then placed through the clevis and secured. The connection allowed for direct loading of the column stub as it pulled downward, simulating column removal.

Figure 3.7 shows the placement of the two draw-wire transducers (DWT) and their connection to the test specimen. These Unimeasure Model PA-30-DS-L5M DWT's collected data regarding vertical deflection. As the column stub moved down, the wires

would extend from the DWT box, transmitting data of how many in. the column stub was moving vertically. Since a DWT was attached to each flange of the column stub, the deflection measurements could be used to determine overall and differential displacement of the column stub.

Strain was collected from a series of seven Vishay "Micro-Measurements" CEA-06-062UW-350 (350 ohm) strain gauges that were connected to each test beam. There was one strain gauge placed approximately in the middle of the beam flange. The other five were located on the beam web at approximately symmetrical points as seen in Figure 3.8. For exact dimensions refer to Figure 3.3.

Data were collected two ways. First, all measured data (force, strain and displacement) were collected through a single data collection portal run through LabView software. Second, the MTS controlling software for the hydraulic actuator collected vertical deflection and force data. Since the data acquisition systems were independent, the data could be compared in an effort to ensure the data collected were consistent and accurate. Figure 3.9 shows a graph comparing the LabView data to the MTS data for force and displacement. It can be seen that very little variation occurs between the two data acquisition systems, which can be attributed to minor differences in calibration between the two systems.

Figure 3.7: Draw Wire Transducer Locations.

Figure 3.8: Strain Gauge Locations.

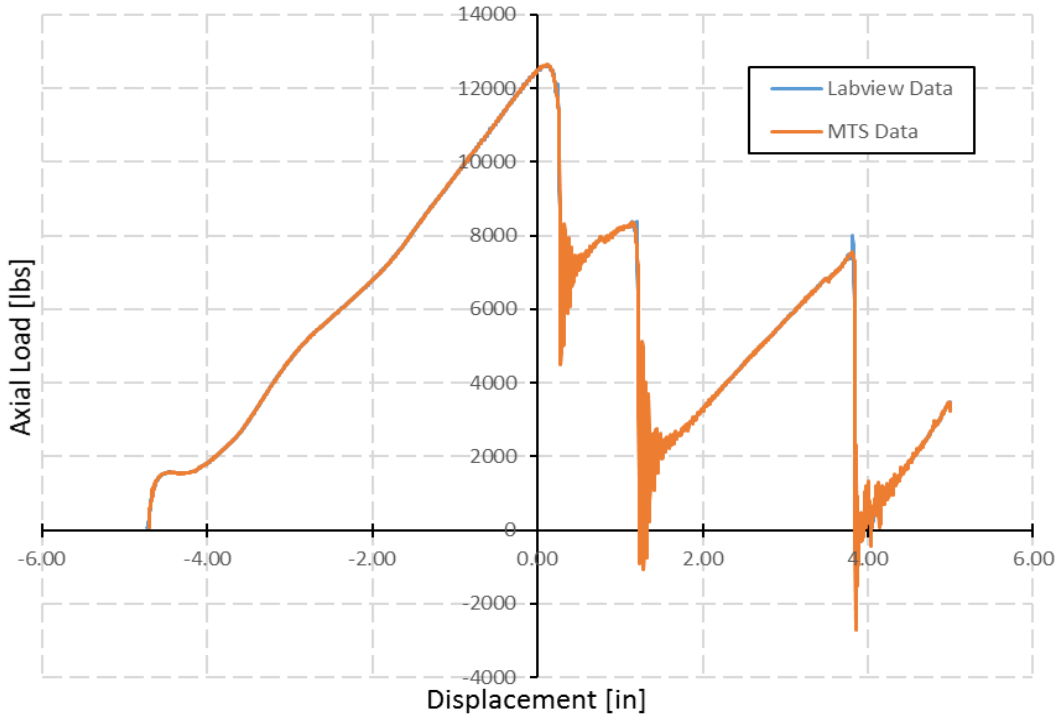

Figure 3.9: MTS versus LabView Data.

3.3 Experimental Safety

Safety precautions during testing were of the utmost concern. Previous experimental safety procedures outlined by Thompson [3] and Friedman [20] were practiced as well as additional safety precautions. The dynamic nature of this testing was

a concern due to the fact that the testing could not be stopped if complete failure were to occur.

Lexan containment shields were placed at the front and back of the specimen to contain bolt shear fragments. Cable winches were attached to the test beams to prevent the beams from falling in the event of total connection failure.

Additional cable winches were attached to the actuator in four directions ensuring the actuator stayed in a straight, upright position. Two winches were attached to the actuator and wrapped around the columns of the test frame to ensure no movement occurred in plane. Two winches were attached to the actuator and wrapped through a plate that was connected to the strong floor to ensure no movement occurred out of plane.

3.4 Experimental Setup

The W18×35 test beams were lifted into the test frame and attached to the true pin connections with a 1-1/4 in. ASTM A490 bolt. The test beams were held in place with a cable winch at each beam end until a specimen was placed and bolted into the frame.

At the beginning of each test a specimen was lifted into place by the use of forklift. These column stubs would be bolted into place and proper bolt tension was determined using direct tension indicating washers. The draw wire transducers were attached to each specimen from above. The actuator was then raised into place and connected to the specimen. Finally, the protective Lexan sheet was installed.

Before each test was run, the instrumentation was verified for accuracy and strain gauges were checked to ensure they were working. The force in the load transducer was verified, ensuring a reading that was relatively low, a few hundred pounds. The strain gauges were verified to be reading accurately by noting they were all reading

approximately the same magnitude of resistance, and the resistance was changing within the margin of error. The data acquisition system was then zeroed, and testing began. Continuous loading commenced until full-stroke of the actuator was completed.

Upon completion of the test, the winches attached to the beams were tightened and the actuator pin was removed from the clevis. Observations were made and photographs were taken, therefore concluding one experimental test. The Lexan and draw wire transducers were then removed and the remaining bolts removed allowing the specimen to be taken down. This experimental procedure was repeated for each test.

This procedure was the same for both static and quasi-dynamic testing; however, the load rate for the quasi-dynamic testing was considerably faster than that of the static. The static tests were performed at a loading rate of one in. per minute. The quasi-dynamic tests were performed at a loading rate of approximately 2.7 in. per second.

Chapter 4

EXPERIMENTAL RESULTS

4.1 Experimental Results Overview

Included within this chapter are experimental results and principal measurements determined from experimental testing. Data collected for each three-, four-, and five-bolt test were applied force, strain, and vertical displacement. The collected data were then converted into shear force, axial force, moments, as well as beam end rotations and differential rotation within the column stub. Maximum bolt forces have been calculated at the point of the connection. Comparisons between static and quasi-dynamic results are included in this chapter, as well as a verification of the statics for the system.

4.2 Data Analysis Process

The following mathematical process outlines the steps taken to systematically assess the experimental data. First, strain gauge measurements at each time step were converted into stresses using Hooke's Law, evaluated as

$$\sigma_n = E * \mu^{-6} * 10^6, \quad (9)$$

where

σ_n = stress at strain gauge 'n', ksi,

E = Modulus of elasticity of steel, 29,000 ksi,

μ^{-6} = measured microstrain.

The modulus of elasticity used in these calculations was 29,000 ksi as materials testing had not been performed for the test beams.

To calculate axial force and moment in the beam at the point of the strain gages, stress at two equidistant strain gauges were used. These gauges were located at the top and bottom flange of the wide flange, strain gauges 0 and 6 on the right beam and 7 and 13 on the left beam. During test D4ST2, strain gauge 13 on the bottom side of the left beam, was not working correctly. Due to this inconsistency, the top-most and bottom-most strain gauges on the web, strain gauges 8 and 12, were used. By solving the stress equation for axial force and moment,

$$\begin{Bmatrix} P \\ M \end{Bmatrix} = \begin{bmatrix} \frac{1}{A} & \frac{-y_t}{I_x} \\ \frac{1}{A} & \frac{-y_b}{I_x} \end{bmatrix}^{-1} \times \begin{Bmatrix} \sigma_{n1} \\ \sigma_{n2} \end{Bmatrix}, \tag{10}$$

where

A = Cross sectional area of a W18×35 equal to 10.3 in.^{2},

σ_n = Stress at given strain gauge ‘n’, ksi,

I_x = Strong axis moment of inertia of a W18×35, equal to 510 in.^{4},

P = Axial force, kips,

M = Moment, kip-in.,

y_t = distance to top location of strain gauge from neutral axis, in.,

y_b = distance to bottom location of strain gauge from neutral axis, in.

The data determined using Equation (10) is valid at the strain gauge location on the beam. However, the forces and moments need to be determined at the point of connection. The measured axial force at the strain gage location and the bolt line are assumed to be equivalent, assuming the axial force is acting along the centroidal line of

the beam. The flexure at the point of connection was determined by using a linear moment distribution,

$$M_c = \frac{Mx_b}{x_{sg}}, \tag{11}$$

where

M_c = moment at the bolt line, kip-in.,

M = moment at the strain gage location, kip-in. per Equation (10),

x_{sg} = horizontal distance from the true pin connection to the strain gage location, equal to 36.125 in.,

x_b = horizontal distance from the true pin connection to the bolt line of the tested connection, equal to 78.38 in.

The beam end rotation was calculated using trigonometry. By using vertical displacement data measured by the draw wire transducers for each side of the beam, the beam end rotation was found by

$$\theta_n = \tan^{-1}\frac{\Delta_n}{x_b}, \tag{12}$$

where

x_b = horizontal distance from the true pin connection to the bolt line of the tested connection, equal to 78.38 in.,

θ_n = beam end rotation at time step ‘n’, radians,

Δ_n= vertical deflection measured by DWT at time step ‘n’, in.

4.3 Experimental Results

The experimental results in this section for the eleven experimental tests have been determined using the processes outlined in Section 4.2.

4.3.1 Three-Bolt Tests

The three-bolt tests included one statically loaded test with a loading rate of one in. per minute, and two dynamically loaded tests with a loading rate of 2.65 in. per second on average. Each test in the three-bolt group had two bolt ruptures.

All three-bolt tests were conducted with ASTM A325 carbon steel bolts. These bolts underwent different bearing locations as the connection was subjected to axial and moment in the beam seen in Figure 4.1.

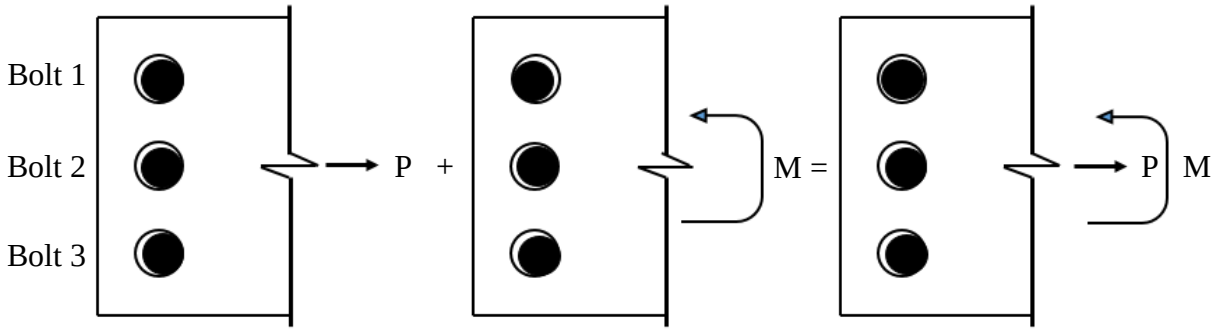

Figure 4.1: Three-Bolt Bearing Pattern.

4.3.1.1 Test S3ST1

Test S3ST1 was a statically loaded test. The test underwent full stroke of the actuator, a full ten in. The failure mechanism for test S3ST1 was bolt shear rupture. This occurred at the locations of the middle and bottom bolt, L2 and L3, on the left side of the specimen. The comparison of the specimen before and after experimental testing can be seen in Figures 4.2(a) and (b).

Figure 4.3 shows the post-test condition of the test specimen. The L2 and L3 bolt holes show noticeable deformation of the holes and at the plate edge perpendicular to the flange. It is also evident that the top bolt on the left side has markings to the right of the hole consistent with the presence of a force couple at the connection. When looking at the

right side of the test specimen, Figure 4.3 (b), there is deformation at the bottom, R3, bolt hole. All other holes do not show the same noticeable elongation on the right side of the specimen. Figure 4.4 shows the post-test condition of the bolts. The figure shows bolts L2 and L3, which sheared, as well as R3, the bottom bolt, which was approaching shear rupture and shows significant deformation.

The forces and moment in the connection versus rotation can be seen in Figures 4.5 and 4.6. The connection resisted forces and moment through flexural resistance up to approximately 0.04 radians of rotation, at which time moment plateaued and catenary action engaged. This is evident by the increase in axial force in the connection. Axial force continued to rise as the test continued until approximately 0.1 radians. At this point, the first bolt ruptured. At this point the axial force and moment in the connection dropped. The axial force began accumulating again until the second bolt failure, at approximately 0.125 radians, when the axial force decreased dramatically. Moment, on the other hand, reversed after the first bolt fractured. At the point of second bolt failure, the moment magnitude dropped.

(a) (b)

Figure 4.2: Test S3ST1 Specimen Comparison.
a) Pre-test. b) Post-test.

(a) (b)

Figure 4.3: Test S3ST1 Connection Specimen Post-Test Condition.
a) Left Side of Test Specimen. b) Right Side of Test Specimen.

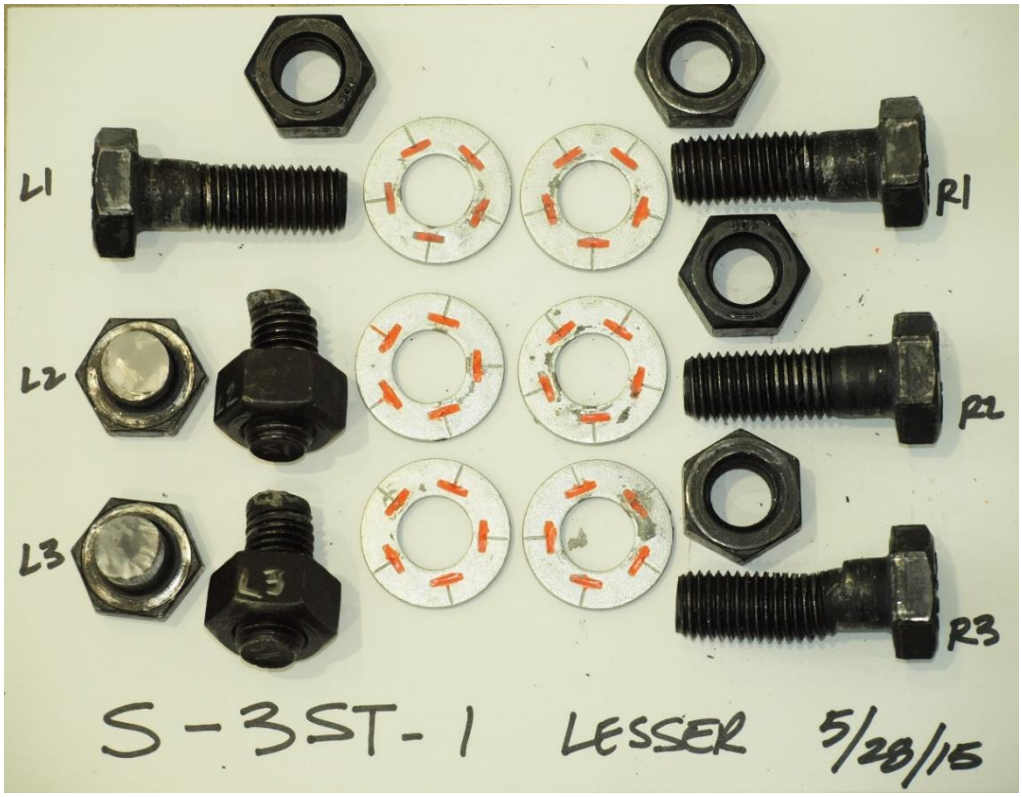

Figure 4.4: Test S3ST1 Test Bolts.

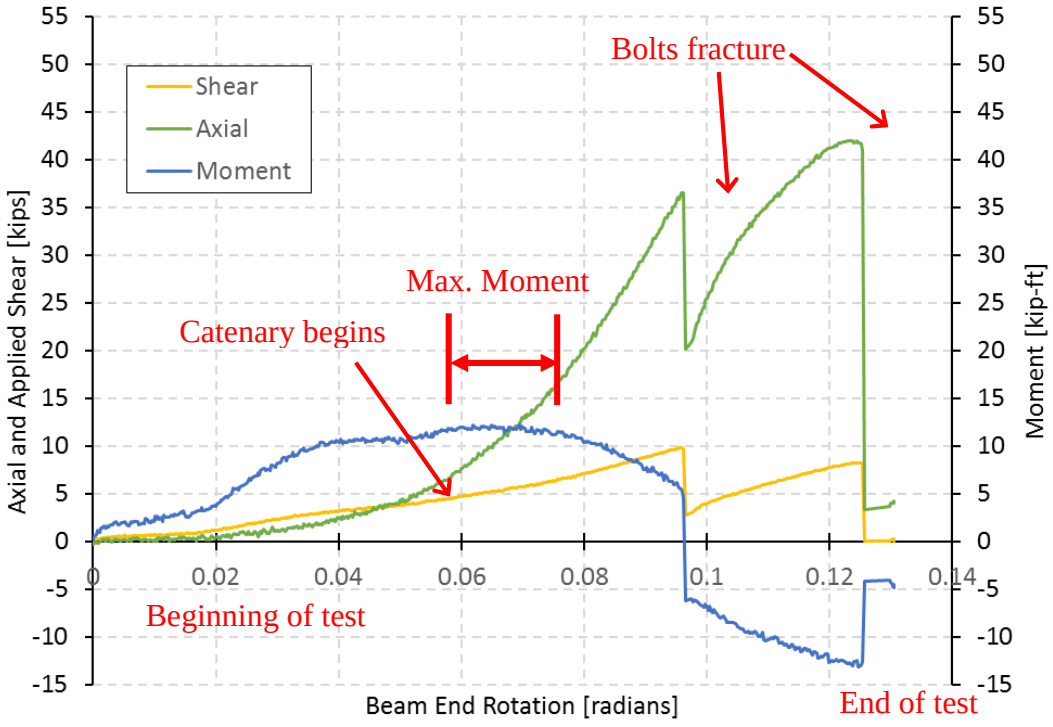

Figure 4.5: Specimen S3ST1 Left Side Bolt Line Forces versus Beam End Rotation.

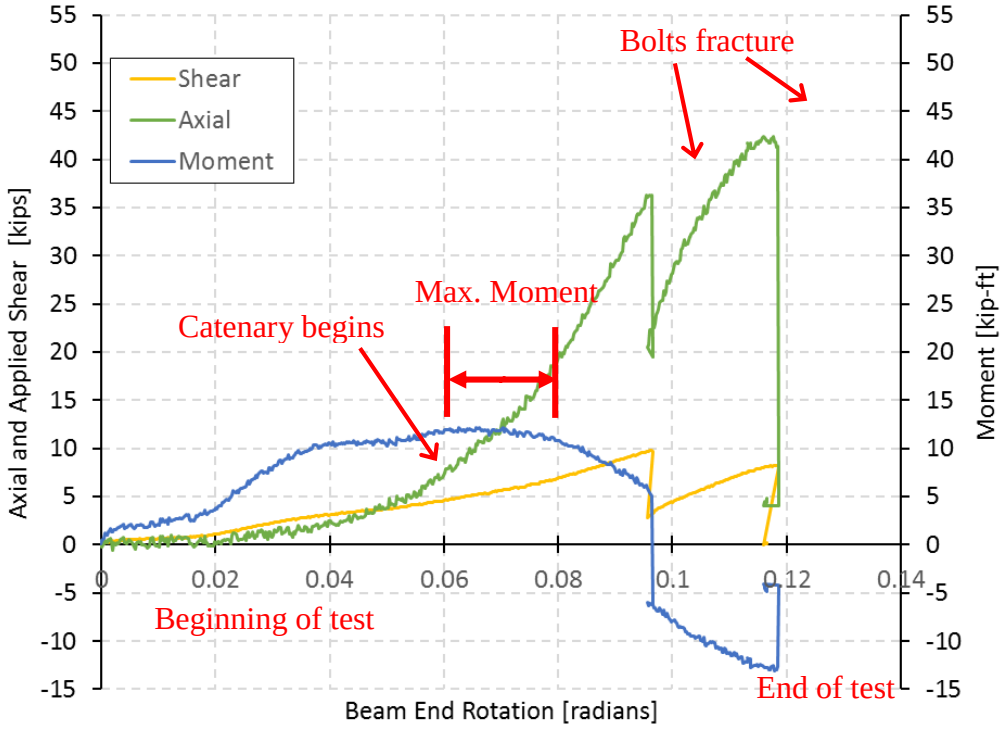

Figure 4.6: Specimen S3ST1 Right Side Bolt Line Forces versus Beam End Rotation.

4.3.1.2 Test D3ST2

Test D3ST2 was the first dynamically loaded three-bolt test. The load rate for this test was 2.67 in. per second. The test underwent a full stroke of the actuator, ten full in. The failure mechanism for test D3ST1 was bolt shear rupture of the middle and bottom bolts, L2 and L3, on the left side of the test specimen. The pre- and post-test configurations can be seen in Figures 4.7 (a) and (b), respectively.

This test showed deformation at the plate, but not as significant as S3ST1. Shown in Figure 4.8 (a), the L2 and L3 bolt holes have deformation perpendicular to the flange. The right side of the specimen had modest deformation of the bottom, R3, bolt hole as seen in Figure 4.8 (b). Figure 4.9 shows the post-test condition of the bolts, where L2 and L3 sheared. Bolt R3 was under significant stress and was approaching the point of shear failure.

The general behavior of this test is similar to that of the S3ST1. Figures 4.10 and 4.11 show the forces and moment in the connection versus rotation. The connection resisted forces and moment through flexural resistance up to approximately 0.05 radians of rotation. This was at which point catenary action began and moment plateaued, as seen by the increase in the axial force in the system. Axial force continued to increase until the first bolt failure occurred at a rotation of 0.105 radians. The axial force and moment dropped in the connection at the point where the first bolt broke. From that point, the axial force began accumulating again until the second bolt failure, at approximately 0.125 radians, when the axial force decreased dramatically on the right side of the test specimen. As can be seen in Figure 4.10 the left side of the specimen had a drop-off of axial force at around 0.125 radians, but didn't fail until about 0.135 radians. The moment, however, followed the same pattern for both sides of the tests.

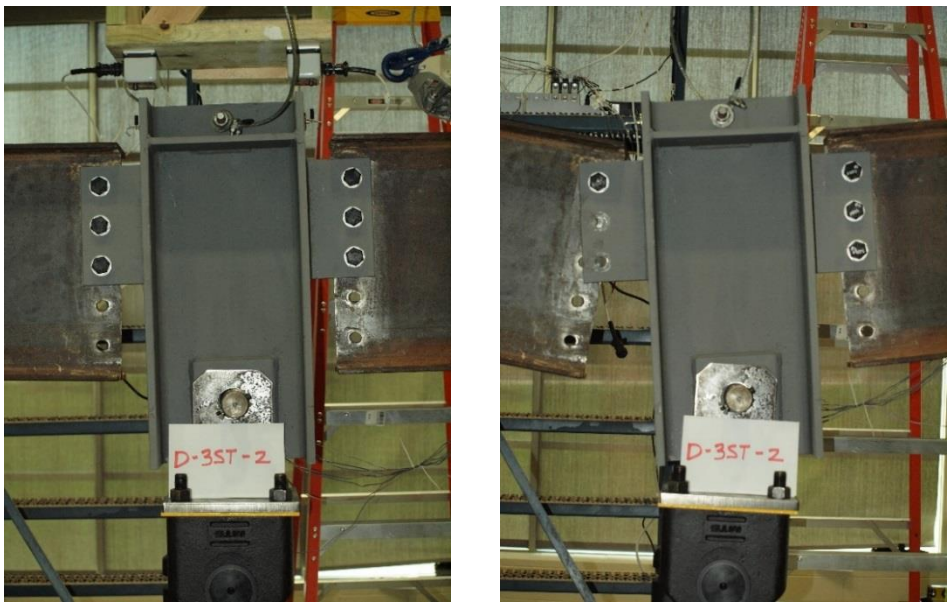

(a) (b)

Figure 4.7: Test D3ST2 Specimen Comparison.
a) Pre-test. b) Post-test.

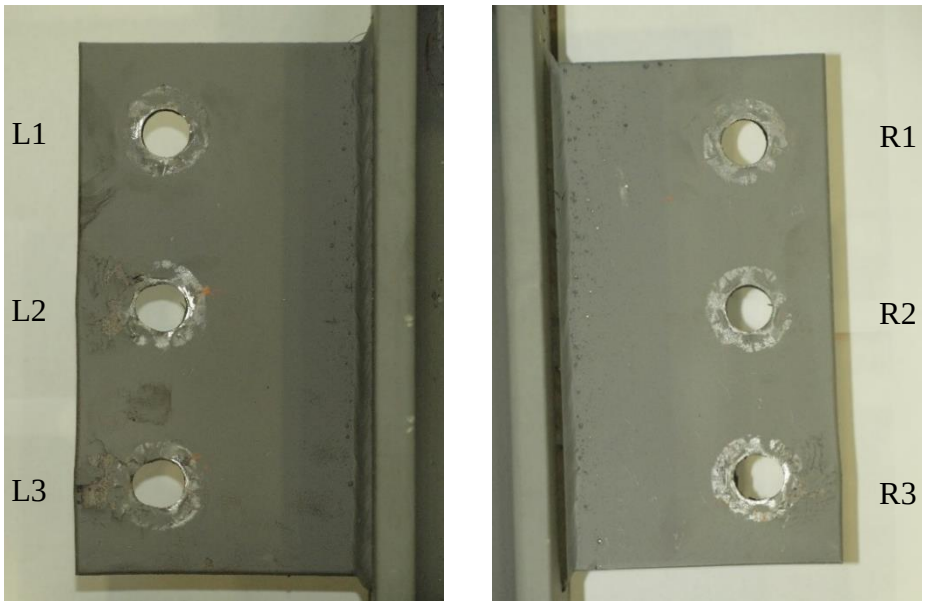

(a) (b)

Figure 4.8: Test D3ST2 Connection Specimen Post-Test Condition.
a) Left Side of Test Specimen. b) Right Side of Test Specimen.

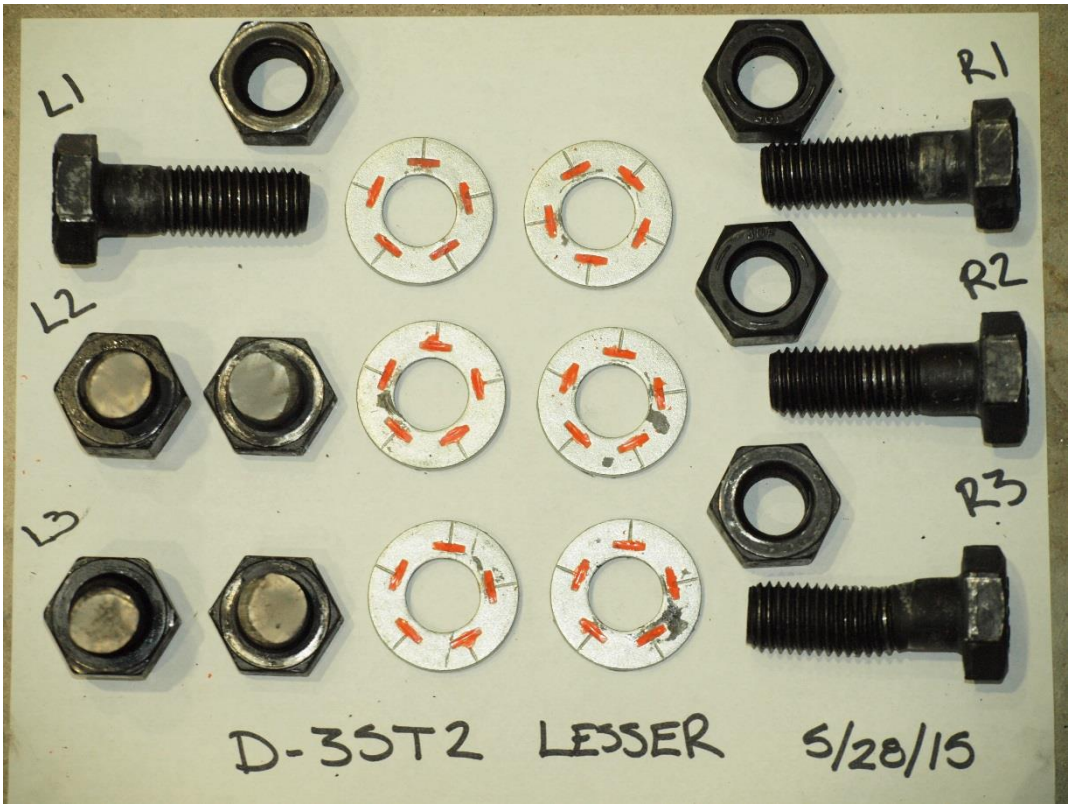

Figure 4.9: Test D3ST2 Test Bolts.

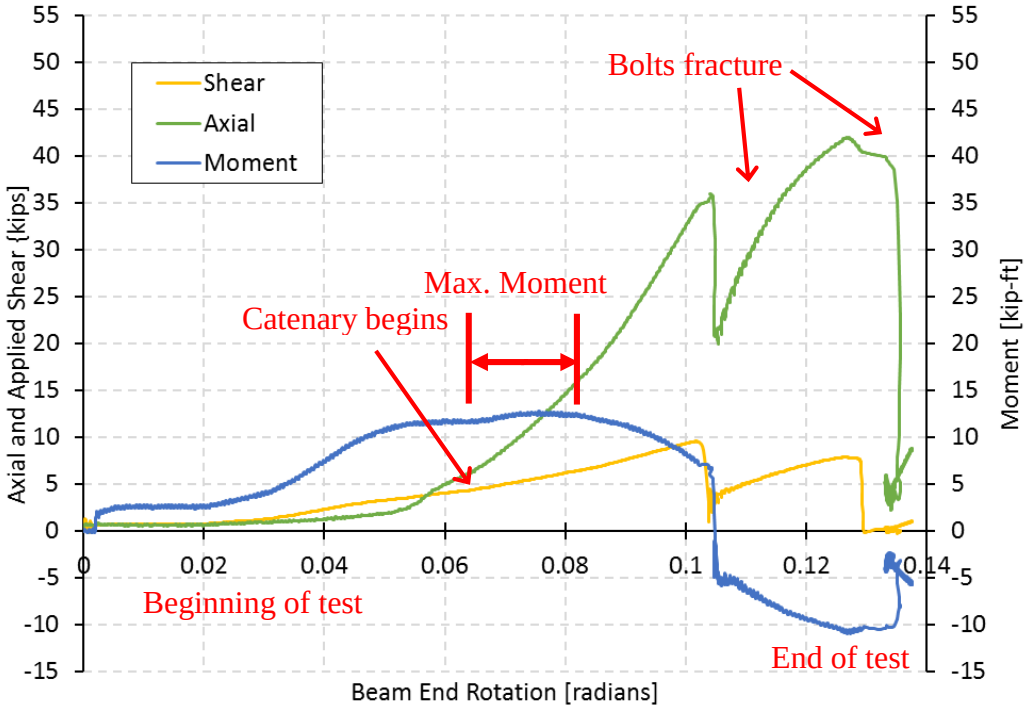

Figure 4.10: Specimen D3ST2 Left Side Bolt Line Forces versus Beam End Rotation.

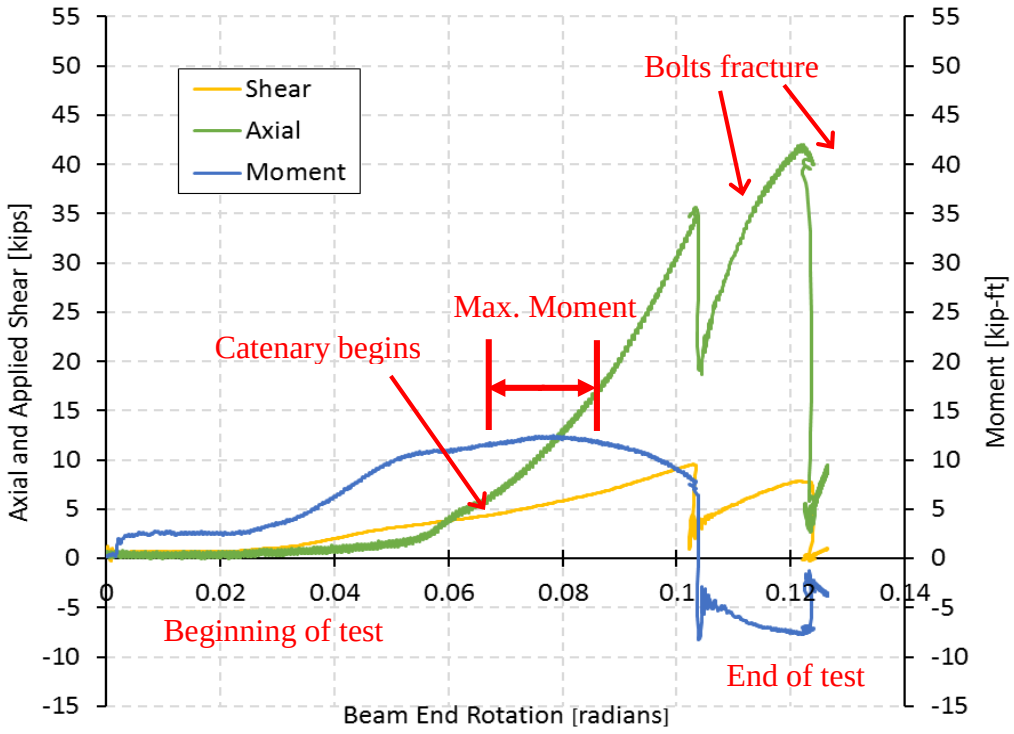

Figure 4.11: Specimen D3ST2 Right Side Bolt Line Forces versus Beam End Rotation.

4.3.1.3 Test D3ST3

Test D3ST3 was the second dynamically loaded three-bolt test. The loading rate of this test was 2.62 in. per second. This test reached the full ten in. of stroke that the actuator allowed. Test D3ST3 failed in bolt shear rupture, with the middle and bottom bolts on the left side rupturing. Figures 4.12 (a) and (b) exhibit the connection in its pre-test and post-test conditions.

Figures 4.13 (a) and (b) show the post-test specimen condition. There is noticeable plate deformation at the middle and bottom bolt holes, L2 and L3, on the left side and the bottom hole on the right side, R3. There is hole deformation clearly showing bolt bearing at the each hole relating back to Figure 4.1. Figure 4.14 shows the post-test condition of the bolts, with L2 and L3 having ruptured and R3 under significant distress. This is consistent with the condition observed for D3ST2.

The same phenomena seen in other three-bolt tests can be seen in D3ST3, as shown in Figures 4.15 and 4.16. When looking at these plots it is obvious that there are missing data. At this point in the experimental testing, it was found that the data acquisition included headers or labels for each column of data in the file for every 10,000 data points. These headers disrupted the data acquisition, skipping data. On this particular test, that occurred during the middle portion of the test, resulting in a missing portion of data. The "data gap" as it is called on the figure, was realized and resolved in subsequent tests.

Due to the missing data, the exact point where the connection's resistance changes from flexural to catenary is inconclusive. However, the axial force did apparently follow the same path, as the axial force magnitudes on each side of the data

gap are consistent with other three-bolt results. The axial force increased until a beam rotation of approximately 0.09 radians, at which point the first bolt failure occurred. At this point, the axial force and moment in the connection decreased. From that point, the axial force began accumulating again until the second bolt failure, occurring at approximately 0.13 radians on the left side and 0.115 radians on the right side. The moment, however, followed a similar pattern for both sides. The moment increased in an opposite direction until the second bolt fracture, and then fell to nearly zero magnitude.

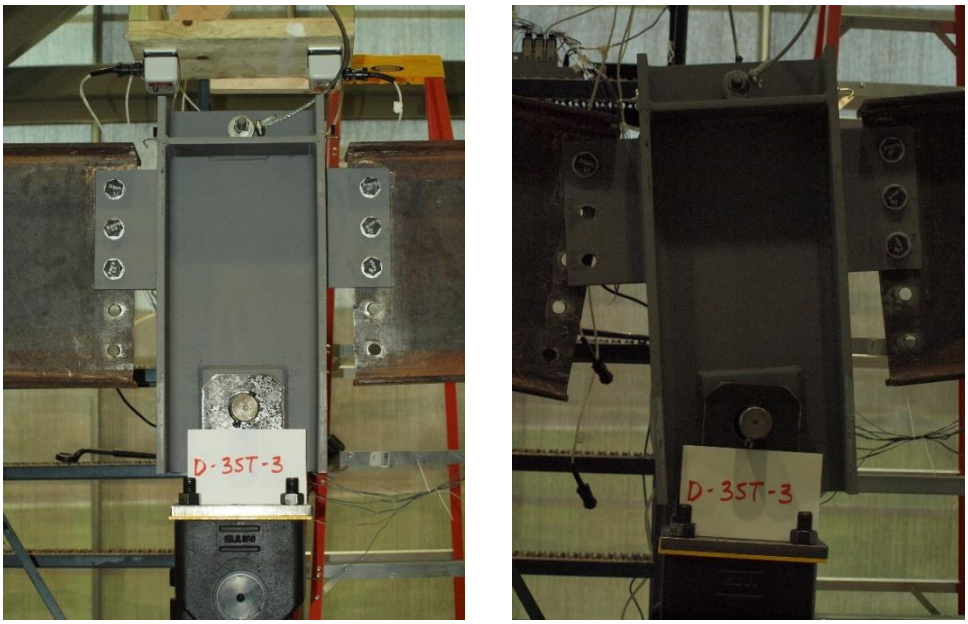

(a) (b)

Figure 4.12: Test D3ST3 Specimen Comparison.
a) Pre-test. b) Post-test.

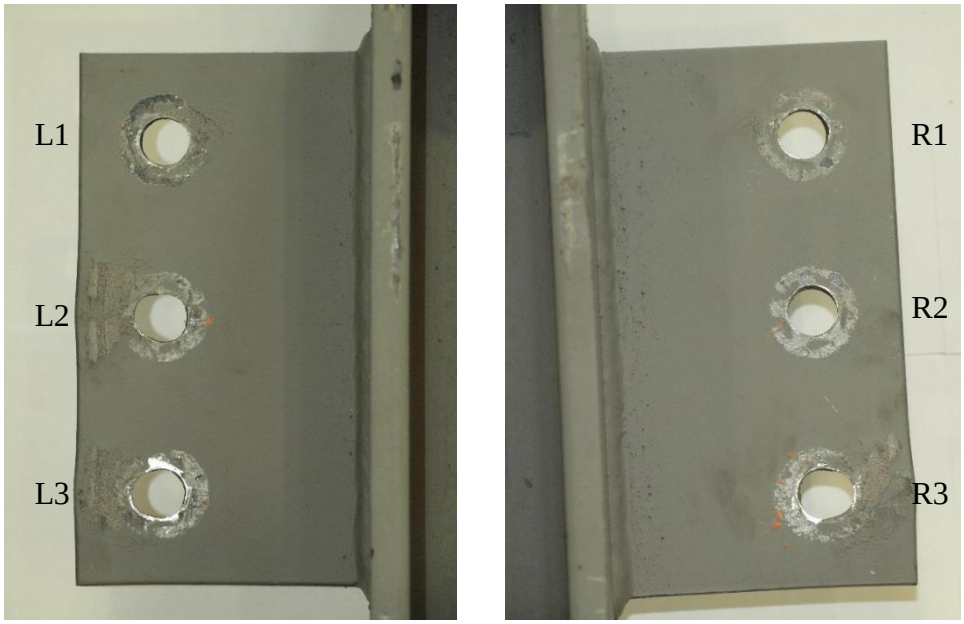

Figure 4.13: Test D3ST3 Connection Specimen Post-Test Condition.
a) Left Side of Test Specimen. b) Right Side of Test Specimen.

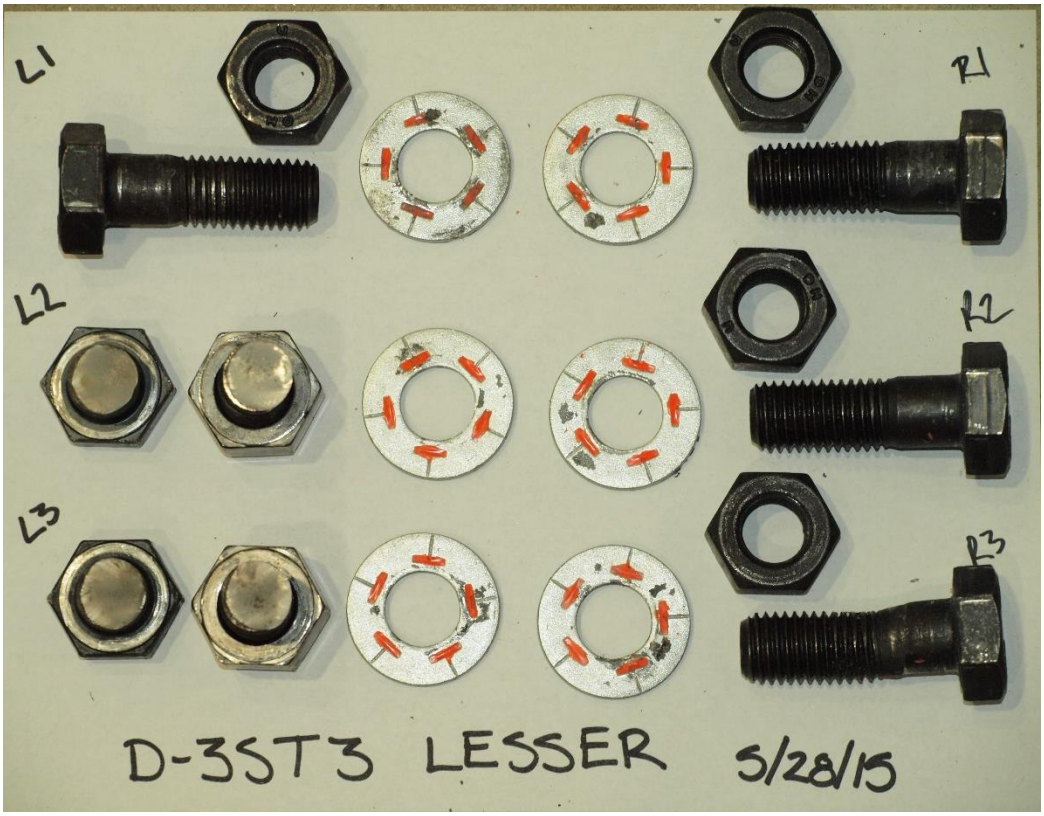

Figure 4.14: Test D3ST3 Test Bolts.

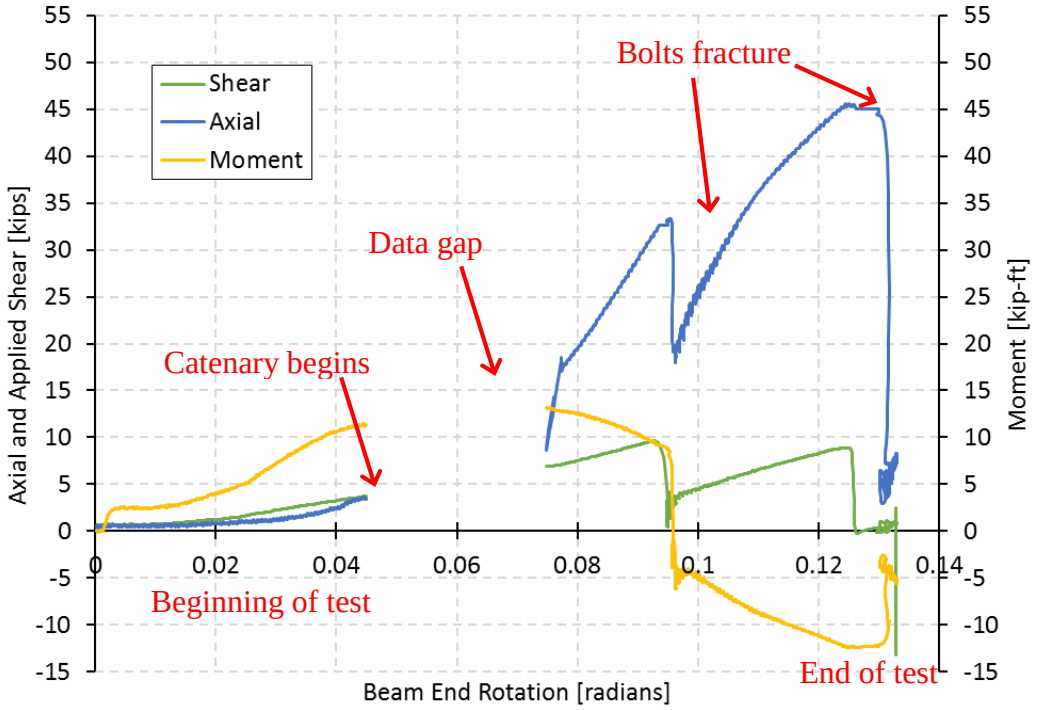

Figure 4.15: Specimen D3ST3 Left Side Bolt Line Forces versus Beam End Rotation.

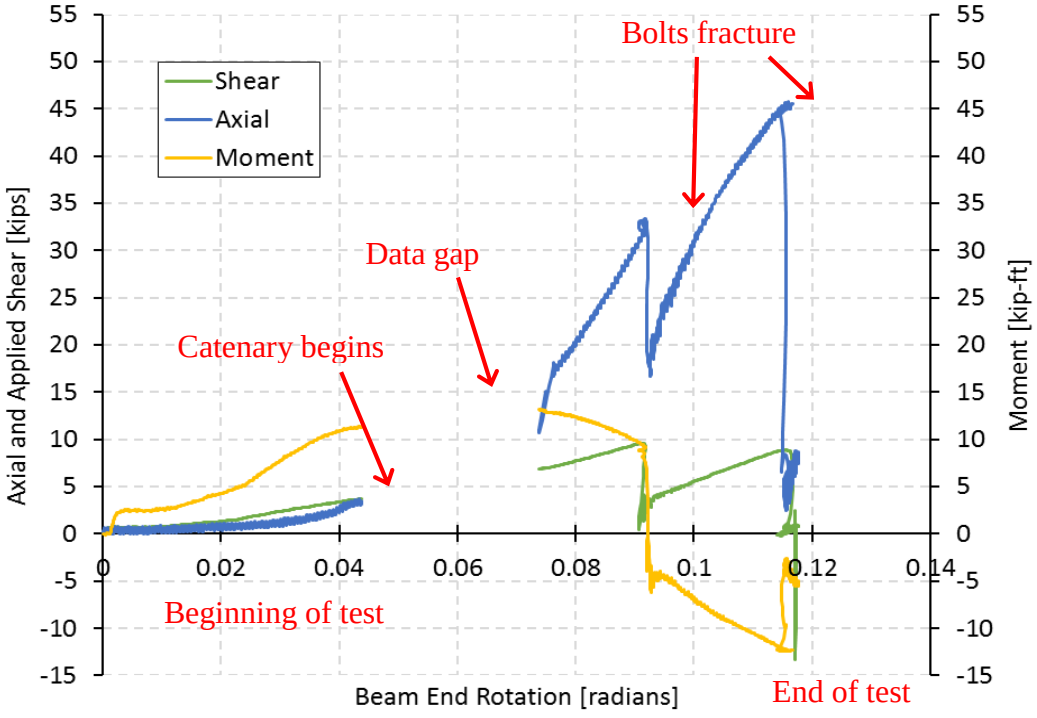

Figure 4.16: Specimen D3ST3 Right Side Bolt Line Forces versus Beam End Rotation.

4.3.1.4 Three-Bolt Summary

All three-bolt tests performed similarly in their behavior. In each case, the connection initially resisted force and moment by a flexural resistance. In each case the resistance changed to catenary as moment approached its maximum. Table 4.1 shows the axial force, shear force and beam rotation at the maximum moment. The point of maximum moment was found by taking an average of the top one percent of the moment magnitudes for the test. This ensured that the maximum moment was found as there was slight fluctuation in the data. The table shows results for only tests S3ST1 and test D3ST2. There were no data at maximum moment for test D3ST3 due to error in the data acquisition system, as discussed in Section 4.3.1.3. Without taking into account the test D3ST3, it can be seen that the bolt line forces at the maximum moment are very similar between the static and dynamic tests, only varying by at most 1.2 kips in axial force.

Table 4.1: Three-Bolt Specimen Bolt Line Forces at Maximum Moment.

Test Specimen	Side of Specimen	Shear Force [Kips]	Moment [Kip-Feet]	Axial Force [Kips]	Beam End Rotation [Radians]
S3ST1	Right	5.32	12.10	10.63	0.0661
	Left	5.30	11.91	10.44	0.0667
D3ST2	Right	5.66	12.26	11.82	0.0708
	Left	5.74	12.46	11.53	0.0736
D3ST3[a]	Right	---	---	---	---
	Left	---	---	---	---

[a] Bolt Line Forces could not be acquired due to error in data acquisition

Unlike at maximum moment, data for bolt line forces measured at initial failure was collected for all three test specimens in this bolt group. These bolt line forces can be seen in Table 4.2. The tests all follow similar trends, although the static test had higher forces and a lower moment magnitude.

Table 4.2: Three-Bolt Specimen Bolt Line Forces at Initial Bolt Failure.

Test Specimen	Side of Specimen	Shear Force [Kips]	Moment [Kip-Feet]	Axial Force [Kips]	Beam End Rotation [Radians]
S3ST1	Right	9.83	6.21	36.22	0.0961
	Left		5.60	35.86	0.0958
D3ST2	Right	9.59	9.89	31.52	0.0866
	Left		9.42	31.99	0.0852
D3ST3	Right	9.60	9.95	31.40	0.0865
	Left		9.52	31.85	0.0851

Each test had a second bolt rupture. This confirms that the connection has innate robustness allowing the connection to sustain load after initial failure. Table 4.3 outlines the bolt line forces at the point of second bolt failure. Both S3ST1 and D3ST3 have similar magnitudes while D3ST2 has slightly lower values. Figure 4.10 shows at second bolt failure that there was slight decrease of axial force followed by increase until final bolt shear rupture. This inconsistency is responsible for lower value of shear force present in test D3ST2.

Table 4.3: Three-Bolt Specimen Bolt Line Forces at Secondary Bolt Failure.

Test Specimen	Side of Specimen	Shear Force [Kips]	Moment [Kip-Feet]	Axial Force [Kips]	Beam End Rotation [Radians]
S3ST1	Right	8.25	-8.94	42.15	0.117
	Left		-12.60	41.90	0.124
D3ST2	Right	7.85	-7.55	41.46	0.121
	Left		-10.79	41.87	0.126
D3ST3	Right	8.86	-7.83	45.71	0.115
	Left		-12.20	45.44	0.124

4.3.2 Four-Bolt Tests

The four-bolt tests included one statically loaded test with a loading rate of one in. per minute and three dynamically loaded tests with loading rates of 2.71 in. per second on average. Each of the four tests resulted in three bolt ruptures.

Tests S4ST1, D4ST2, and D4ST3 used ASTM A325 carbon steel bolts. D4ST4 used galvanized ASTM A325 bolts. Bolt bearing within each bolt hole can be seen in Figure 4.17.

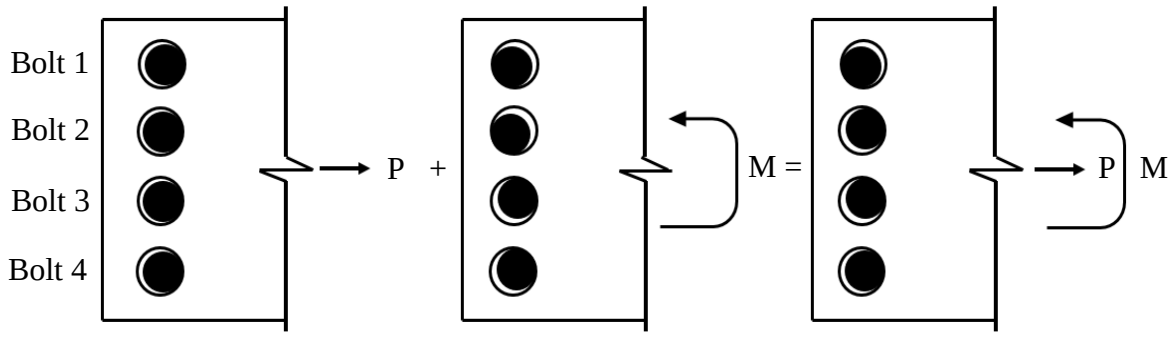

Figure 4.17: Four Bolt-Bearing Pattern.

4.3.2.1 Test S4ST1

Test S4ST1 was a statically loaded test. The test underwent full stroke of the actuator, ten in. The failure mechanism for test S4ST1 was bolt shear rupture on the right side. The bottom three bolts on the right side of the specimen ruptured. Figures 4.18 (a) and (b) show the pre-test and post-test configuration.

Figures 4.19 (a) and (b) show each shear tab in their post-test conditions. The right side, where bolt rupture occurred, shows significant deformation in the bottom bolt hole, R4, while less pronounced deformations occurred at the middle two holes, R2 and R3. On the left side, modest deformation occurred at the L4 bolt hole. The plate edge had noticeable deformation of the holes perpendicular to the flange on the right side. The left side had minor plate edge deformation located at L4. The post-test condition of the bolts is shown in Figure 4.20. Bolt L4 does not show the same level of distress as seen in the three-bolt tests.

Figures 4.21 and 4.22 show the connections gaining flexural and tensile forces simultaneously, with the flexural forces immediately rising and beginning to plateau prior to the initial bolt fracture. The tensile forces increase slowly until about 0.02 radians and then rapidly increase as catenary action begins up to the point of bolt rupture. After the first bolt break, axial force and moment both decrease significantly. After bolt failure, axial force and moment continue to increase until the second bolt break. After this, moment reverses and drops in magnitude while axial forces accrue again. After the third bolt breaks, axial force, shear and moment all drop to near-zero magnitudes.

(a) (b)

Figure 4.18: Test S4ST1 Specimen Comparison.
a) Pre-test. b) Post-test.

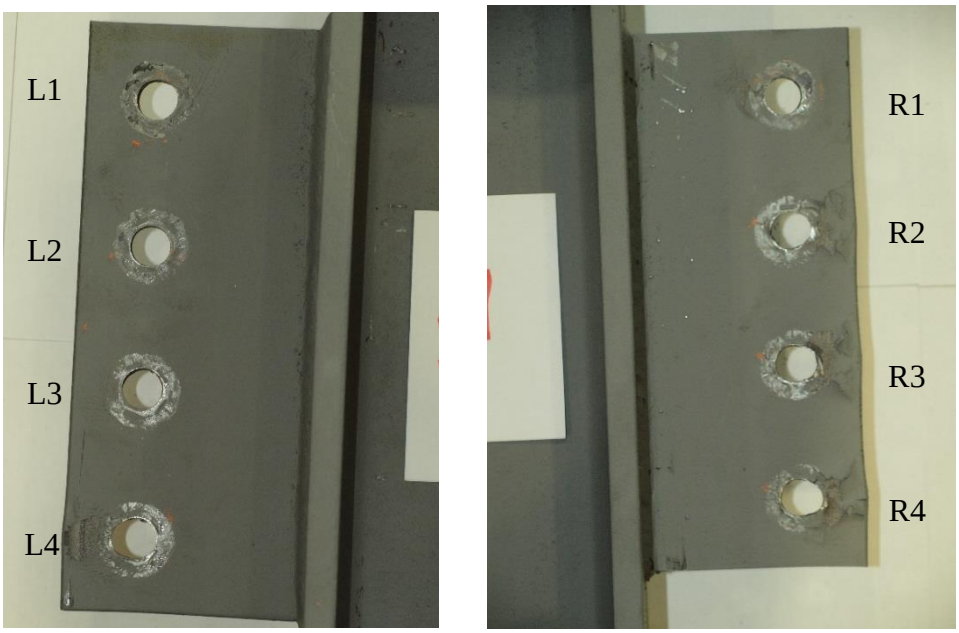

(a) (b)

Figure 4.19: Test S4ST1 Connection Specimen Post-Test Condition.
a) Left Side of Test Specimen. b) Right Side of Test Specimen.

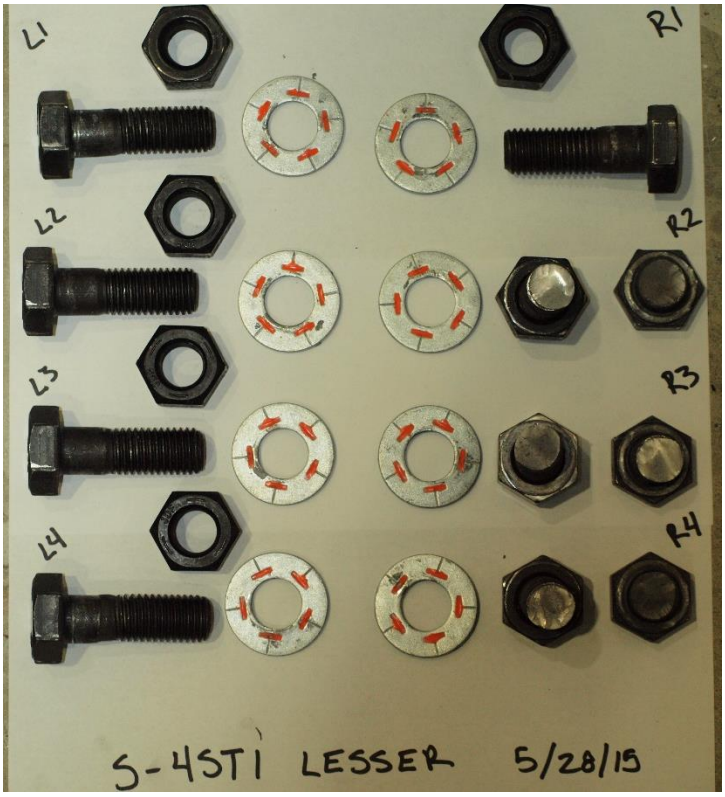

Figure 4.20: Test S4ST1 Test Bolts.

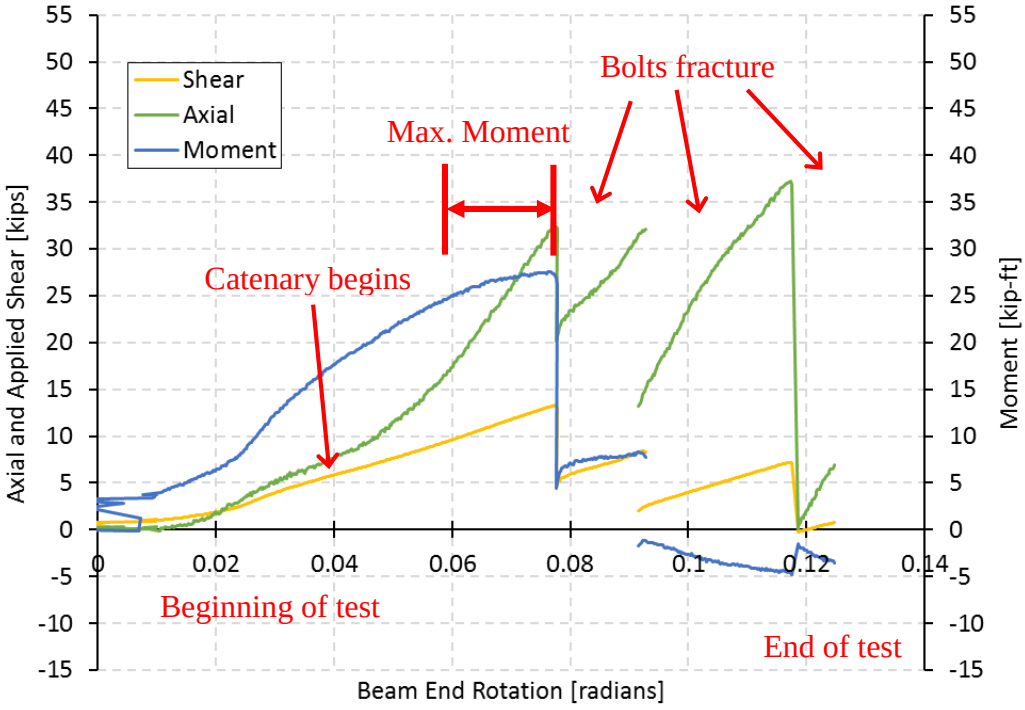

Figure 4.21: Specimen S4ST1 Left Side Bolt Line Forces versus Beam End Rotation.

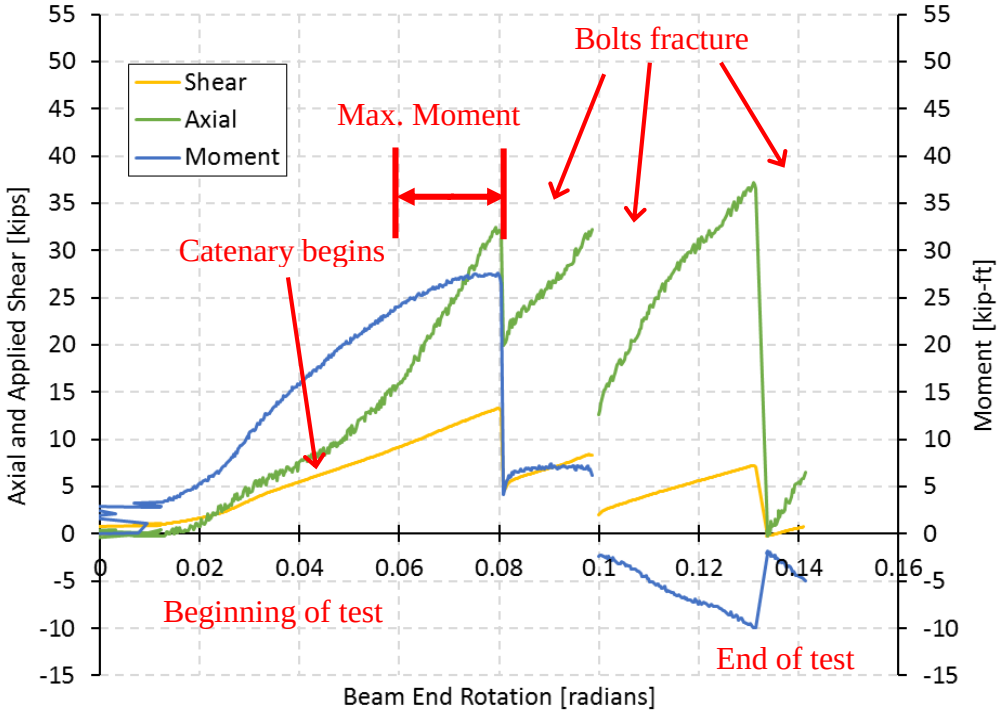

Figure 4.22: Specimen S4ST1 Right Side Bolt Line Forces versus Beam End Rotation.

4.3.2.2 Test D4ST2

Test S4ST1 was a dynamically loaded test. The loading rate was 2.62 in. per second. The test underwent full stroke of the actuator, ten in. Test D4ST2 had bolt shear rupture on the left side as its failure mechanism. Bolts L2, L3, and L4 ruptured on that side. Figures 4.23 (a) and (b) show the connections pre-test and post-test, respectively.

D4ST2 exhibited less plate deformation than seen in prior tests, as shown in Figure 4.24 (a) and (b). There was, however, noticeable stress marks on the bolt holes consistent with those made from a force couple. The post-test condition of the bolts in this test are shown in Figure 4.25. The bottom three bolts on the left side (L2, L3, and L4) have sheared, as well as bolt R4 showing considerable deformation. The washer for L2 was not found after testing.

The general behavior of D4ST2 was very similar to that of S4ST1. Both moment and axial force accrued until connection failure; however, at the first bolt break, the moment hits a maximum and drops dramatically due to the fracture of the bolt. Figures 4.26 and 4.27 show this behavior. The moment plateaus at approximately 11 kip-feet prior to the second bolt break. Axial force, on the other hand, doesn't begin to accrue significantly until about 0.01 radians, and then begins to increase rapidly until initial bolt rupture. This trend signifies that catenary action is in effect from approximately 0.01 radians through the first bolt break. Axial force drops after the first bolt breaks, and begins to accrue up to the point of the second bolt fracture. The trend is similar between the second and third bolt fractures. It can be seen that axial force reaches magnitudes consistently between 30 and 35 kips at the point of bolt fractures, which is an interesting trend.

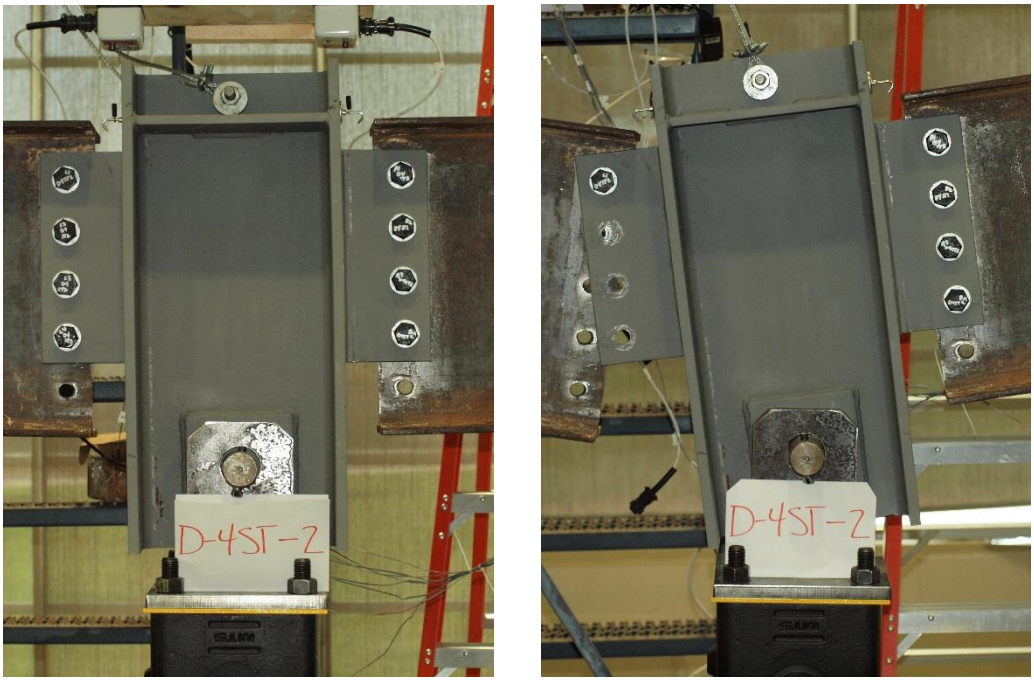

(a) (b)

Figure 4.23: Test D4ST2 Specimen Comparison.
a) Pre-test. b) Post-test.

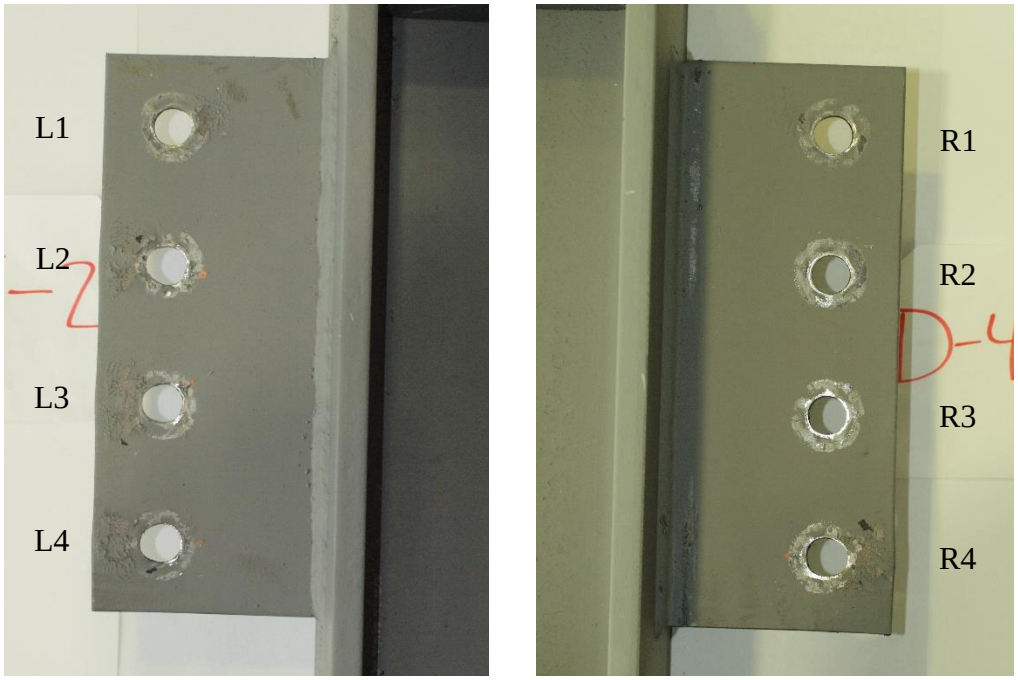

(a) (b)

Figure 4.24: Test D4ST2 Connection Specimen Post-Test Condition.
a) Left Side of Test Specimen. b) Right Side of Test Specimen.

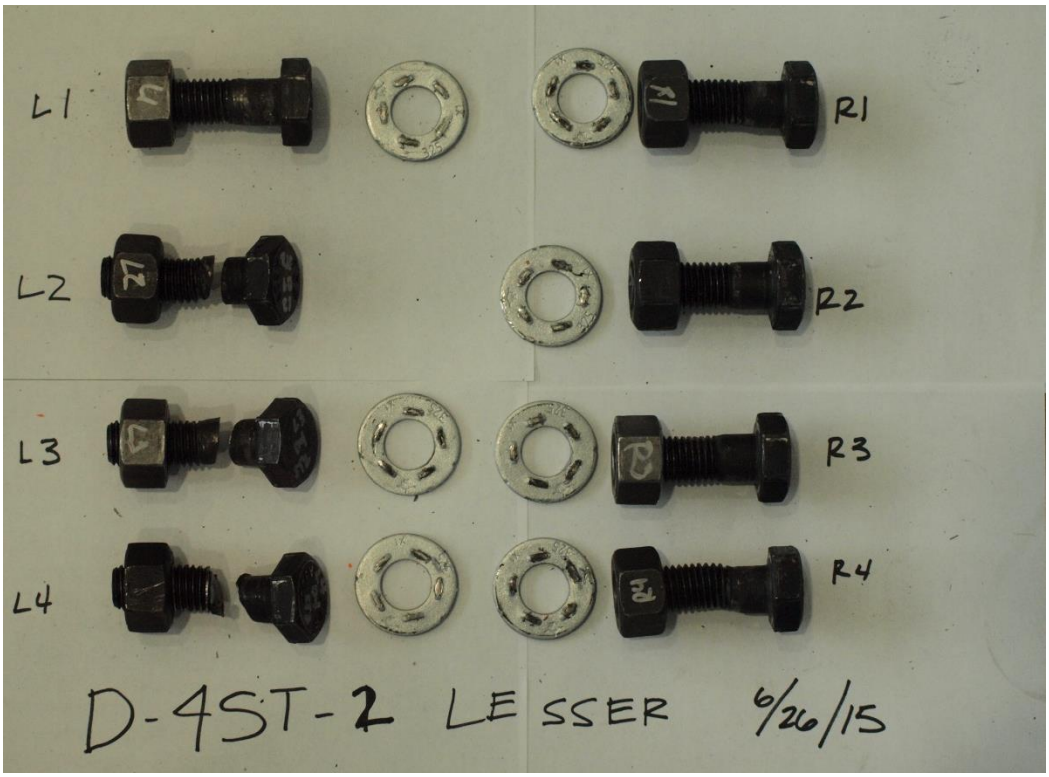

Figure 4.25: Test D4ST2 Test Bolts.

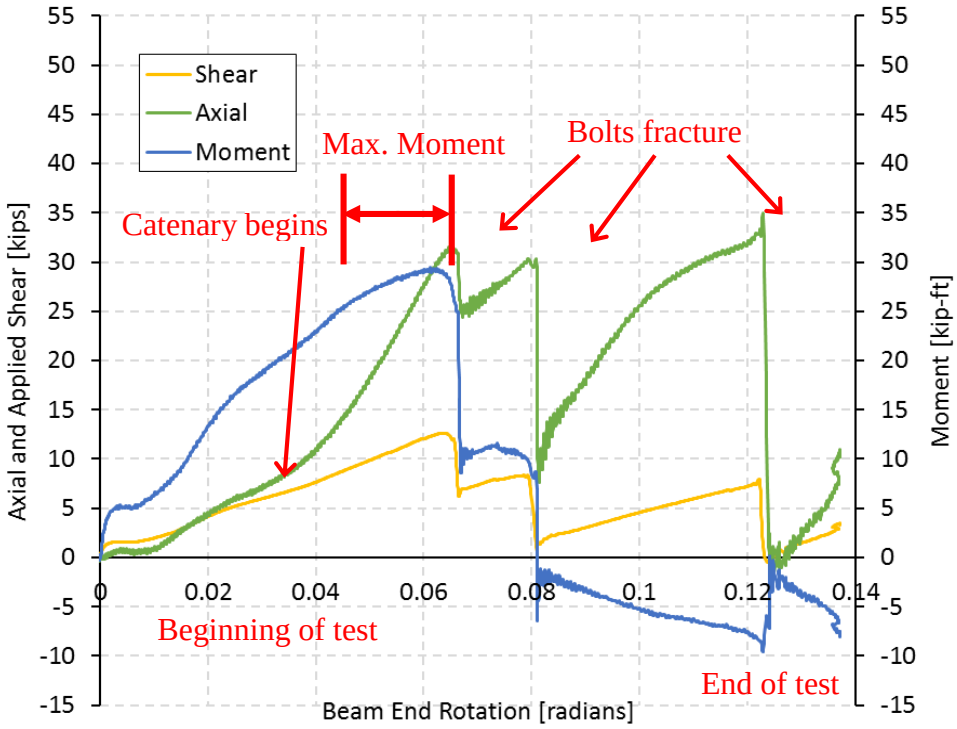

Figure 4.26: Specimen D4ST2 Left Side Bolt Line Forces versus Beam End Rotation.

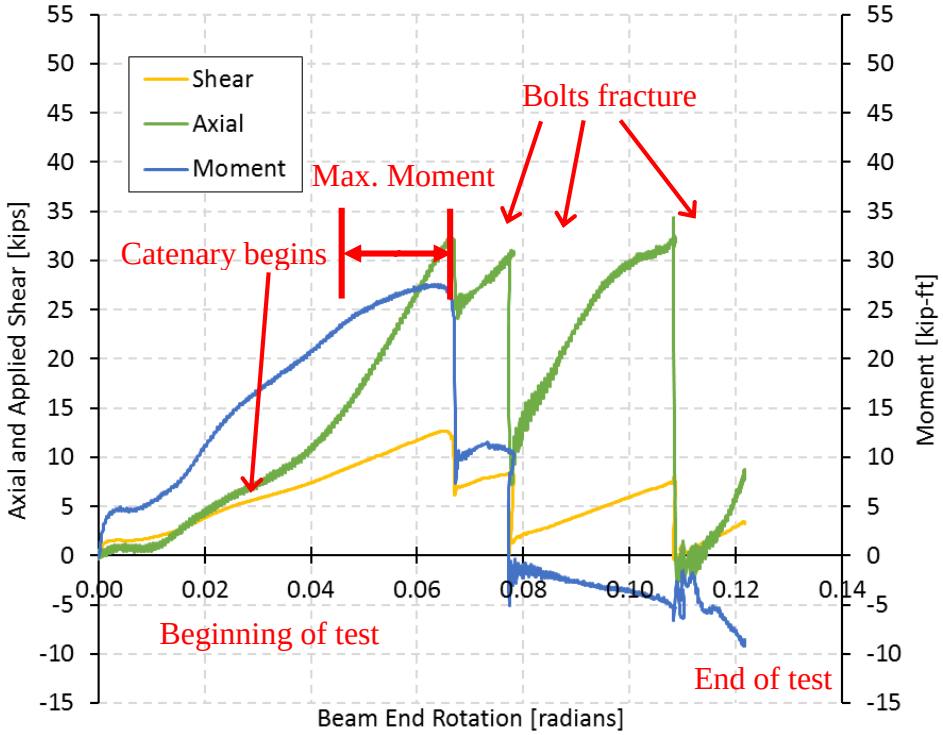

Figure 4.27: Specimen D4ST2 Right Side Bolt Line Forces versus Beam End Rotation.

4.3.2.3 Test D4ST3

D4ST3 was a dynamically loaded test. The test underwent full stroke of the actuator, 10 in. The loading rate of this test was 2.8 in. per second. Figures 4.28 (a) and (b) show the pre-test and post-test configuration. The connection failure was due to bolt shear rupture on the right side of the specimen. Again, the bottom three (R2, R3, and R4) bolts failed.

Figure 4.29 shows the bottom bolt hole on the right side (R4) having elongation parallel to the line of action of the axial force. The edge of the plate has deformed in the same direction, indicating significant force magnitude due to combined axial force and moment at this bolt. Other bolt holes show less deformation, but still show evidence of stress around the perimeter of the hole. The top bolt holes (R1 and L1) show evidence of force acting toward the W12 column stub, as is expected due to the direction of the force due to moment resistance. Figure 4.30 shows the bolts in their post-test configuration. The bottom three bolts the right side, R2, R3, and R4, have ruptured. The bottom bolt on the left side, L4, shows deformation due to shear force, as do the top bolts, R1 and L1.

When looking at Figures 4.31 and 4.32, one can see that at the beginning of the test the axial, shear, and moment all begin at an elevated magnitude at approximately 0.03 radians. This was due to the same data acquisition error noted in test D3ST3, except this error occurred at the beginning for test D4ST3. After the acquisition error, data continued to be collected, allowing the comparison of forces beyond 0.03 radians. The moment accrued until about 28 kip-feet, where it plateaued and the initial bolt broke. The axial force increased rapidly until initial bolt break, reaching about 36 kips. The initial failure dropped the forces and moments present in the connection. The axial load began

to rise again while moment remained at a low magnitude and plateaued before decreasing at the second bolt failure. The forces once again dropped at the second bolt failure. The shear and axial force increased again after the second bolt break, while moment remained at a low magnitude and switched direction. A third bolt break occurred, dropping the force magnitudes once again. The shear and axial forces increased and moment slightly increased in magnitude until test completion.

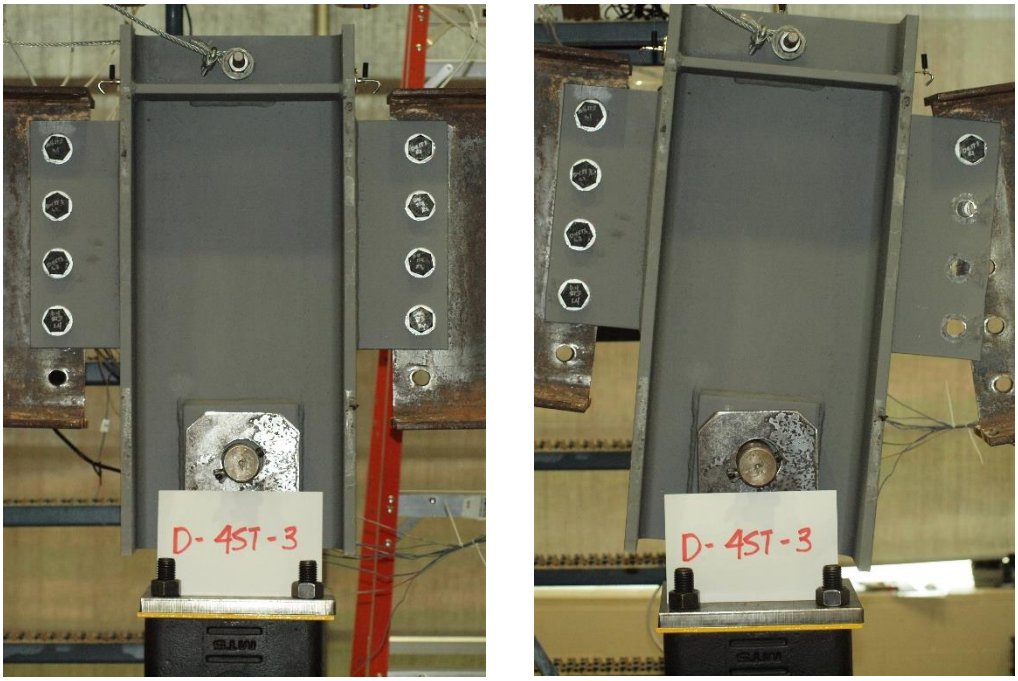

(a) (b)

Figure 4.28: Test D4ST3 Specimen Comparison.
a) Pre-test. b) Post-test.

(a) (b)

Figure 4.29: Test D4ST3 Connection Specimen Post-Test Condition.
a) Left Side of Test Specimen. b) Right Side of Test Specimen.

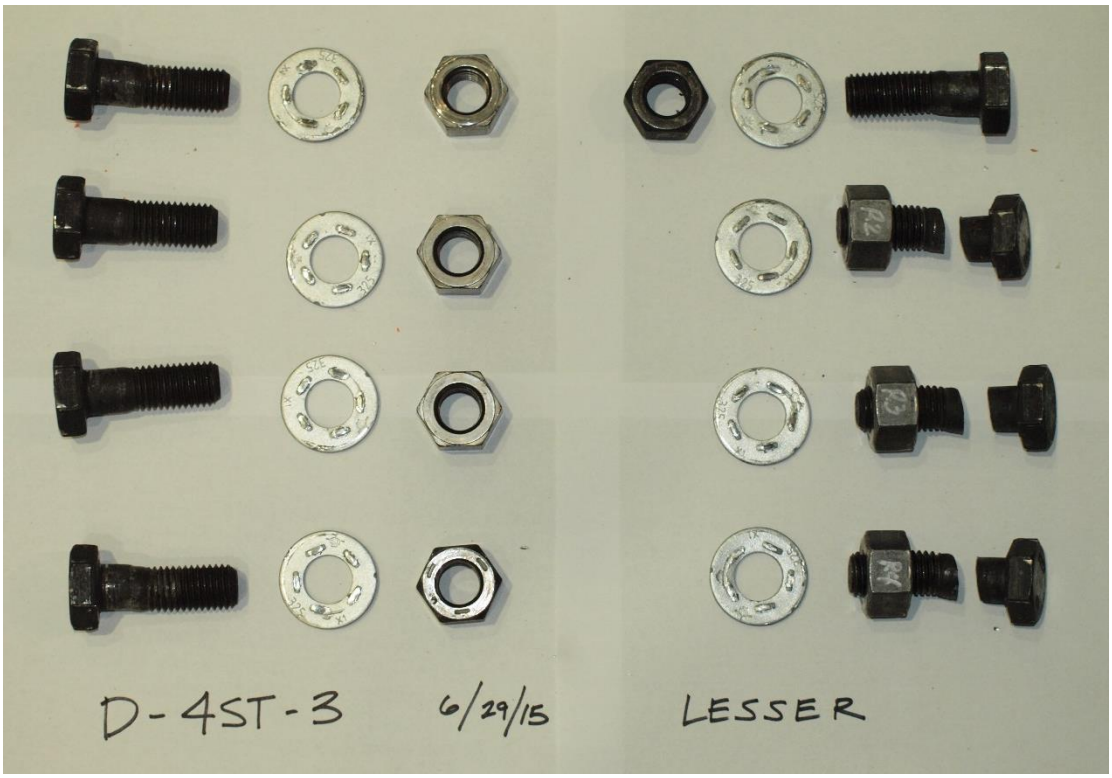

Figure 4.30: Test D4ST3 Test Bolts.

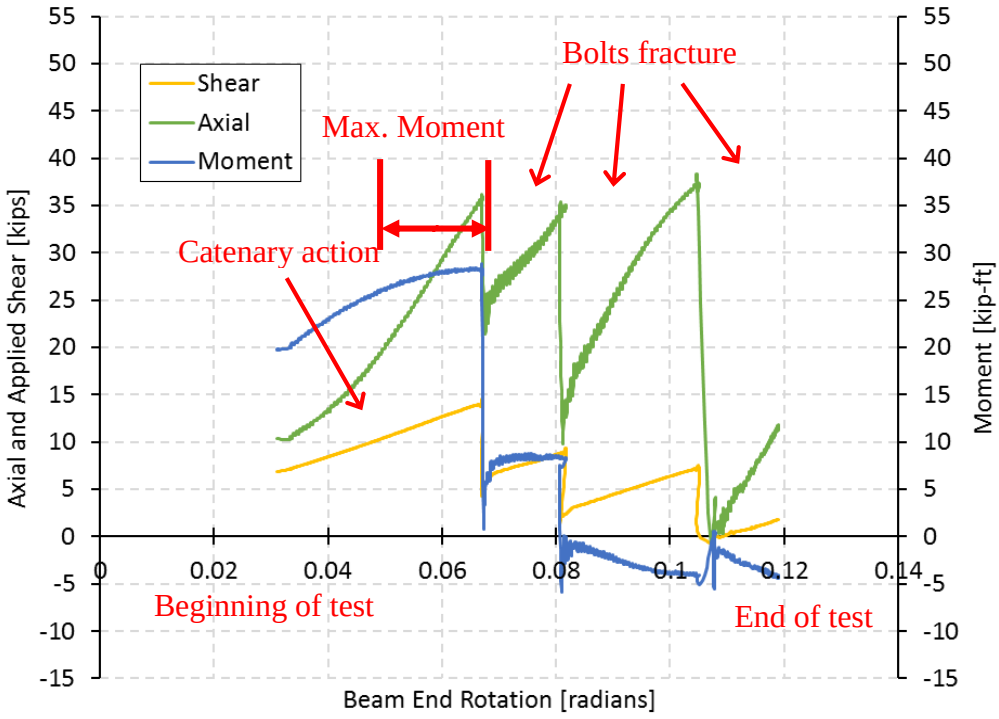

Figure 4.31: Specimen D4ST3 Left Side Bolt Line Forces versus Beam End Rotation.

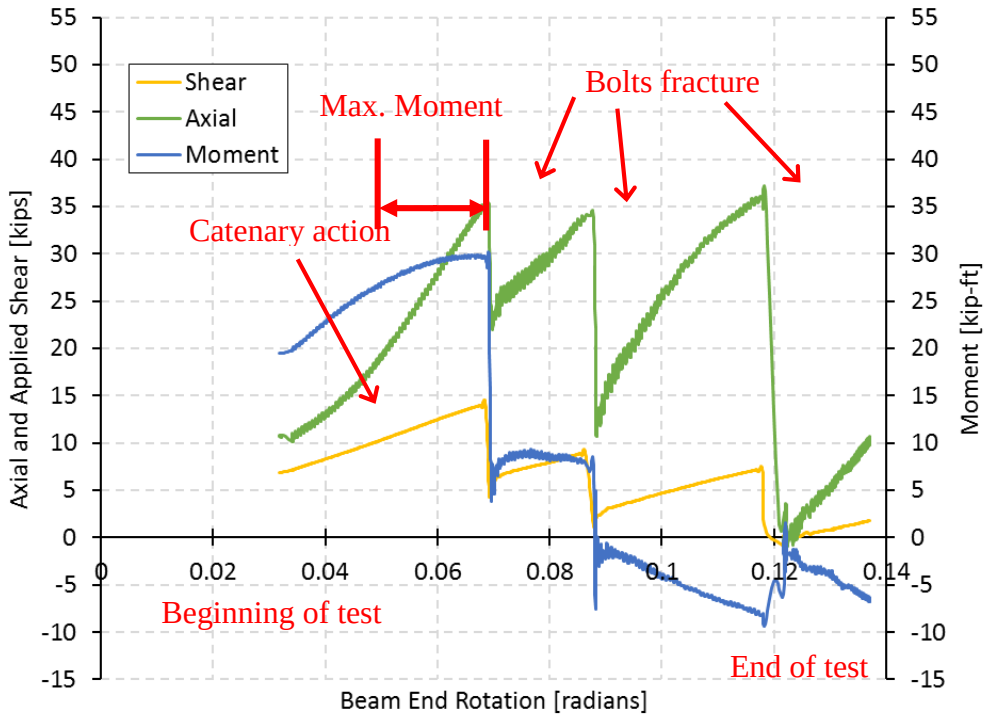

Figure 4.32: Specimen D4ST3 Right Side Bolt Line Forces versus Beam End Rotation.

4.3.2.4 Test D4ST4

D4ST4 was a dynamically loaded test that underwent a full ten in. of stroke. The loading rate was 2.62 in. per second. Test D4ST4 used galvanized bolts. Galvanized bolts were used because the test was part of a secondary round of experiments, and a second lot of bolts was purchased at a later date. Galvanized bolts were delivered instead of carbon bolts, and the decision was made to move forward with the testing using the galvanized bolts. This specimen's failure mechanism was bolt shear rupture of bolts R2, R3, and R4 on the right side. Figures 4.33 (a) and (b) show the specimen pre-test and post-test.

There was minimal deformation located on any of the bolt holes as shown in Figures 4.34 (a) and (b). There are noticeable stress marks located around the bolt holes indicating a force couple. The post-test condition of the bolts can be seen in Figure 4.35. R2, R3, and R4 have sheared. Bolt L4 has deformed due to shear. Other bolts (L2 and L3) do not show as much deformation.

Figures 4.36 and 4.37 show the forces and moment versus rotation for D4ST4. Although the same trends as the previous dynamic tests are present in D4ST4, there is a noticeable shift in the rotations and forces. The moment was comparable to previous tests, while the axial force was more than 10 kips less at initial bolt break. The first bolt break in D4ST4 occurred 0.02 radians sooner than the previous four-bolt dynamic tests. These differences are attributed to the use of the galvanized bolts.

(a) (b)

Figure 4.33: Test D4ST4 Specimen Comparison.
a) Pre-test. b) Post-test.

(a) (b)

Figure 4.34: Test D4ST4 Connection Specimen Post-Test Condition.
a) Left Side of Test Specimen. b) Right Side of Test Specimen.

Figure 4.35: Test D4ST4 Test Bolts.

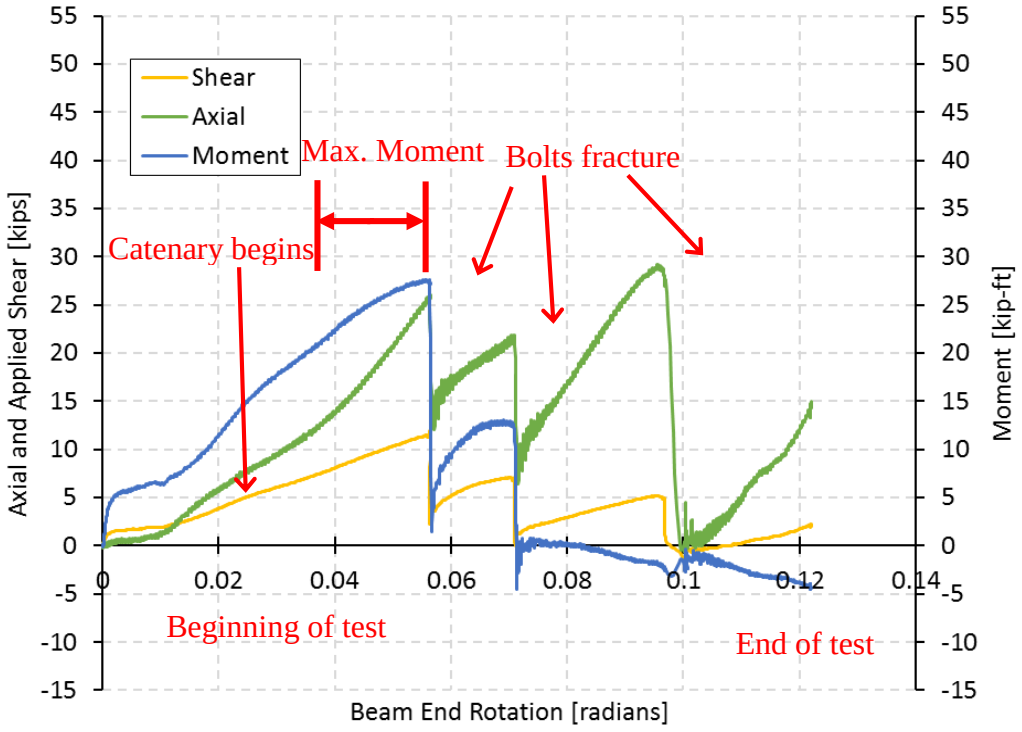

Figure 4.36: Specimen D4ST4 Left Side Bolt Line Forces versus Beam End Rotation.

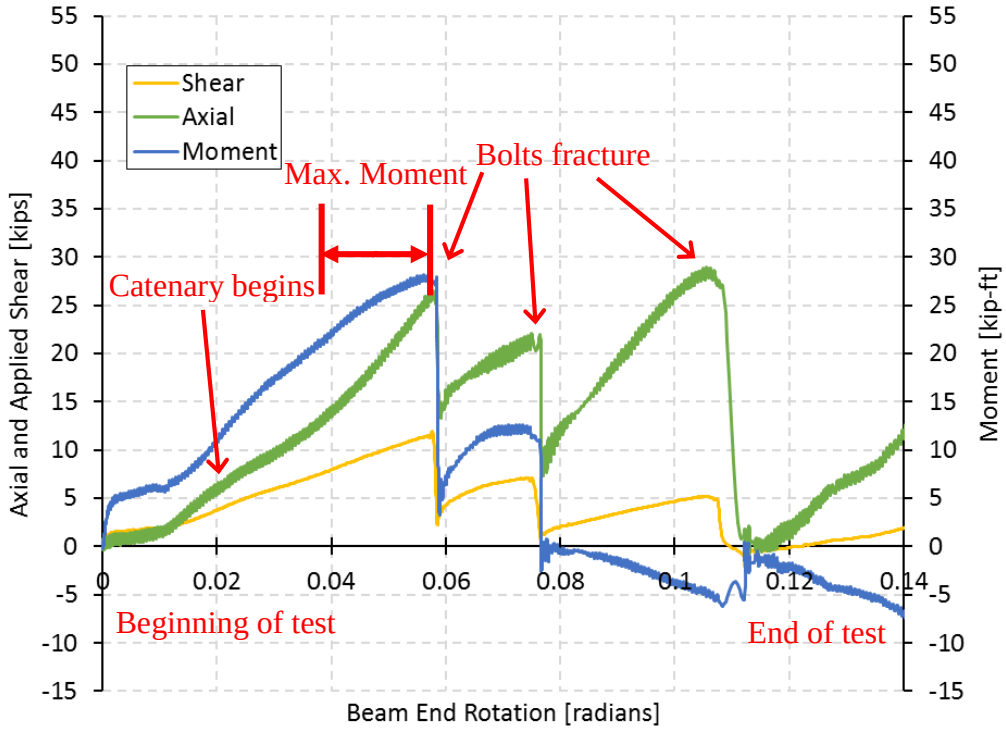

Figure 4.37: Specimen D4ST4 Right Side Bolt Line Forces versus Beam End Rotation.

4.3.2.5 Four-Bolt Summary

As was seen in the three-bolt tests, the four-bolt configurations initially resisted the applied loading through flexural resistance and after some magnitude of rotation catenary action engaged. However, catenary action engaged with less rotation in the four-bolt configurations than was seen with the three-bolt results. In each four-bolt test, the bolts ruptured as moment reached maximum and catenary was fully engaged.

Axial force, shear, and beam rotation at the maximum moment can be seen in Table 4.4. As with the three-bolt tests, the maximum moment was taken as the top 1% of moment and averaged. Tests S4ST1, D4ST2, and D4ST3 were similar with minor differences, as test S4ST1 had forces that were slightly lower. It can be seen in the table that D4ST4 is significantly different in bolt line forces. These differences are due to the change from carbon steel bolts to galvanized A325 bolts. The use of galvanized bolts contributed to a reduced capacity in the connection.

Table 4.4: Four-Bolt Specimen Bolt Line Forces at Approximate Maximum Moment.

Test Specimen	Side of Specimen	Shear Force [Kips]	Moment [Kip-Feet]	Axial Force [Kips]	Beam End Rotation [Radians]
S4ST1	Right	12.88	27.41	31.41	0.0752
	Left	12.95	27.47	31.01	0.0780
D4ST2	Right	12.23	27.37	32.35	0.0613
	Left	12.27	29.14	31.25	0.0631
D4ST3	Right	13.39	29.68	33.89	0.0656
	Left	13.21	31.84	33.56	0.0672
D4ST4	Right	10.90	27.61	24.59	0.0546
	Left	10.77	27.30	24.67	0.0561

Bolt line forces collected at the point of initial failure can be seen in Table 4.5. Once again it can be seen that test D4ST4 had much less capacity than that of the tests utilizing carbon steel bolts. Measured moment at initial failure is similar among each of

the tests; however, noticeable difference between bolt line forces is observed. D4ST2 was the one test that acquired failure at a lower shear force when compared to the other specimen with similar bolts, while axial force and moment remained similar to the other four-bolt tests. A second and third failure mechanism was found for these tests, meaning that once again this set of connections had enough robustness to continue sustaining applied shear.

Table 4.5: Four-Bolt Specimen Bolt Line Forces at Initial Bolt Failure.

Test Specimen	Side of Specimen	Shear Force [Kips]	Moment [Kip-Feet]	Axial Force [Kips]	Beam End Rotation [Radians]
S4ST1	Right	13.26	27.62	31.91	0.0773
	Left		27.28	32.26	0.0798
D4ST2	Right	12.56	27.11	31.77	0.0638
	Left		28.76	30.59	0.0653
D4ST3	Right	14.02	29.87	34.26	0.0665
	Left		32.05	34.18	0.0677
D4ST4	Right	11.92	27.36	26.42	0.0564
	Left		27.30	25.98	0.0576

Second and third bolt failures occurred, meaning that the applied load was resisted by means of force redistribution within the connection. The bolt line forces for the second and third bolt failures can be seen in Tables 4.6 and 4.7. It is evident that the galvanized bolts failed at much lower loads as well as at less rotation compared to those of the carbon bolts. Although evident that galvanized bolts were an outlier, the other tests were very inconsistent. There are certain similarities between S4ST1 and D4ST3, but the bolt line forces are not as similar as they had been for the three-bolt results as shown in Table 4.2 and 4.3.

Table 4.6: Four-Bolt Specimen Bolt Line Forces at Secondary Bolt Failure.

Test Specimen	Side of Specimen	Shear Force [Kips]	Moment [Kip-Feet]	Axial Force [Kips]	Beam End Rotation [Radians]
S4ST1	Right	8.41	6.84	32.06	0.0980
	Left		8.02	44.22	0.0925
D4ST2	Right	8.37	10.75	30.01	0.0775
	Left		10.29	30.01	0.0786
D4ST3	Right	9.37	8.00	44.23	0.0862
	Left		8.23	34.18	0.0817
D4ST4	Right	7.09	11.24	21.75	0.0751
	Left		12.10	21.31	0.0709

Table 4.7: Four-Bolt Specimen Bolt Line Forces at Tertiary Bolt Failure.

Test Specimen	Side of Specimen	Shear Force [Kips]	Moment [Kip-Feet]	Axial Force [Kips]	Beam End Rotation [Radians]
S4ST1	Right	7.2	-9.94	37.16	0.131
	Left		-4.57	37.18	0.117
D4ST2	Right	7.9	-5.41	32.44	0.109
	Left		-8.46	33.04	0.122
D4ST3	Right	7.5	-8.20	36.02	0.118
	Left		-4.15	37.38	0.105
D4ST4	Right	5.19	-4.34	27.69	0.105
	Left		-1.79	28.71	0.095

4.3.3 Five-Bolt Tests

There were a total of four five-bolt tests performed. These included one statically loaded test with a loading rate of one in. per minute and three dynamically loaded tests with an average loading rate of 2.72 in. per second. All tests performed resulted in four out of the five bolts rupturing on one side of the column stub.

Tests S5ST1, D5ST2, and D5ST3 used ASTM A325 carbon steel bolts. D5ST4 used galvanized ASTM A325 bolts. Bolt bearing within each bolt hole can be seen in Figure 4.38.

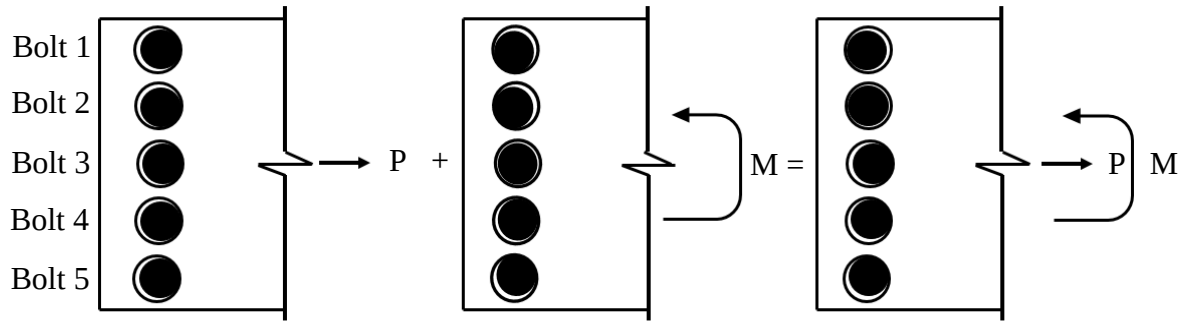

Figure 4.38: Five-Bolt Bearing Pattern.

4.3.3.1 S5ST1

Test S5ST1 was a statically loaded test. The test underwent a full ten in. stroke. The failure mechanism for test S5ST1 was bolt shear rupture on the left side of the specimen. This failure occurred to the bottom four bolts on the left side, L2 through L5. Figures 4.39 (a) and (b) show the specimen pre-test and post-test configuration.

Shown in Figures 4.40 (a) and (b) are the shear tab connections in their post-test configurations at each side of the specimen. Noticeable bolt hole deformation occurred at all bolt holes on the left side of the specimen while on the right side significant deformation can be seen at R5 while less deformation is noticeable at R4 and R5. Bolt hole R2 shows significant elongation. Stress markings around both the top and bottom holes on both sides of the specimen confirm the presence of a force couple. At the plate edge deformation occurred due to the forces acting at each bolt hole. Figure 4.41 shows the post-test condition of the bolts. The bottom four bolts on the left side failed. Bolts R4 and R5 sustained noticeable deformation.

As seen in Figures 4.42 and 4.43, the connection behavior shows a significantly higher measured moment when compared to three- and four-bolt tests. At the beginning of the test, there is slight inconsistency in the data as can be seen in the plots, which was

assumed to be the applied load engaging the specimen. The moment and axial forces both increase magnitudes immediately. Catenary begins at the start of the test and increases nearly linearly until the first bolt failure. After the first bolt fails, forces and moment increase again until the second bolt fails. After the second bolt break, axial forces increase yet again while moment decreases significantly and remains nearly constant until the point of the third bolt failure. After this, moment reverses and maintains a relatively low magnitude, whereas axial force continues to increase until the fourth bolt breaks and the test is concluded.

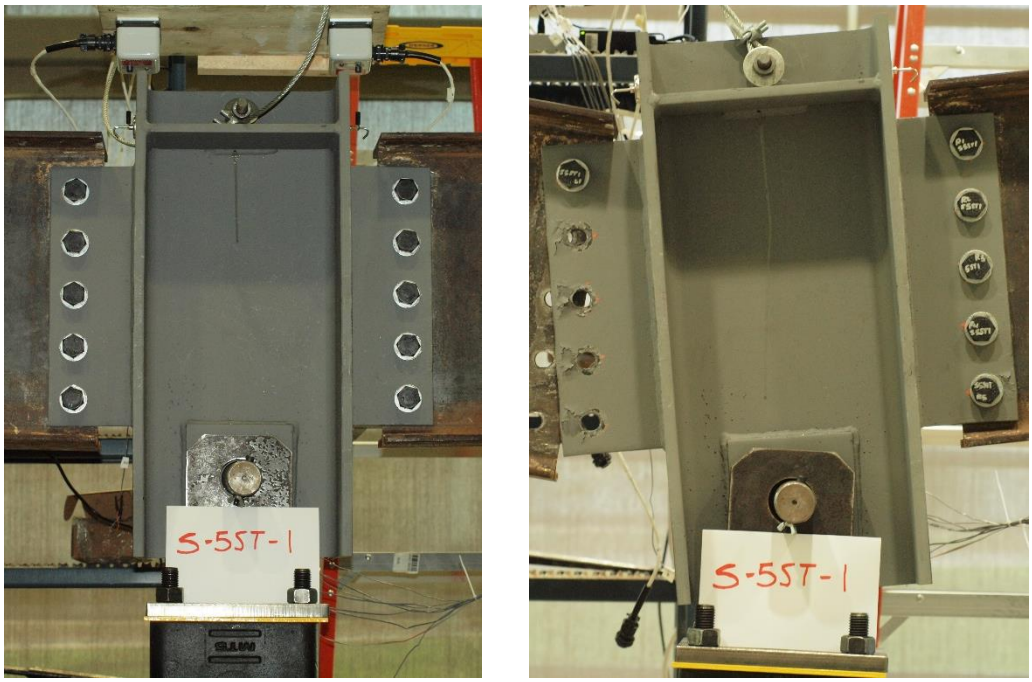

(a) (b)

Figure 4.39: Test S5ST1 Specimen Comparison.
a) Pre-test. b) Post-test.

(a) (b)

Figure 4.40: Test S5ST1 Connection Specimen Post-Test Condition.
a) Left Side of Test Specimen. b) Right Side of Test Specimen.

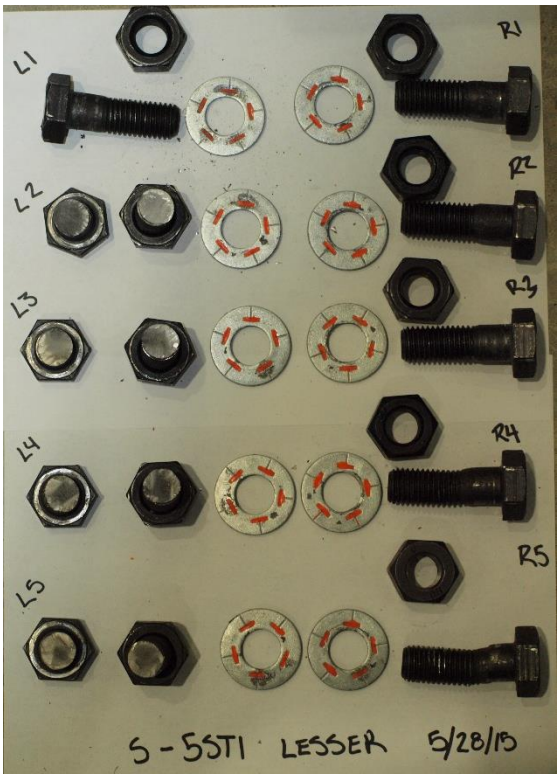

Figure 4.41: Test S5ST1 Test Bolts.

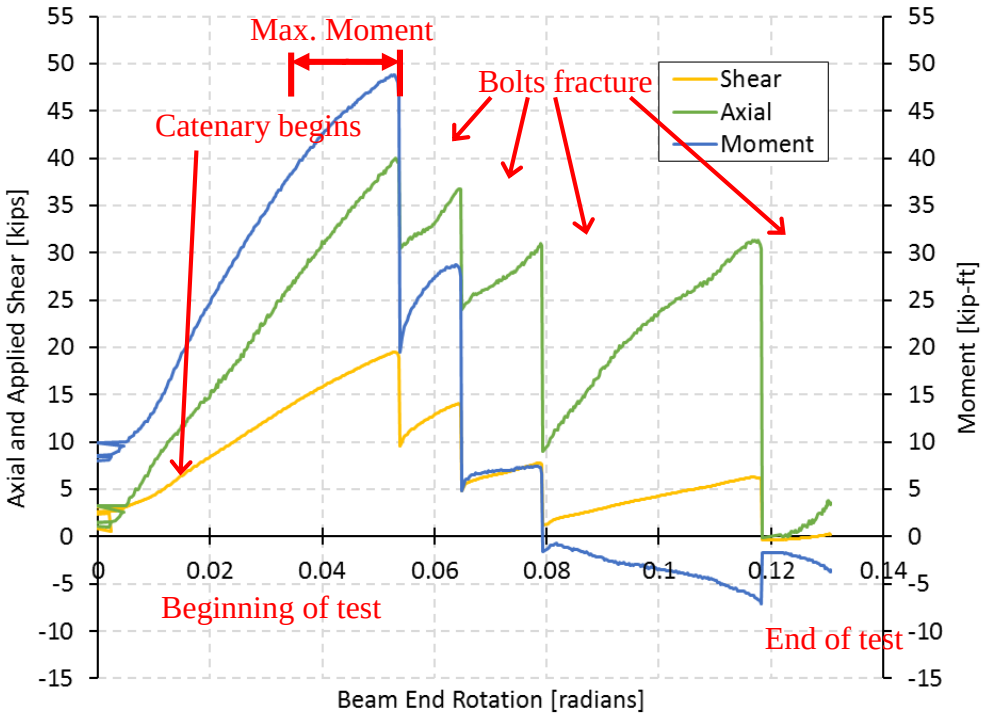

Figure 4.42: Specimen S5ST1 Left Side Bolt Line Forces versus Beam End Rotation.

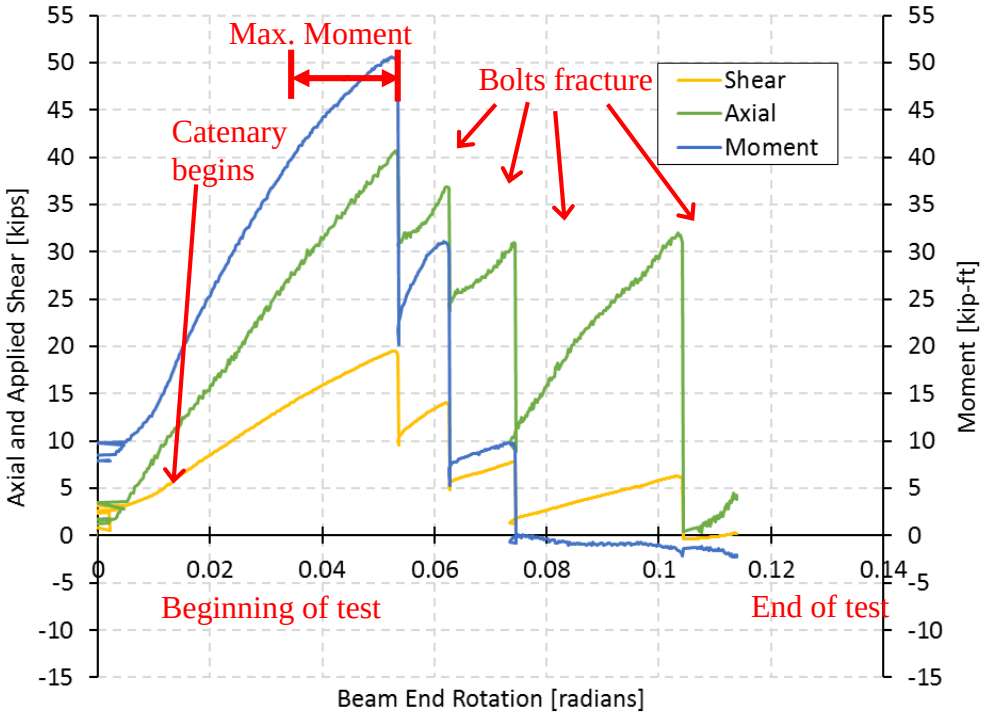

Figure 4.43: Specimen S5ST1 Right Side Bolt Line Forces versus Beam End Rotation.

4.3.3.2 Test D5ST2

Test D5ST2 was the first five-bolt dynamic test with a loading rate of 2.74 in. per second. The test specimen underwent full stroke of the actuator. Bolts L2, L3, and L4 ruptured on the left side. Figures 4.44 (a) and (b) show the specimen pre-test and post-test.

Figures 4.45 (a) and (b) show the test specimen's shear tabs post-test. The bolt hole elongation on the left side occurred on every bolt hole. The right side only sustained noticeable deformation on the bottom hole, R5. Surficial stress marks on both sides show evidence of the force couple. Plate edge deformation can be seen on both sides of the test specimen. Figure 4.46 shows the post-test condition of the bolts. It can be seen that the left side bolts. L2 through L5, failed. On the right side, R5 sustained noticeable deformation, while the rest of the bolts on the right side didn't showed less deformation than seen in R5.

As seen in Figures 4.47 and 4.48, the test started with forces and moment present in the system. The moment, axial, and shear forces in the connection increased until first bolt break. Upon first bolt fracture, the forces and moment dropped but reengaged and increased until the second bolt break. The moment plateaued prior to the second bolt fracture, whereas shear and axial forces peaked at the second bolt fracture. After the second bolt fractured the moment in the connection decreased significantly and remained relatively constant until the third bolt fractured. The axial and shear forces increased between the second and third bolt fractures, but the increases were not as substantial as seen prior to the second bolt fracture. Following the third bolt break the moment reverses and maintains low magnitudes, but the axial force again increases until the fourth bolt

breaks. The peak axial magnitudes at the point of the third and fourth bolt fractures are nearly identical.

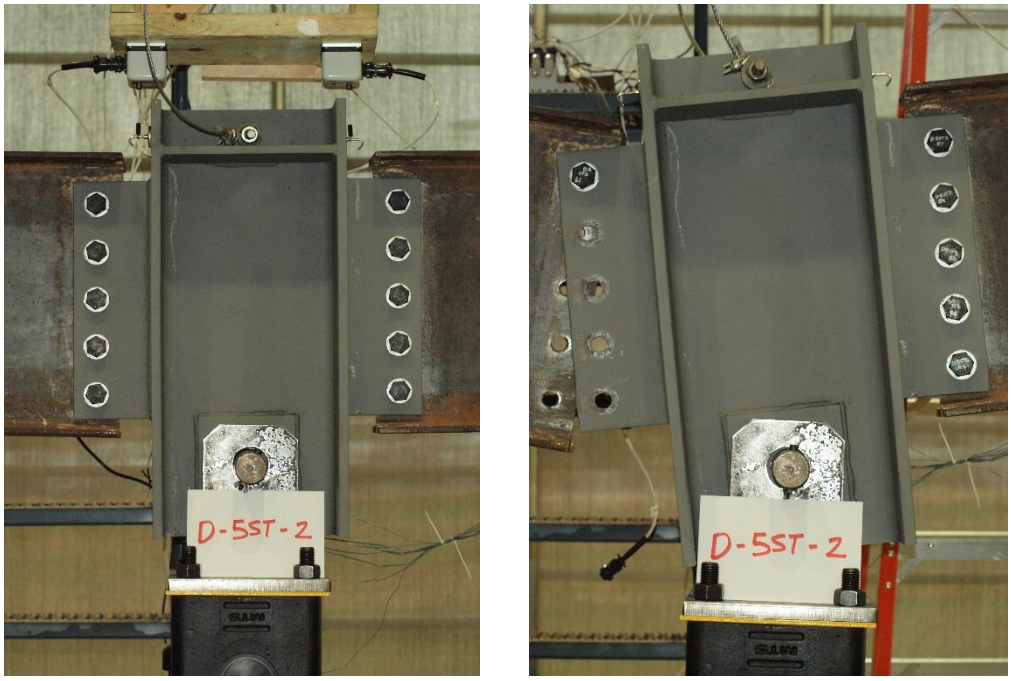

(a) (b)

Figure 4.44: Test D5ST2 Specimen Comparison.
a) Pre-test. b) Post-test.

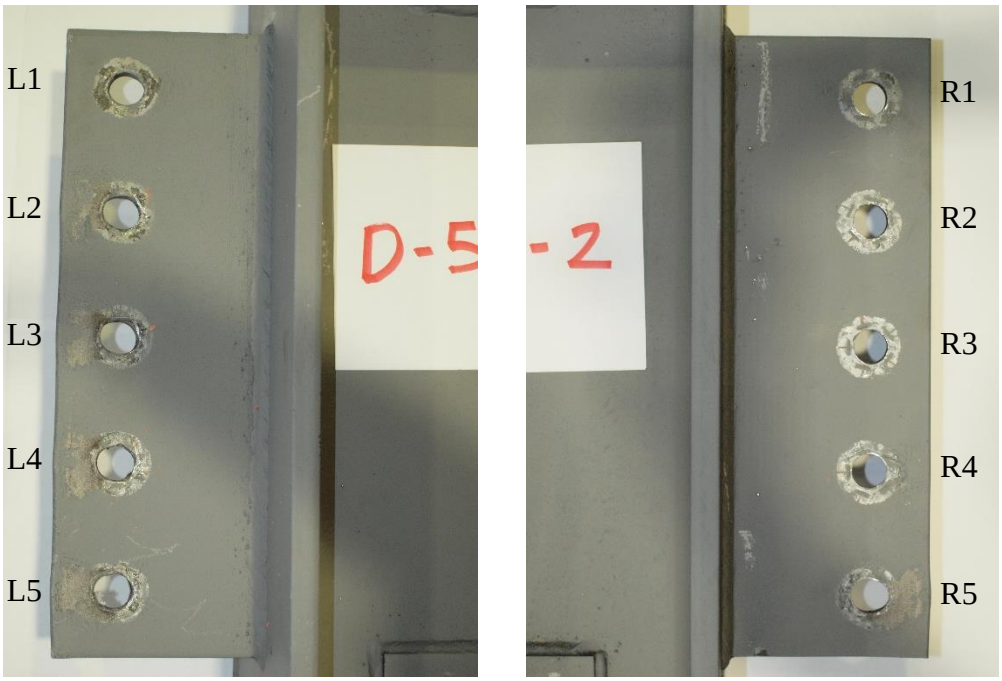

(a) (b)

Figure 4.45: Test D5ST2 Connection Specimen Post-Test Condition.
a) Left Side of Test Specimen. b) Right Side of Test Specimen.

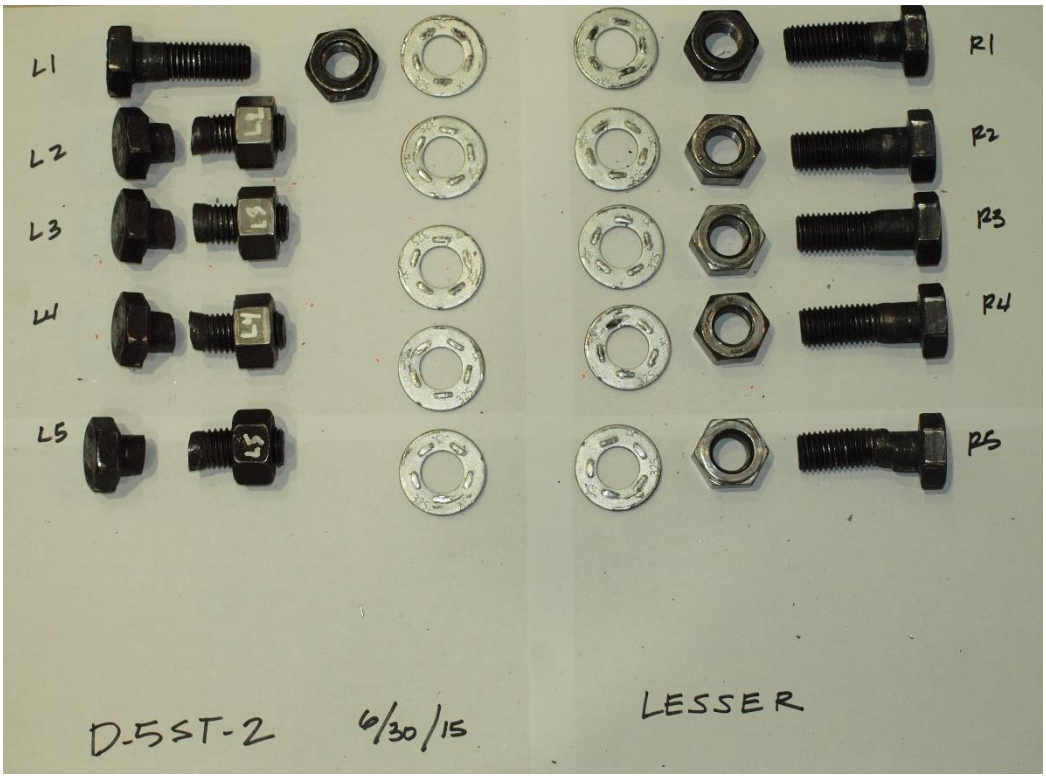

Figure 4.46: Test D5ST2 Test Bolts.

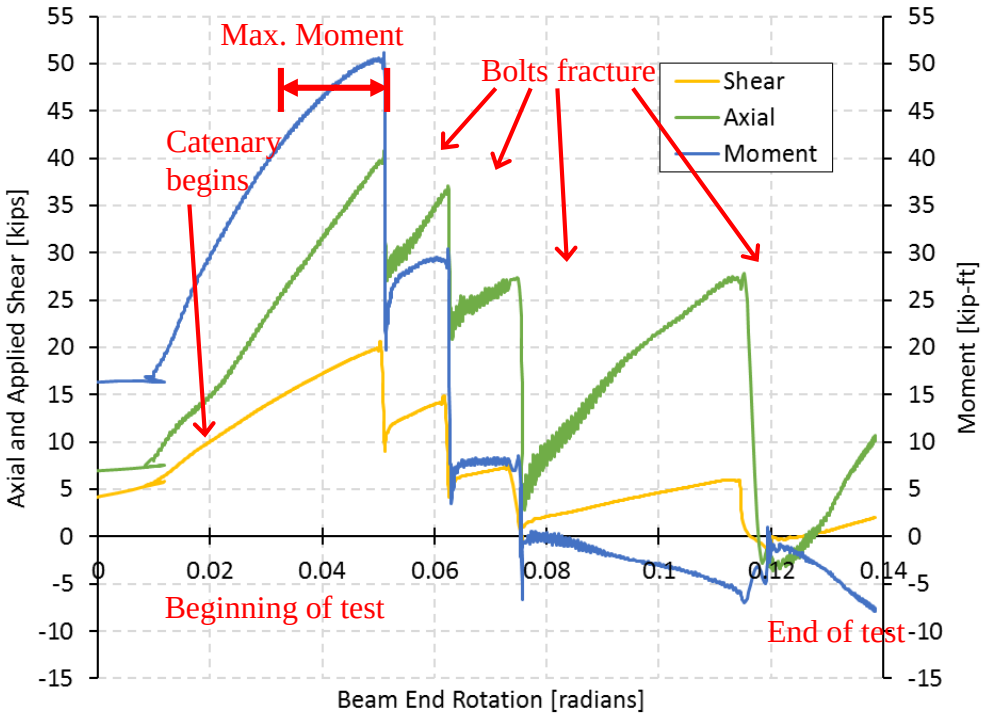

Figure 4.47: Specimen D5ST2 Left Side Bolt Line Forces versus Beam End Rotation.

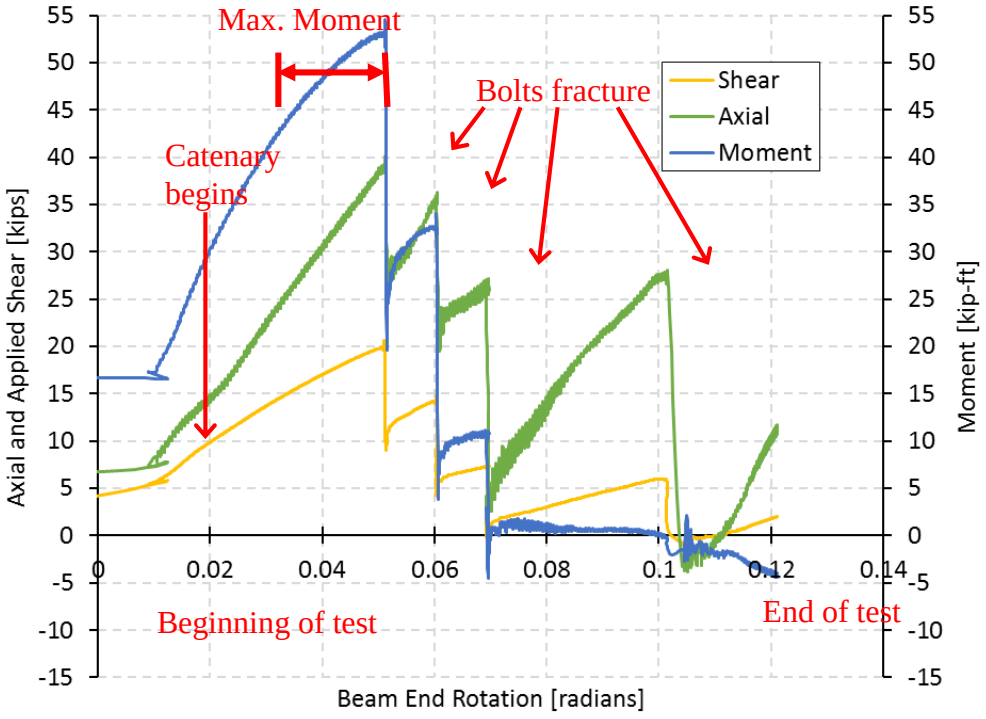

Figure 4.48: Specimen D5ST2 Right Side Bolt Line Forces versus Beam End Rotation.

4.3.3.3 Test D5ST3

Test D5ST3 was the second dynamically loaded five-bolt test. It underwent a full stroke of the actuator resulting in a loading rate of 2.69 in. per second. The failure mechanism for the D5ST3 test was bolt shear rupture on the left side of the specimen of L2, L3, L4, and L5. Figures 4.49 (a) and (b) show images of the pre-test and post-test configuration. Bolt shear of bolts L2, L3, L4, and L5 bolt can be seen in Figure 4.49 (b).

Bolt hole deformation can be seen at all of the bolts on the left side of the specimen. As seen in Figure 4.50 (a). Figure 4.50 (b), the bottom bolt hole on the right side, R5, shows some perceptible elongation while the rest do not show the same observable deformation. Both the left and right sides show stress at the bolt holes consistent with a force couple being applied to the connection plate. The plate edge deformation was minimal on both sides of the test specimen, but more perceptible on the left side where the bolt fractures occurred.

Figure 4.51 shows the post-test bolt condition. On the left side, bolts L2 through L5 are ruptured while L1 showed no noticeable deformation. On the right side, R1, R4, and R5 show noticeable deformation.

Figures 4.52 and 4.53 show very similar results to that seen in D5ST2. The moment, axial force, and shear force began increasing at the start of the test. This test showed that the forces increased rapidly, but slowed momentarily at approximately 0.01 radians, then increasing rapidly again. Both flexural and catenary actions were present until first bolt break, which occurred at approximately 0.05 radians of rotation. The moment and forces in the connection drop after the first bolt break, but then increase again up to the point of the second bolt fracture. As with D5ST2, the moment plateaued

prior to the second bolt fracture, and it even dropped somewhat as fracture was impending. Moment decreased significantly after the second bolt fracture and remained constant until the third bolt broke. The axial and shear forces increased again between the second and third bolt fractures, but not at the same rate as seen before the second bolt broke. After the third bolt fractured, the moment reversed and remained at relatively low magnitudes, whereas the axial force increased until the fourth bolt broke. In this test, the peak axial forces at the points where the second, third and fourth bolts broke were similar in magnitude.

(a) (b)

Figure 4.49: Test D5ST3 Specimen Comparison.
a) Pre-test. b) Post-test.

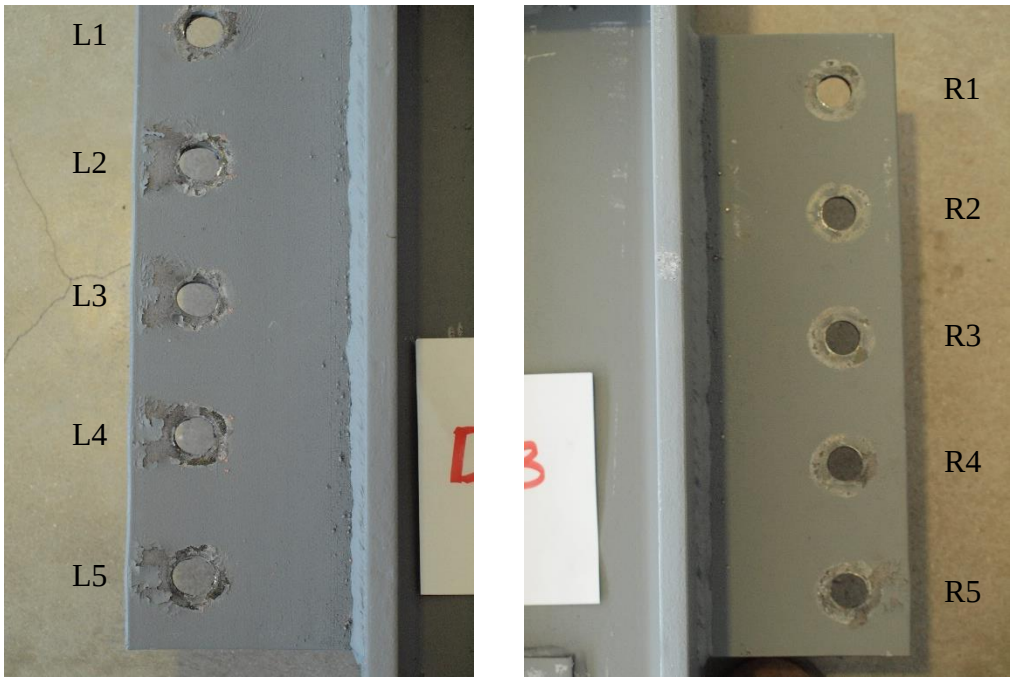

(a) (b)

Figure 4.50: Test D5ST3 Connection Specimen Post-Test Condition.
a) Left Side of Test Specimen. b) Right Side of Test Specimen.

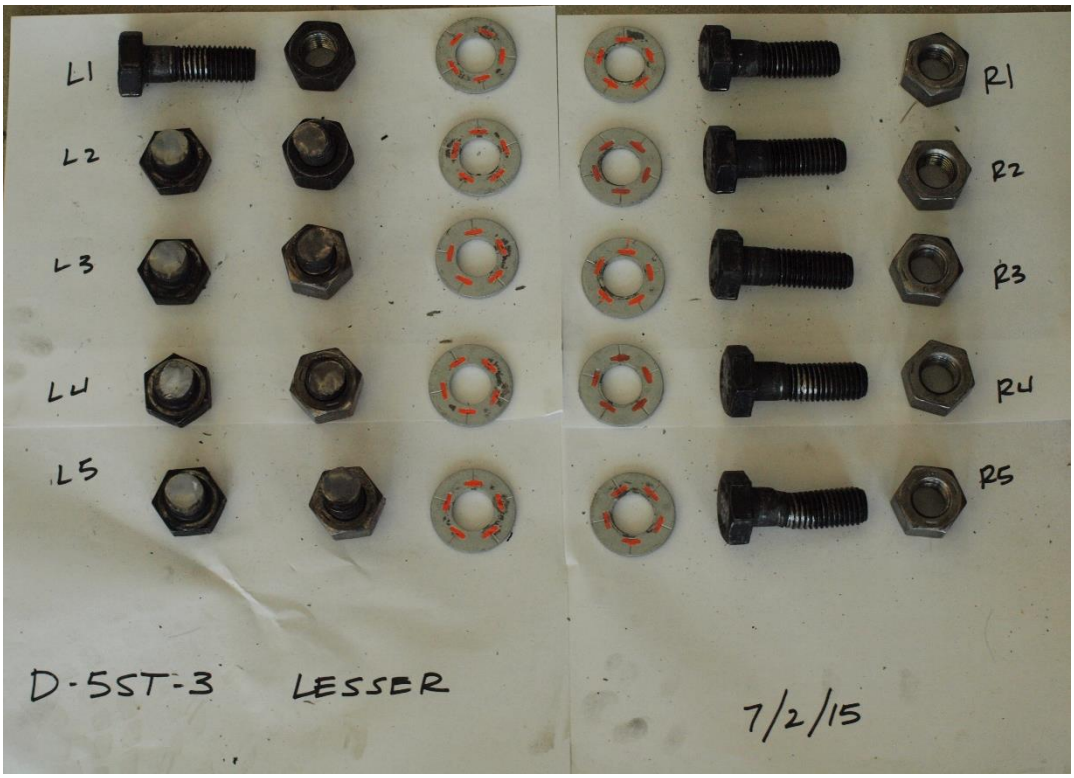

Figure 4.51: Test D5ST3 Test Bolts.

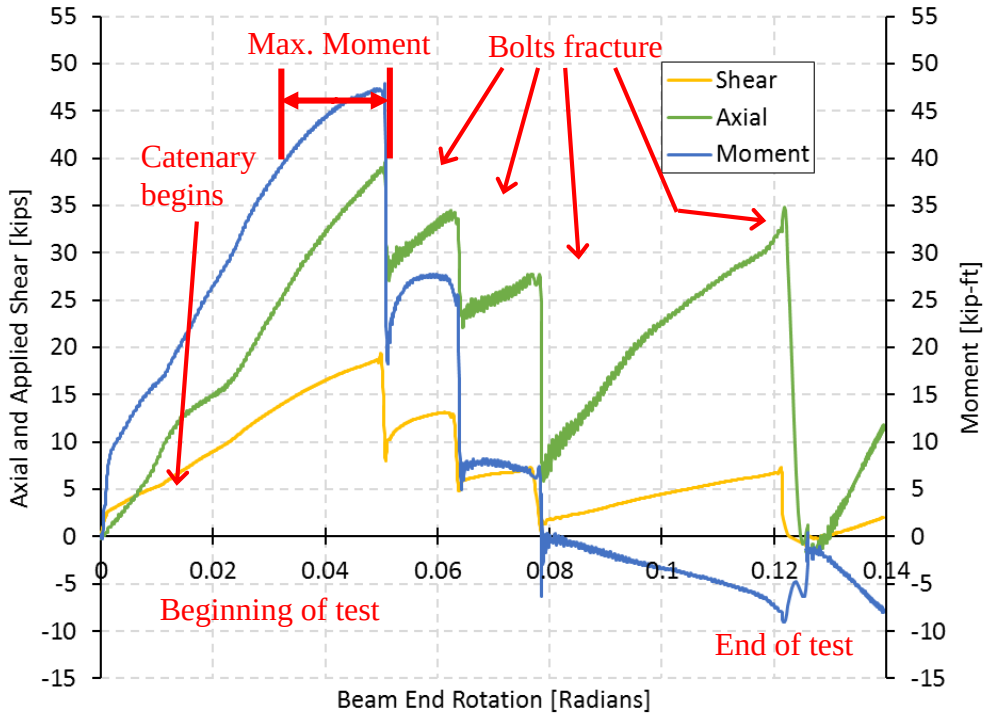

Figure 4.52: Specimen D5ST3 Left Side Bolt Line Forces versus Beam End Rotation.

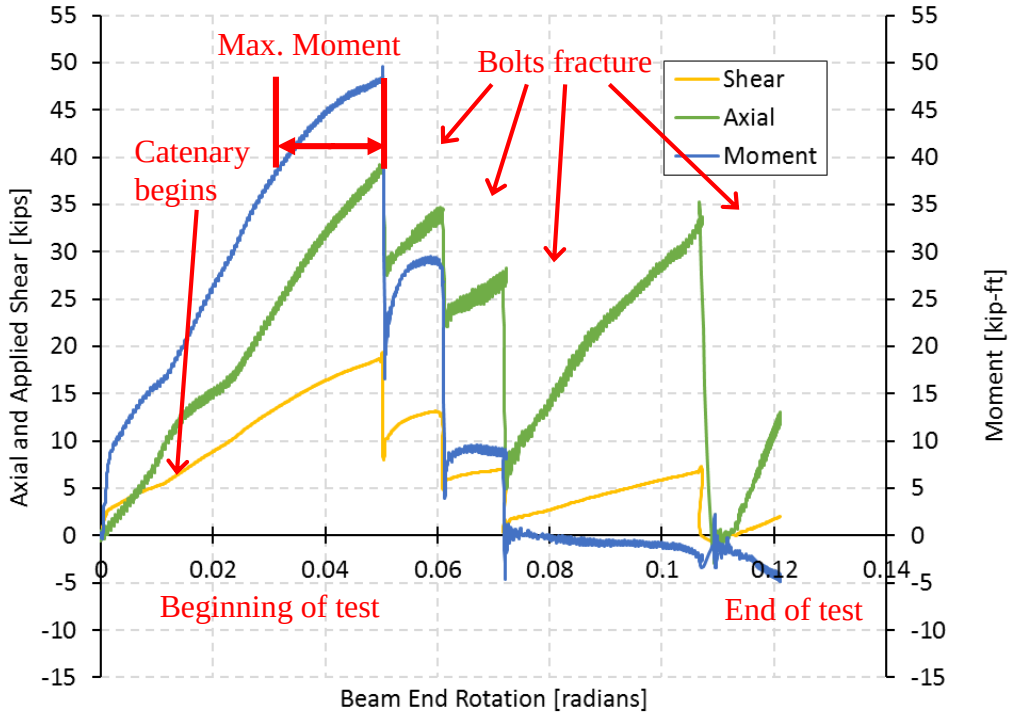

Figure 4.53: Specimen D5ST3 Right Side Bolt Line Forces versus Beam End Rotation.

4.3.3.4 Test D5ST4

Test D4ST4 was the fourth dynamically loaded five-bolt test. If underwent a full stroke of the actuator and had a loading rate of 2.86 in. per second. Test D5ST4 had a failure mechanism of bolt shear rupture on the left side of the column stub. This rupture occurred at L2, L3, L4, and L5. Figures 4.54 (a) and (b) show the connection pre-test and post-test.

Noticeable deformation of the bolt holes can be seen at L4 and L5. The bolt hole deformations can be seen in Figures 4.55 (a) and (b). Around the bottom two bolts, L5 and R5, stress can be seen; however, no significant stress can be seen near the top bolt holes on either side of the test specimen. The array of post-test bolts can be seen in Figure 4.56. Besides the bolts on the left side which ruptured, the bolt with the most noticeable deformation was R5. The rest of the bolts showed only minor deformation.

Figures 4.57 and 4.58 show the axial and shear force and moment versus rotation for each side of the test specimen. This test follows similar trends as in D5ST2 and D5ST3. The forces and moment increase immediately at the beginning of the test, and the applied load is resisted by both flexural and catenary action. Initial bolt failure occurred at axial and shear forces with much lower magnitudes than previous 5ST tests; however, the moment magnitude at initial bolt fracture was similar to the previous tests. In addition, the initial bolt fractured at less rotation than the other five bolt dynamic tests. Initial bolt failure occurred at approximately 0.04 radians with an axial force magnitude approximately 26 kips and shear force magnitude approximately 17 kips. The trends are very similar to those seen in other five-bolt dynamic tests, albeit with lower axial and

shear force magnitudes. Moment trends and magnitudes are very similar to the previous tests.

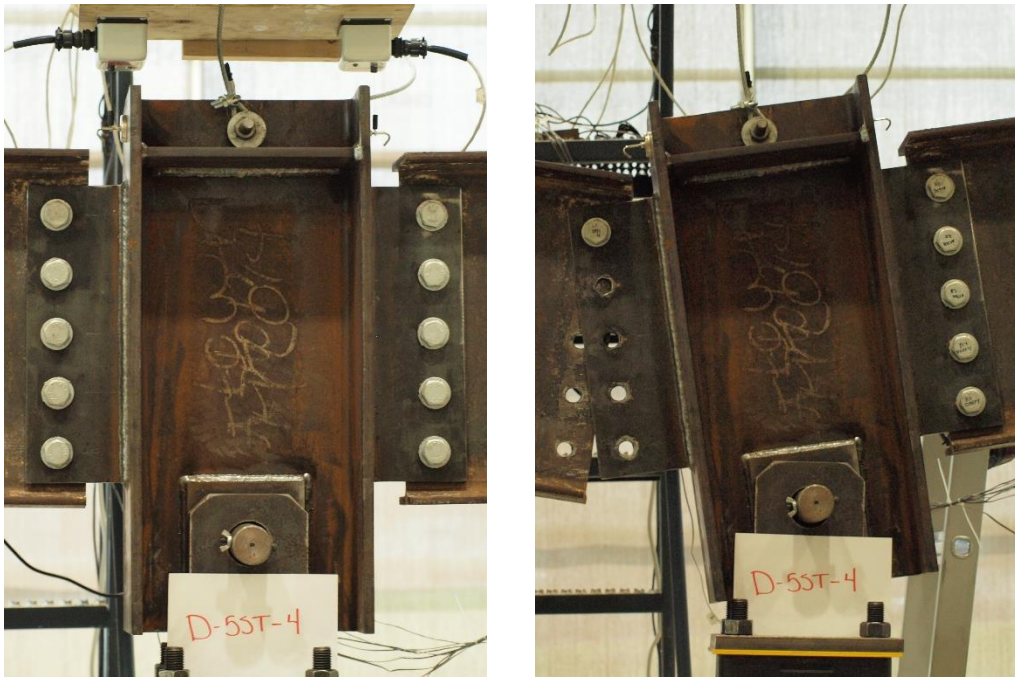

(a) (b)

Figure 4.54: Test D5ST4 Specimen Comparison.
a) Pre-test. b) Post-test.

(a) (b)

Figure 4.55: Test D5ST4 Connection Specimen Post-Test Condition.
a) Left Side of Test Specimen. b) Right Side of Test Specimen.

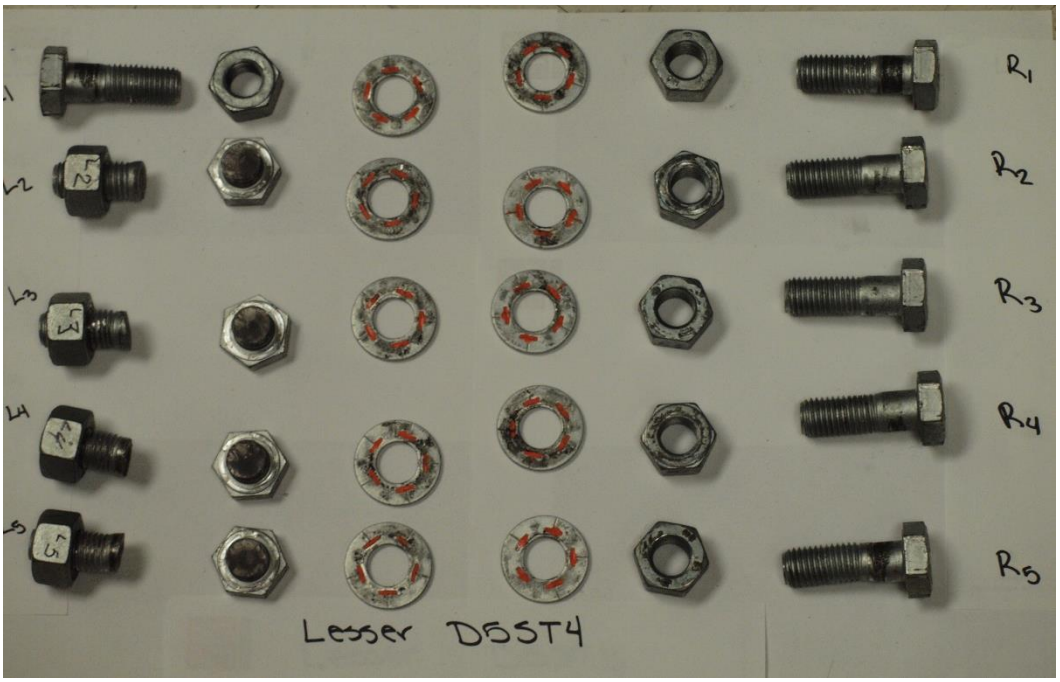

Figure 4.56: Test D5ST4 Test Bolts.

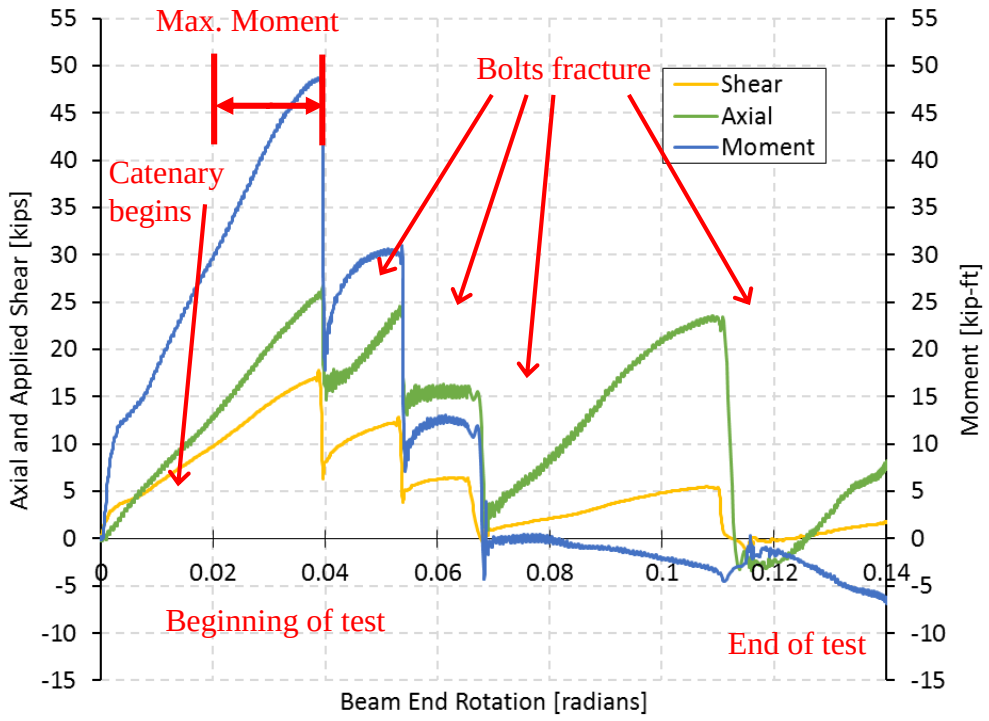

Figure 4.57: Specimen D5ST4 Left Side Bolt Line Forces versus Beam End Rotation.

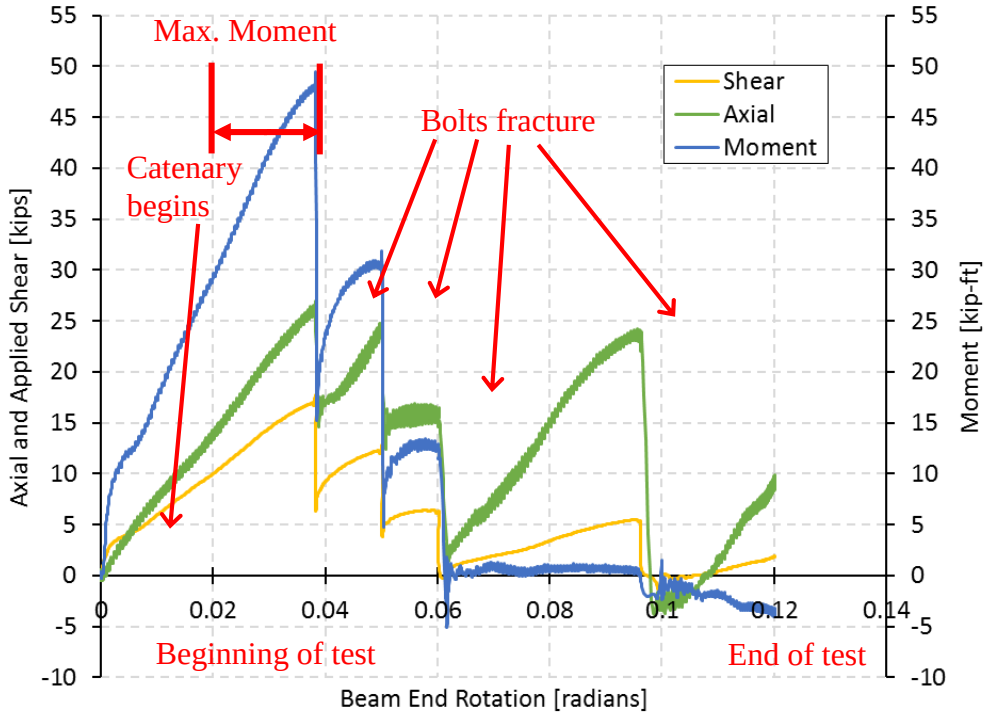

Figure 4.58: Specimen D5ST4 Right Side Bolt Line Forces versus Beam End Rotation.

4.3.3.5 Five-Bolt Summary

The five-bolt configuration followed the same trend as seen in the three and four-bolt tests, where force and moment were initially resisted through flexural resistance. However, catenary action was engaged in all five bolt tests at the beginning of the test, as opposed to the three- and four-bolt tests where resistance transitioned from flexural to catenary. Bolt rupture occurred at the point of maximum moment during all tests in the five-bolt configuration.

Table 4.8 shows the experimental data at the point of maximum moment. The top 1% of calculated moment was averaged to determine the maximum value. The values are similar between all tests with the exception of test D5ST4, where the use of galvanized bolts impacted the capacities. Applied shear for D5ST4 is lower than the other five-bolt tests, but the table clearly shows the applied shear decreasing for each test after S5ST1.

Table 4.8: Five-Bolt Specimen Bolt Line Forces at Approximate Maximum Moment.

Test Specimen	Side of Specimen	Shear Force [Kips]	Moment [Kip-Feet]	Axial Force [Kips]	Beam End Rotation [Radians]
S5ST1	Right	19.45	50.54	40.25	0.0528
	Left	19.47	48.78	39.66	0.0526
D5ST2	Right	18.94	52.92	38.58	0.0497
	Left	19.05	50.33	39.42	0.0504
D5ST3	Right	17.84	47.90	38.14	0.0488
	Left	17.93	47.14	38.31	0.0495
D5ST4	Right	16.12	47.93	25.43	0.0372
	Left	16.18	47.22	24.89	0.0367

The bolt line forces at initial failure can be seen in Table 4.9. This table shows there are extreme differences between D5ST4 and the other three tests. The point at which initial failure occurs is more than 0.01 radians less, but also the measured axial and

shear forces are approximately 15 and 10 kips lower, respectively. All other tests show similar magnitudes at the point of initial bolt failure.

Table 4.9: Five-Bolt Specimen Bolt Line Forces at Initial Bolt Failure.

Test Specimen	Side of Specimen	Shear Forces [Kips]	Moment [Kip-Feet]	Axial Force [Kips]	Beam End Rotation [Radians]
S5ST1	Right	19.52	50.53	40.61	0.0532
	Left		48.79	39.90	0.0530
D5ST2	Right	19.91	52.83	39.03	0.0498
	Left		50.30	39.43	0.0505
D5ST3	Right	19.34	48.01	39.19	0.0499
	Left		47.15	38.94	0.0501
D5ST4	Right	17.31	47.84	25.91	0.0383
	Left		48.57	25.54	0.0377

Each of the test specimens had four bolt failures, and the axial force recovered to a similar magnitude each time prior to the next bolt failing. The resistance magnitudes developed for the secondary, tertiary, and quaternary failures are shown in Tables 4.10, 4.11, and 4.12. As mentioned previously, D5ST4 utilized galvanized bolts and it can be seen throughout the data that the values for shear, axial force, and rotation are considerably lower than the other three tests which utilized carbon bolts. Results did not show the same difference between moment magnitudes.

Table 4.10: Five-Bolt Specimen Bolt Line Forces at Secondary Bolt Failure.

Test Specimen	Side of Specimen	Shear Forces [Kips]	Moment [Kip-Feet]	Axial Forces [Kips]	Beam End Rotation [Radians]
S5ST1	Right	14.04	31.04	36.85	0.0621
	Left		28.56	36.73	0.0642
D5ST2	Right	14.84	32.36	35.52	0.0605
	Left		29.08	36.08	0.0618
D5ST3	Right	13.00	28.16	33.44	0.0608
	Left		26.18	33.74	0.0627
D5ST4	Right	11.92	30.44	23.14	0.0501
	Left		30.20	23.95	0.0530

Table 4.11: Five-Bolt Specimen Bolt Line Forces at Tertiary Bolt Failure.

Test Specimen	Side of Specimen	Shear Force [Kips]	Moment [Kip-Feet]	Axial Forces [Kips]	Beam End Rotation [Radians]
S5ST1	Right	7.78	9.66	31.02	0.0742
	Left		7.34	30.95	0.0789
D5ST2	Right	7.60	11.06	25.51	0.0696
	Left		8.19	25.99	0.0730
D5ST3	Right	7.37	8.19	28.10	0.0723
	Left		6.38	27.50	0.0766
D5ST4	Right	5.96	12.35	16.60	0.0592
	Left		12.13	16.14	0.0642

Table 4.12: Five-Bolt Specimen Bolt Line Forces at Quaternary Bolt Failure.

Test Specimen	Side of Specimen	Shear Force [Kips]	Moment [Kip-Feet]	Axial Force [Kips]	Beam End Rotation [Radians]
S5ST1	Right	6.27	-1.47	31.82	0.103
	Left		-6.26	31.20	0.117
D5ST2	Right	6.02	-0.17	27.26	0.101
	Left		-5.88	27.06	0.114
D5ST3	Right	7.29	-2.06	32.67	0.107
	Left		-7.89	32.33	0.121
D5ST4	Right	4.85	0.71	23.35	0.095
	Left		-3.09	22.92	0.108

4.4 Comparison of Static and Quasi-Dynamic Tests

Each bolt configuration included one static test and at least two quasi-dynamic tests. This section will discuss the comparisons between the static and quasi-dynamic tests for each bolt configuration.

4.4.1 Three-Bolt Tests

Figures 4.59 and 4.60 show tests for the three-bolt configuration. The statically loaded test, S3ST1, is shown as a set of dashed lines. This is compared against the quasi-dynamic tests D3ST2 and D3ST3, shown as solid lines.

The trends for both the static and dynamic tests are similar. In all cases, the maximum moment magnitudes occur at approximately the same magnitude of beam

rotation. The axial force and shear force magnitudes are similar when bolts break. The static test and one of the dynamic tests, D3ST3, are nearly on top of one another. D3ST2 lags the others by approximately 0.01 radians of beam rotation.

Since one of the experiments had gaps in the data, it is difficult to draw firm conclusions from the results. It can be said, however, that the three-bolt configuration does not match the hypothesis that the connection when subjected to dynamic loading will exhibit failure modes with less rotation than when subjected to a static loading.

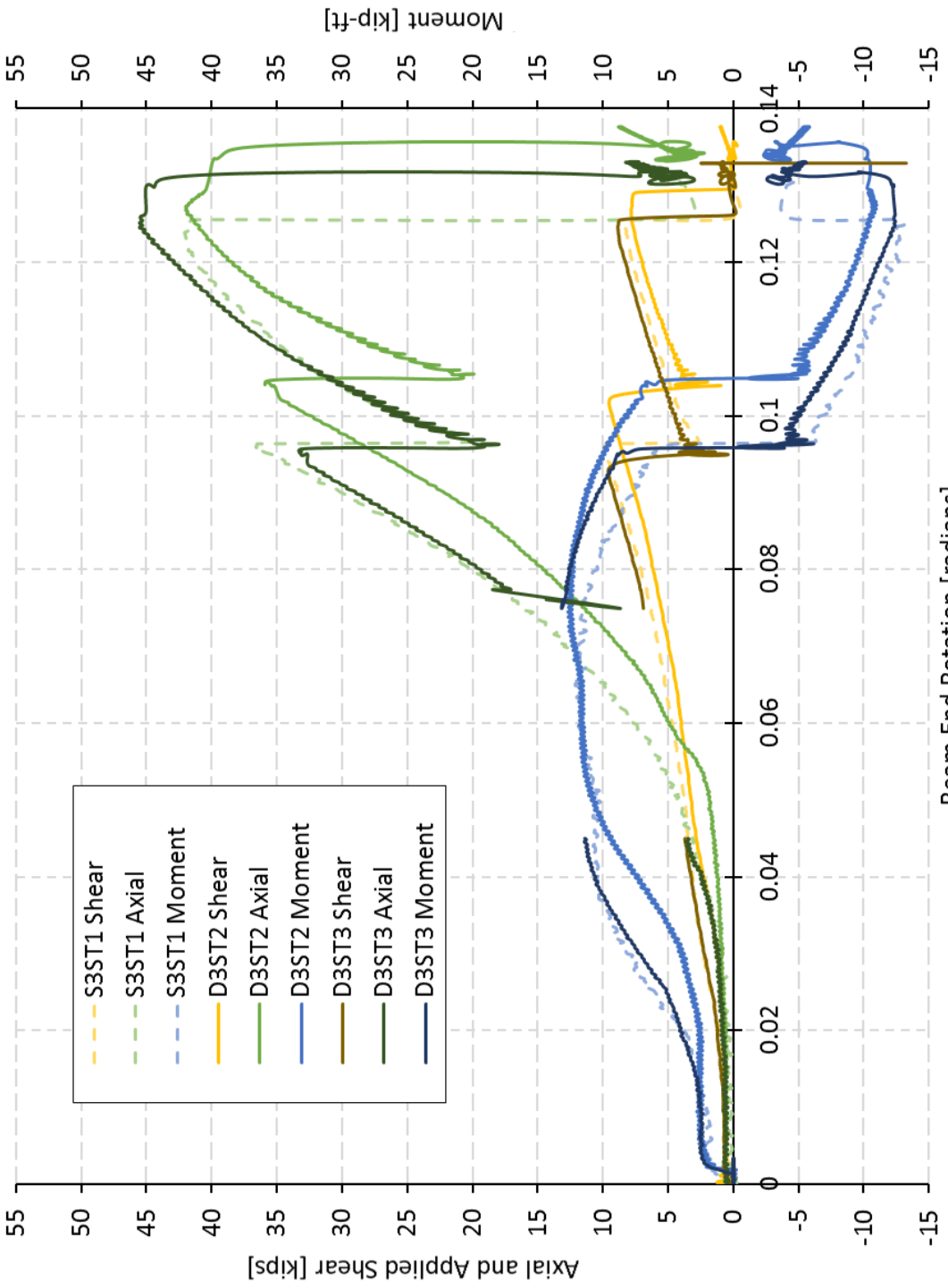

Figure 4.59: Three-Bolt Left Side Bolt Line Forces versus Beam End Rotation.

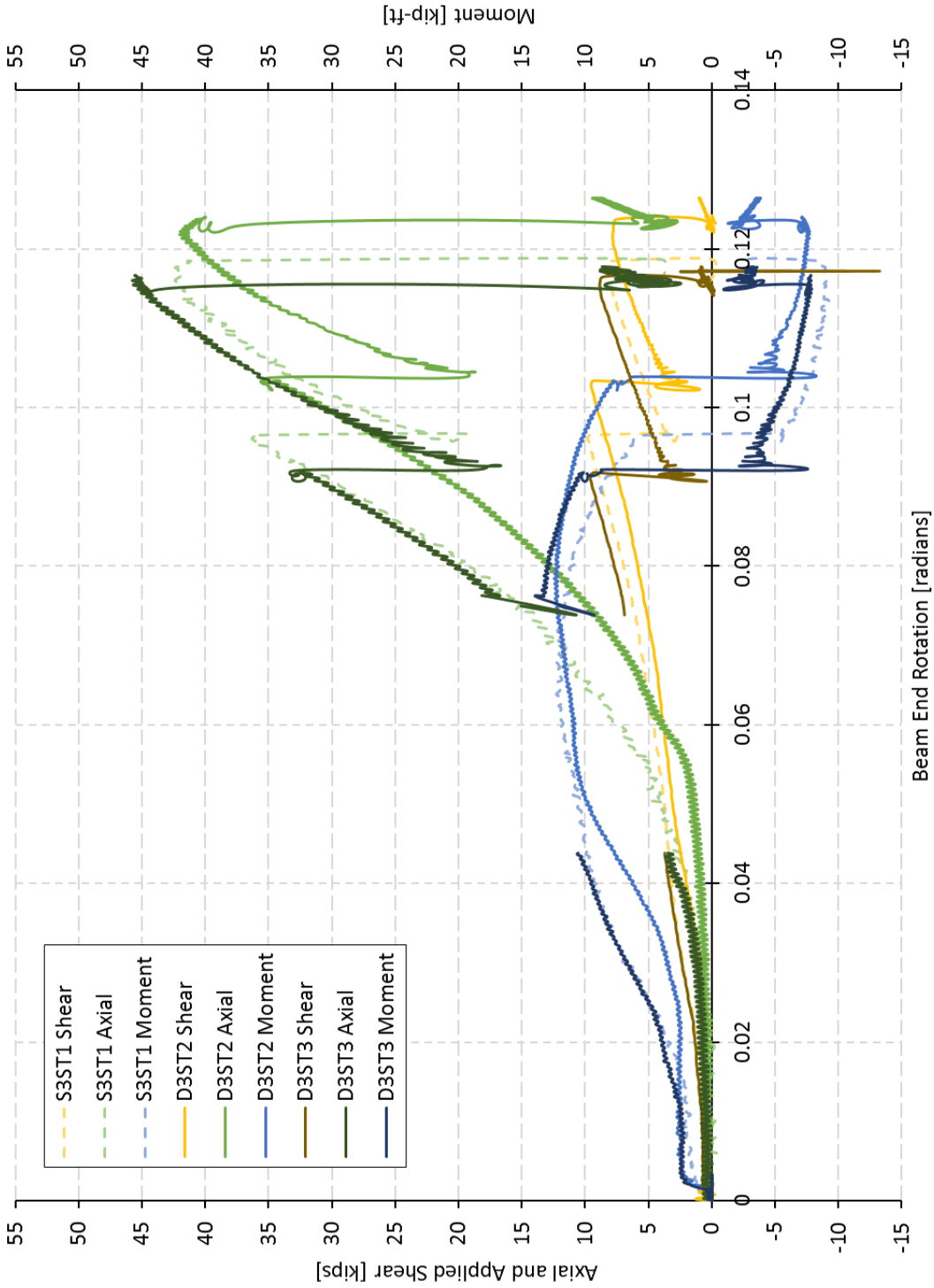

Figure 4.60: Three-Bolt Right Side Bolt Line Forces versus Beam End Rotation.

4.4.2 Four-Bolt Tests

Figures 4.61 and 4.62 compare the axial, shear, and moment for the four bolt configuration tests. The statically loaded test and quasi-dynamically loaded tests have comparable bolt line force and moment magnitudes. (The specimen using galvanized bolts has less axial, shear and moment magnitudes as previously discussed, but the trends are similar to the other tests.) It is clearly evident from these plots that the quasi-dynamically loaded tests had bolts fail at less rotation, approximately 0.015 radians less than that seen in the static tests. This agrees with the initial hypothesis that limit states for dynamically loaded connections will occur with less rotation than they will under a static loading. However, the rotation magnitudes are closer together when the third bolt fractures.

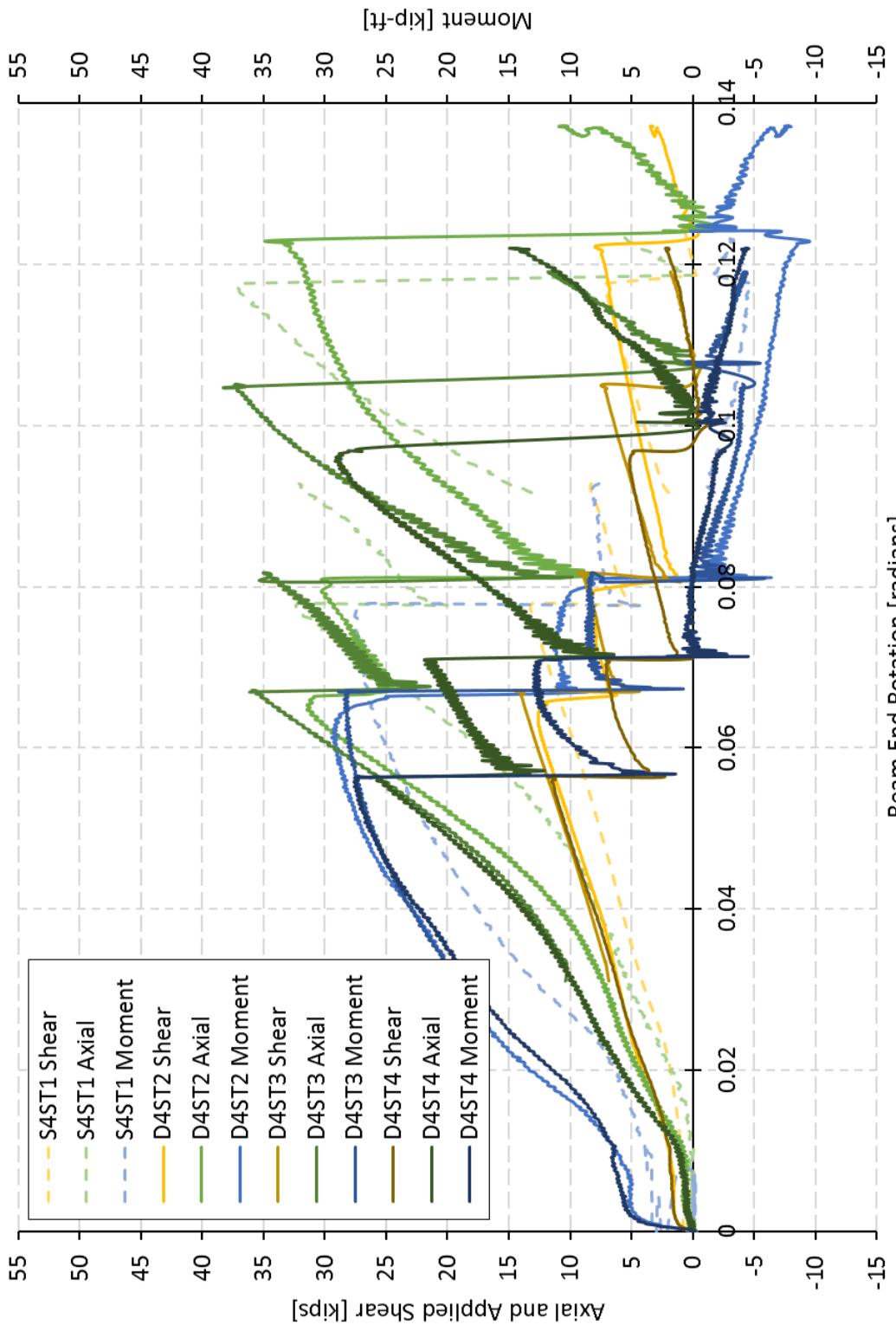

Figure 4.61: Four-Bolt Left Side Bolt Line Forces versus Beam End Rotation.

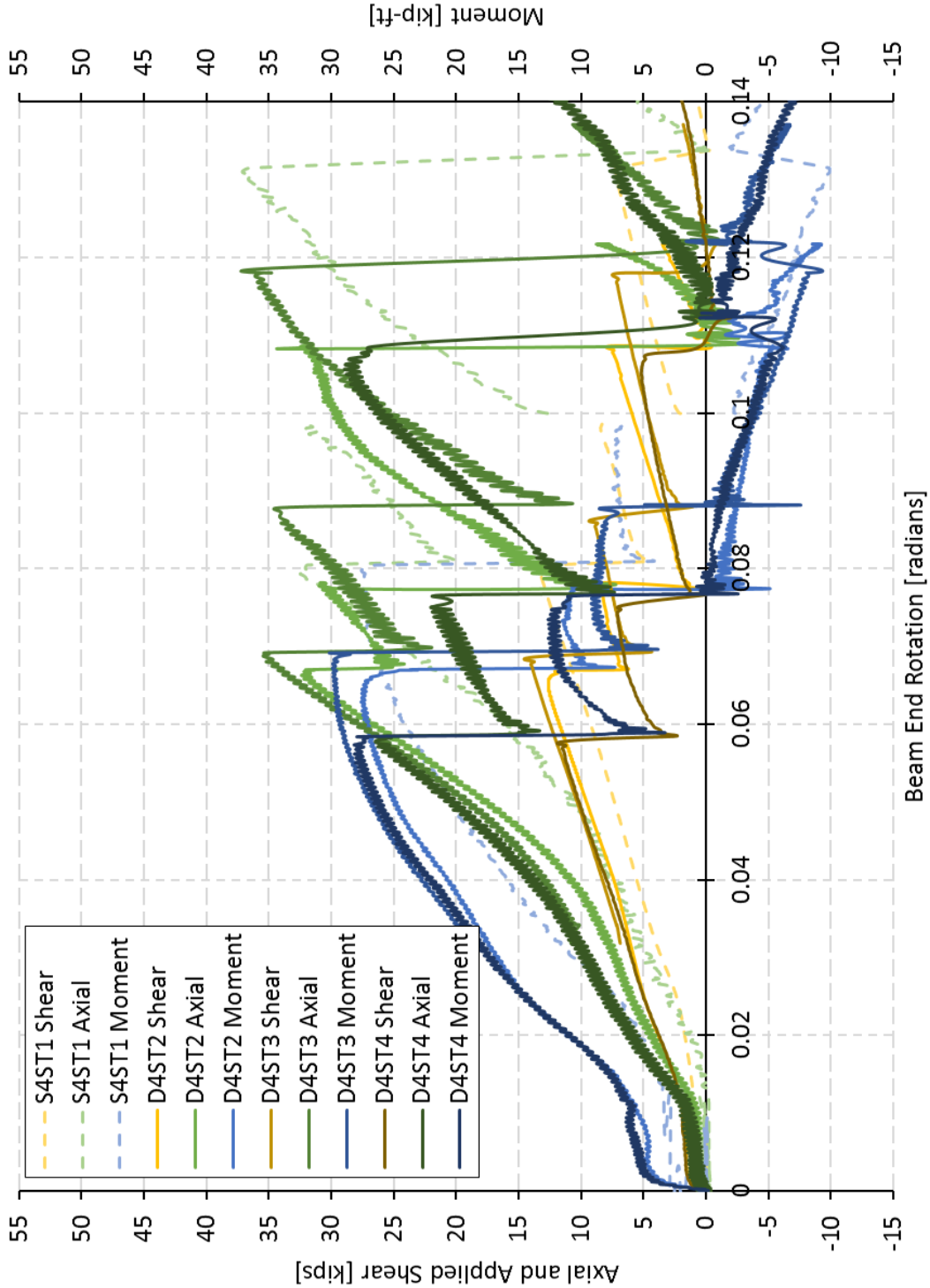

Figure 4.62: Four-Bolt Right Side Bolt Line Forces versus Beam End Rotation.

4.4.3 Five-Bolt Tests

Figures 4.63 and 4.64 show tests S5ST1 and D5ST3 bolt line forces. The bolt line forces do not show much shear, rotation, axial, and moment magnitude variation as the test proceeded, typically less than 1% difference. It was found that the initial bolt shear rupture occurred with slightly less rotation for the quasi-dynamic tests as compared to the static test. The difference is approximately 0.005 radians. This is much less than was seen for the four-bolt configuration. The second and third bolt failure occurred nearly at the same rotation magnitudes for static and quasi-dynamic tests.

The galvanized bolts in this test configuration showed the same trend as with the four-bolt configuration. As the bolts began to fail, the bolts fail at 0.005 radians less than dynamic tests utilizing non-galvanized bolts. The bolts rupture under less axial and shear force magnitudes, but the moment magnitudes are similar to that of the other tests.

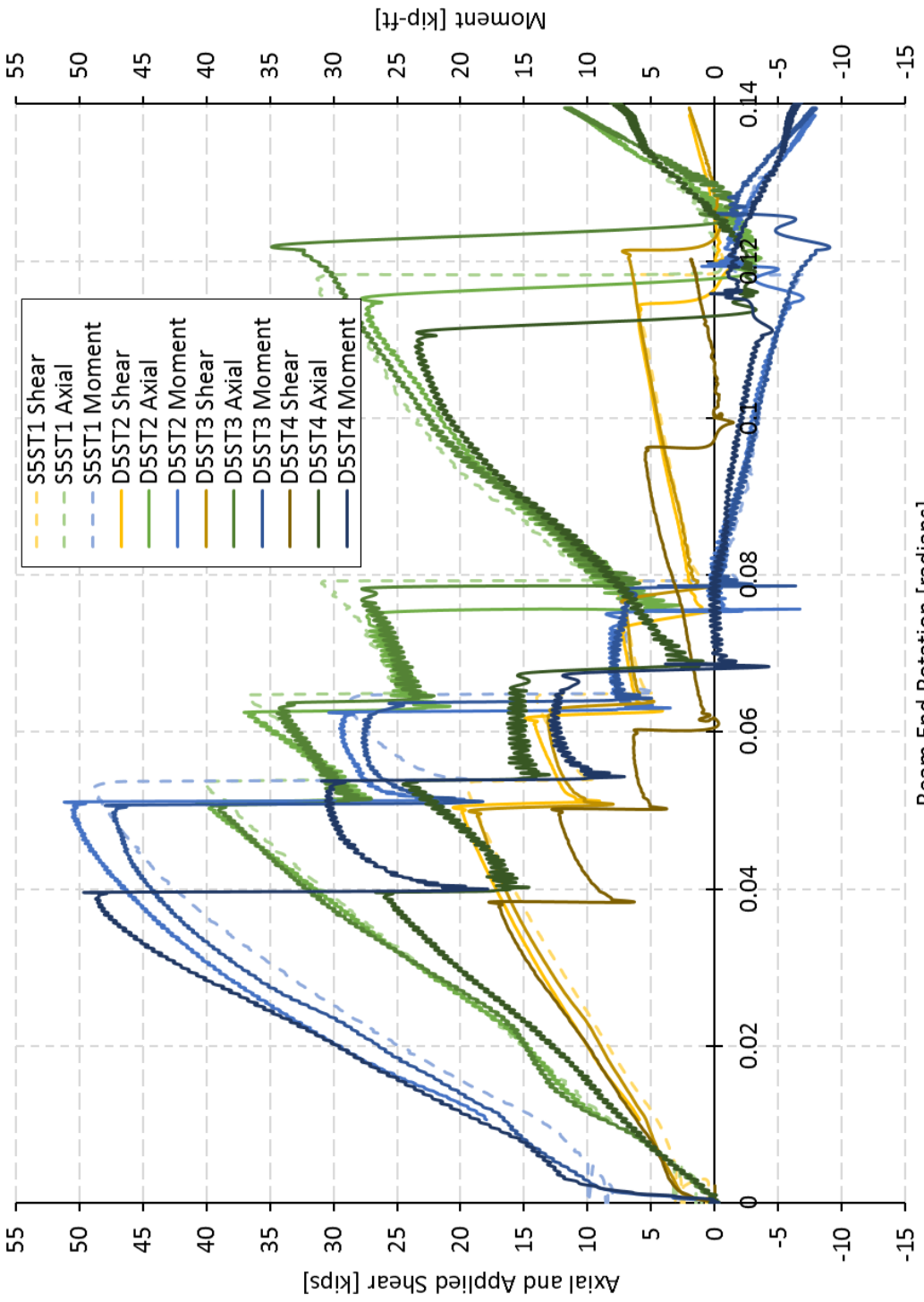

Figure 4.63: Five-Bolt Left Side Bolt Line Forces versus Beam End Rotation.

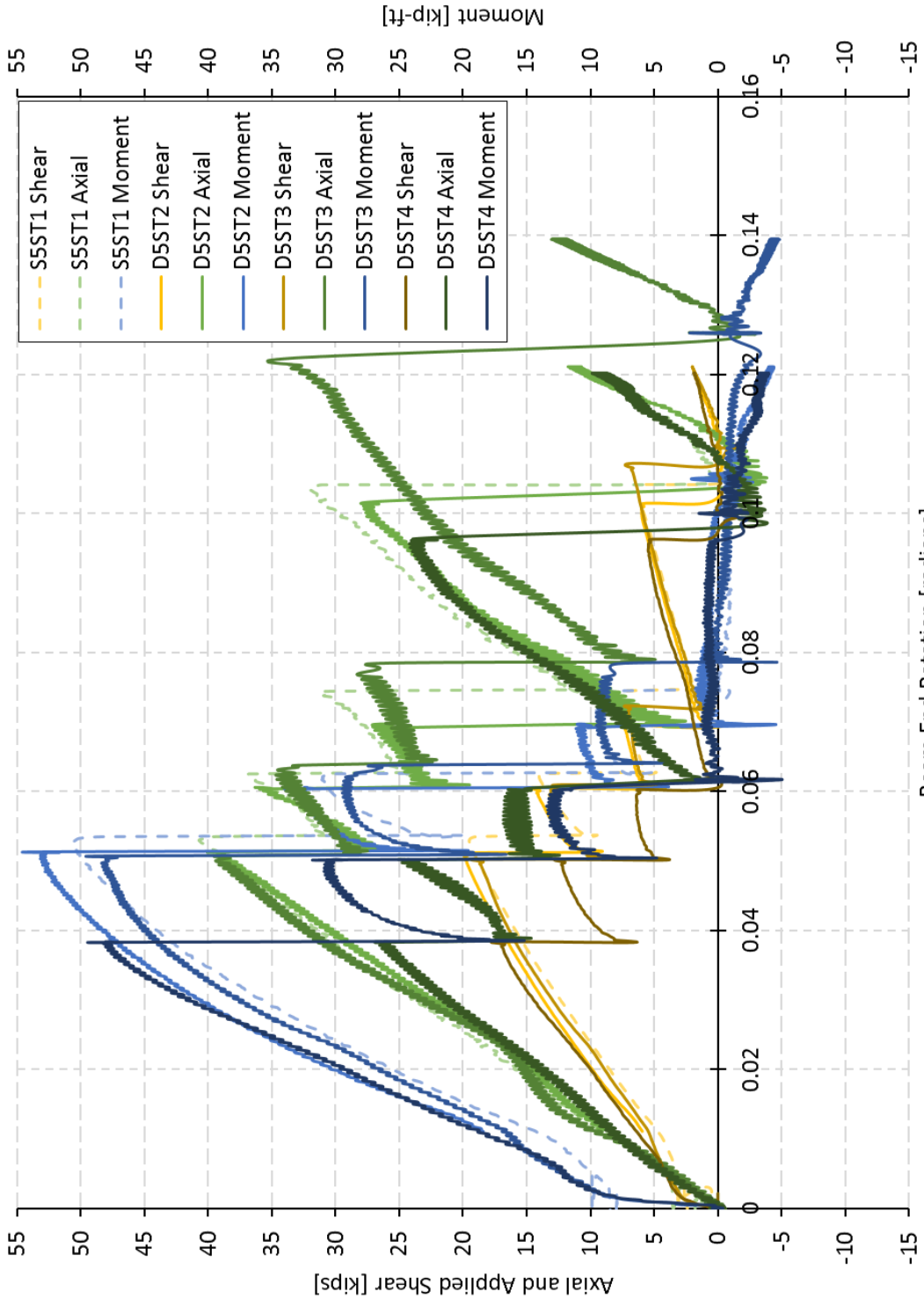

Figure 4.64: Five-Bolt Right Side Bolt Line Forces versus Beam End Rotation.

4.4.4 Summary

When comparing the static tests performed in this research to the quasi-dynamic tests, it was found that four- and five-bolt configuration in the quasi-dynamic tests fail with less rotation than the corresponding static tests.

The three-bolt tests are somewhat inconclusive with respect to the hypothesis, due to the data gap present in one of the tests.

It is conclusive that as the number of bolts increase, the difference in rotation begins to decrease. As the number of bolts increase, more work must be done in the system to achieve failure. More bolts are able to resist more work, resulting in higher bolt line forces being resisted.

4.5 Comparison with Previous Research

As discussed previously, this is an expansion on the work done by Thompson [3]. A fundamental difference between the current research and the tests conducted by Thompson is that the current tests resulted in multiple bolt failures, whereas not every test by Thompson proceeded past the first bolt failure. Thus, comparisons may only be made up to the point of first bolt rupture in the three-bolt configuration and the second bolt rupture in the four- and five-bolt configurations. All quasi-dynamically loaded tests were used in the comparison plots shown in this section.

4.5.1 Three-Bolt Tests

Figures 4.65 and 4.66 demonstrate the bolt line forces of Thompson's statically loaded tests, shown as dashed lines, and the quasi-dynamically loaded test results, shown as solid lines. The initial bolt failure of the quasi-dynamic test occurred under less rotation than the initial failure in Thompson's static test. Unlike the comparison between

the static tests in this research, the dynamically loaded tests were found to fail sooner than Thompson's [3] static tests. The net difference in rotation between those failures is slightly more than 0.02 radians.

The forces of these tests differ between the test results seen in Section 4.4. The moment is similar in maximum magnitude; however, axial and shear in the static test is almost consistent with that of the second bolt rupture found in the quasi-dynamic test. It was found that the statically loaded test acquired about 7 kips of shear, 50 kips of axial force, and 13 kip-feet of moment. The bolt line forces for the dynamically loaded tests for the three bolt configuration can be found in Section 4.3.1.4. The dynamic tests failed between 0.005 and 0.01 radians sooner with about 2 kips more shear, between 5 and 9 kips less axial force, and equivalent moment present in the system.

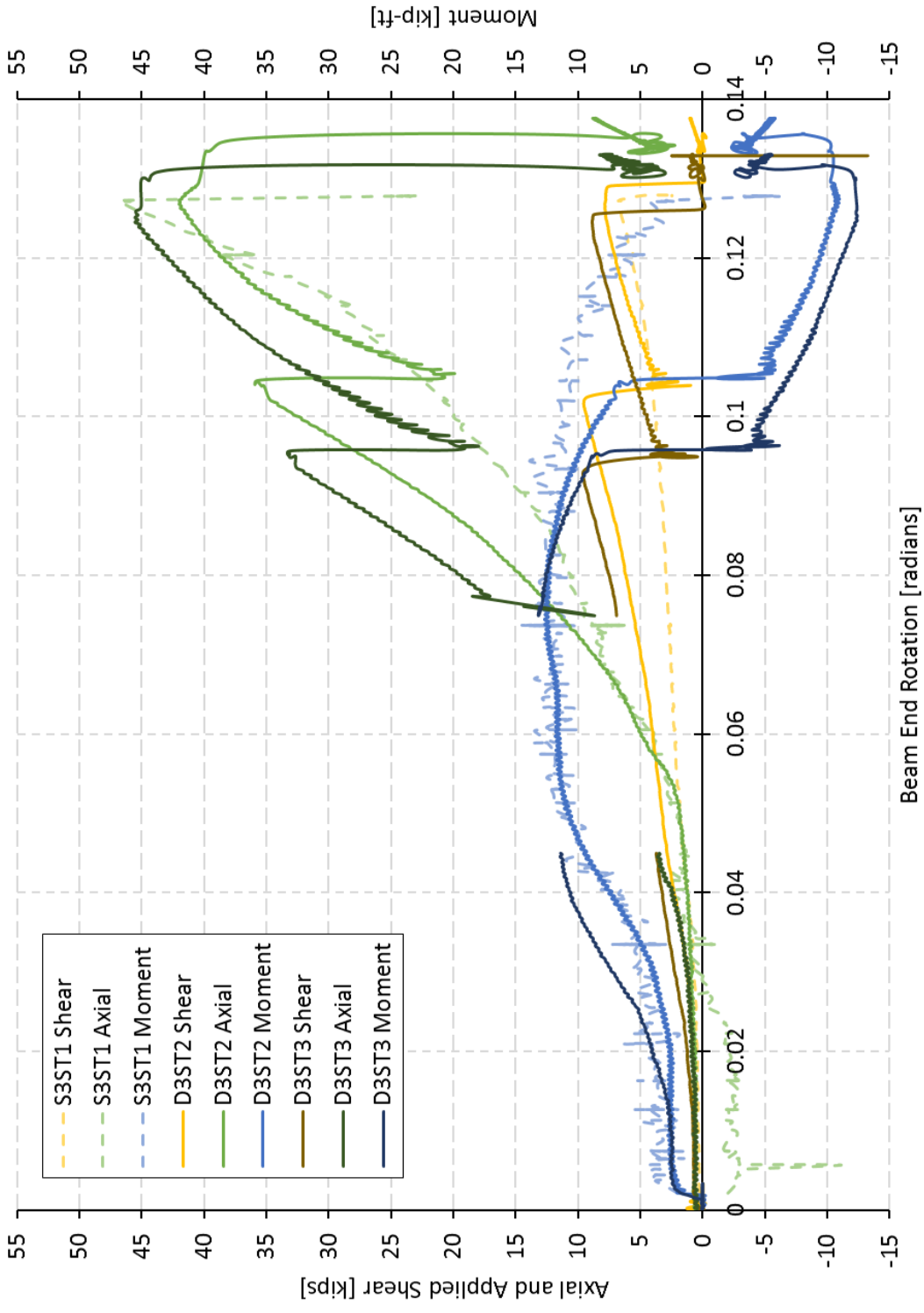

Figure 4.65: Three-Bolt Left Side Bolt Line Forces versus Beam End Rotation.

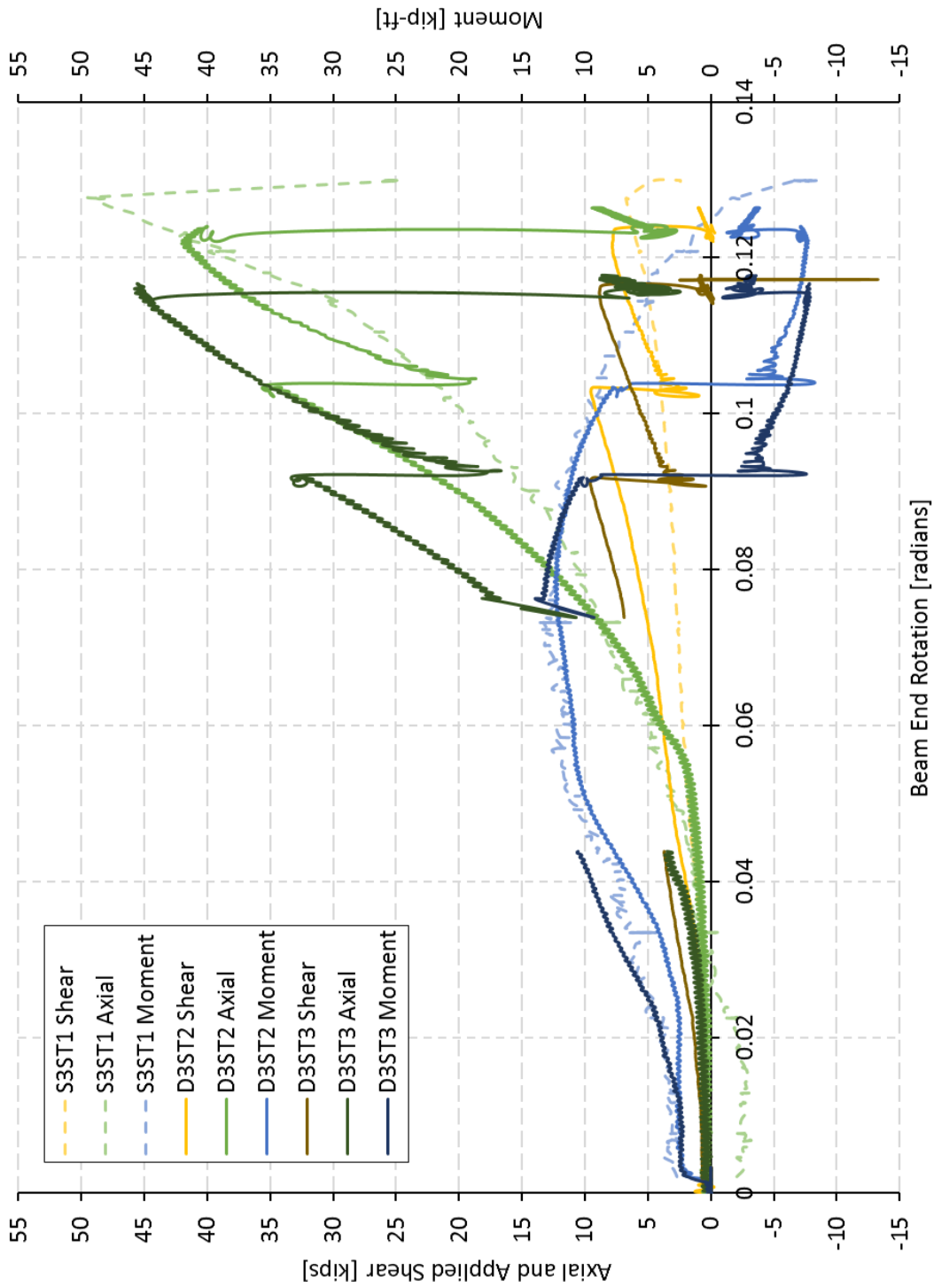

Figure 4.66: Three-Bolt Right Side Bolt Line Forces versus Beam End Rotation.

4.5.2 Four-Bolt Tests

Figures 4.67 and 4.68 show the four-bolt configuration comparisons. The bolt line forces in the plots are similar for axial force and moment up to the point of first bolt rupture. Shear force in Thompson's statically loaded test was much lower than that found in the quasi-dynamic test, about 7 kips less. After initial failure, the bolt line forces do not show any similarities. At secondary bolt failure, Thompson's static test showed similar shear, but the axial forces began to increase rapidly reaching about 67 kips at test completion. This was almost 35 kips higher than the dynamically loaded tests. The moment for Thompson's static test decreased after the first bolt break. The dynamic tests show that the axial moment rises, but bolts break two more times. Thompson's testing shows a sharp decline in moment capacity after the first bolt broke, whereas the current testing shows that moment recovers after the first bolt breaks.

This comparison agrees with observations from Section 4.4 that bolt shear rupture occurs at a lower rotation magnitude in quasi-dynamic loading tests as compared to static loading, the rotational difference being about 0.03 radians lower for quasi-dynamic loading. This is 0.02 radians more than what was found in the comparisons of the current research.

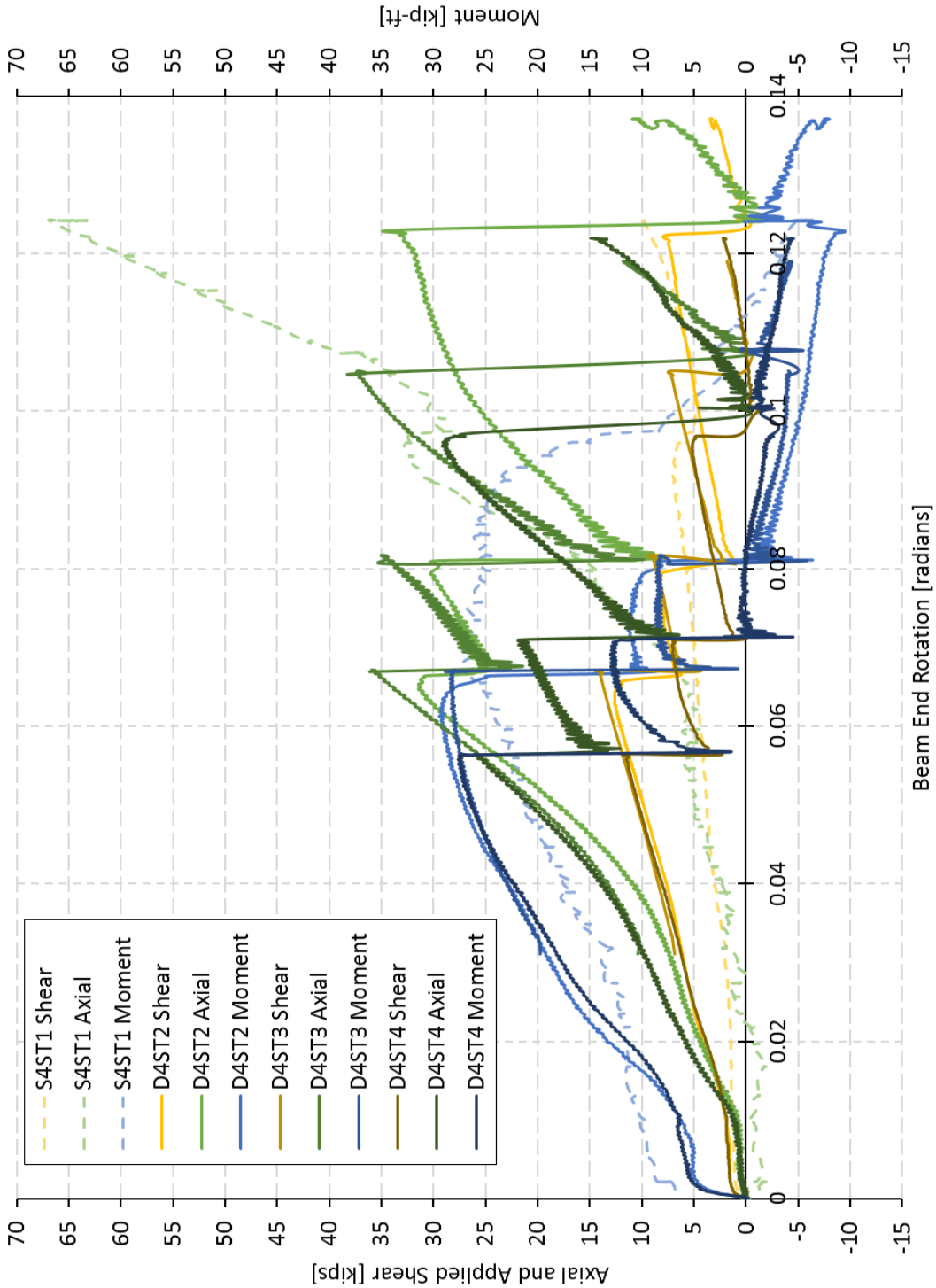

Figure 4.67: Four-Bolt Left Side Bolt Line Forces versus Beam End Rotation.

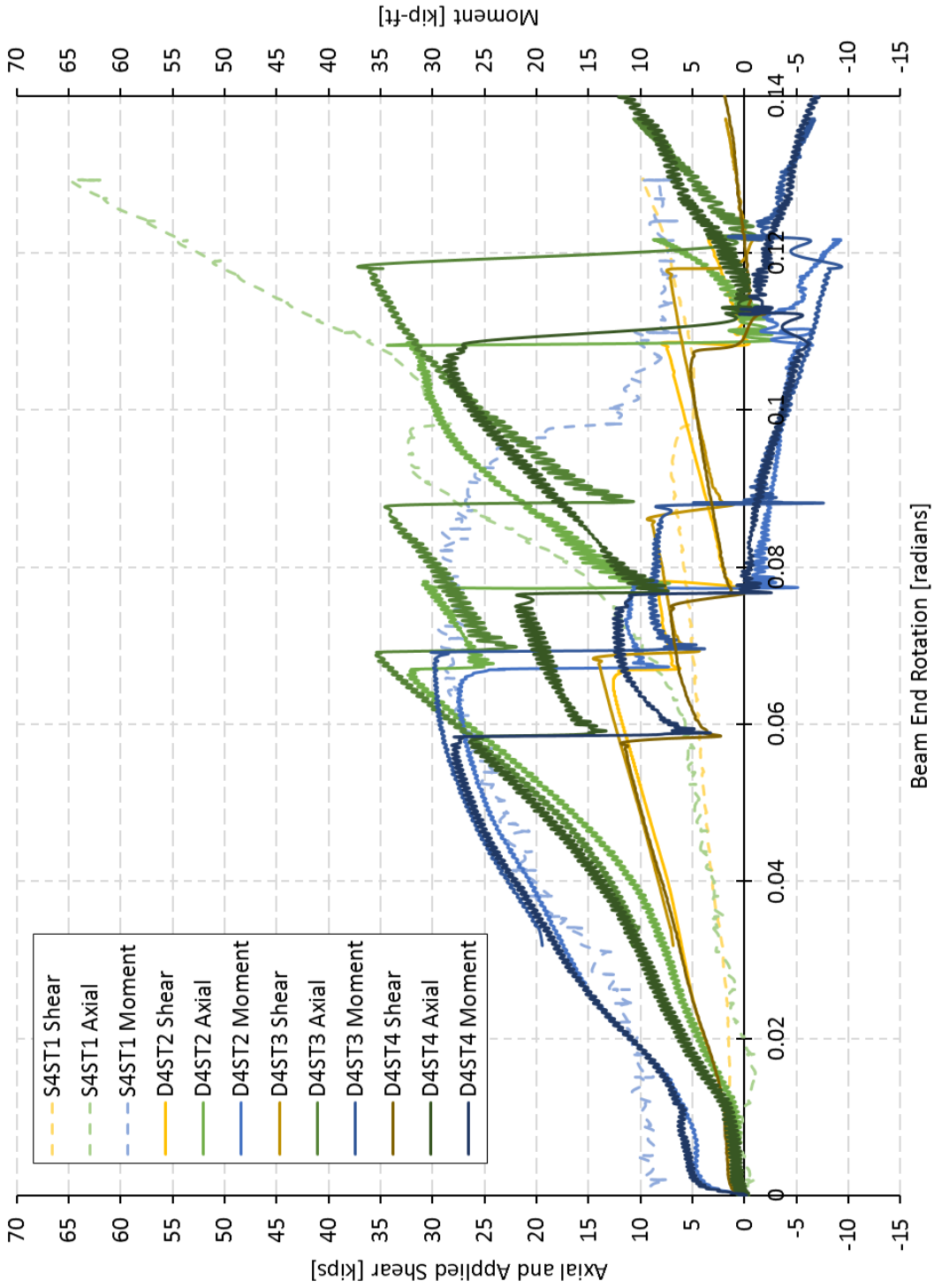

Figure 4.68: Four-Bolt Right Side Bolt Line Forces versus Beam End Rotation.

4.5.3 Five-Bolt Tests

A comparison of the five-bolt configurations can be seen in Figures 4.69 and 4.70. The plots show that moment followed the similar trends and magnitudes between Thompson's results and the results of the current research. In addition, trends in moment remained similar up to the point of the second bolt fracture. Shear force was slightly lower in Thompson's static test, around 6 kips less during the entire test. The axial force was found to be 15% higher in Thompson's test than in the dynamic testing, a difference of about 6 kips. Another difference between the statically loaded tests and the dynamically loaded tests is that the axial forces in the second bolt failure occurs at slightly higher axial forces in the static tests while the dynamic tests decrease in axial force after each bolt failure. Also, it can be seen that Thompson's static test shows that the axial force did not begin to significantly increase until about 0.03 radians while the dynamic tests began increasing as soon as testing began.

The five-bolt configurations confirm the hypothesis that dynamically loaded connections will experience bolt failures at less rotation than statically loaded connections. The difference in rotation between the two tests was slightly higher than 0.045 radians. As a comparison, the difference in the four-bolt tests was about 0.005 radians.

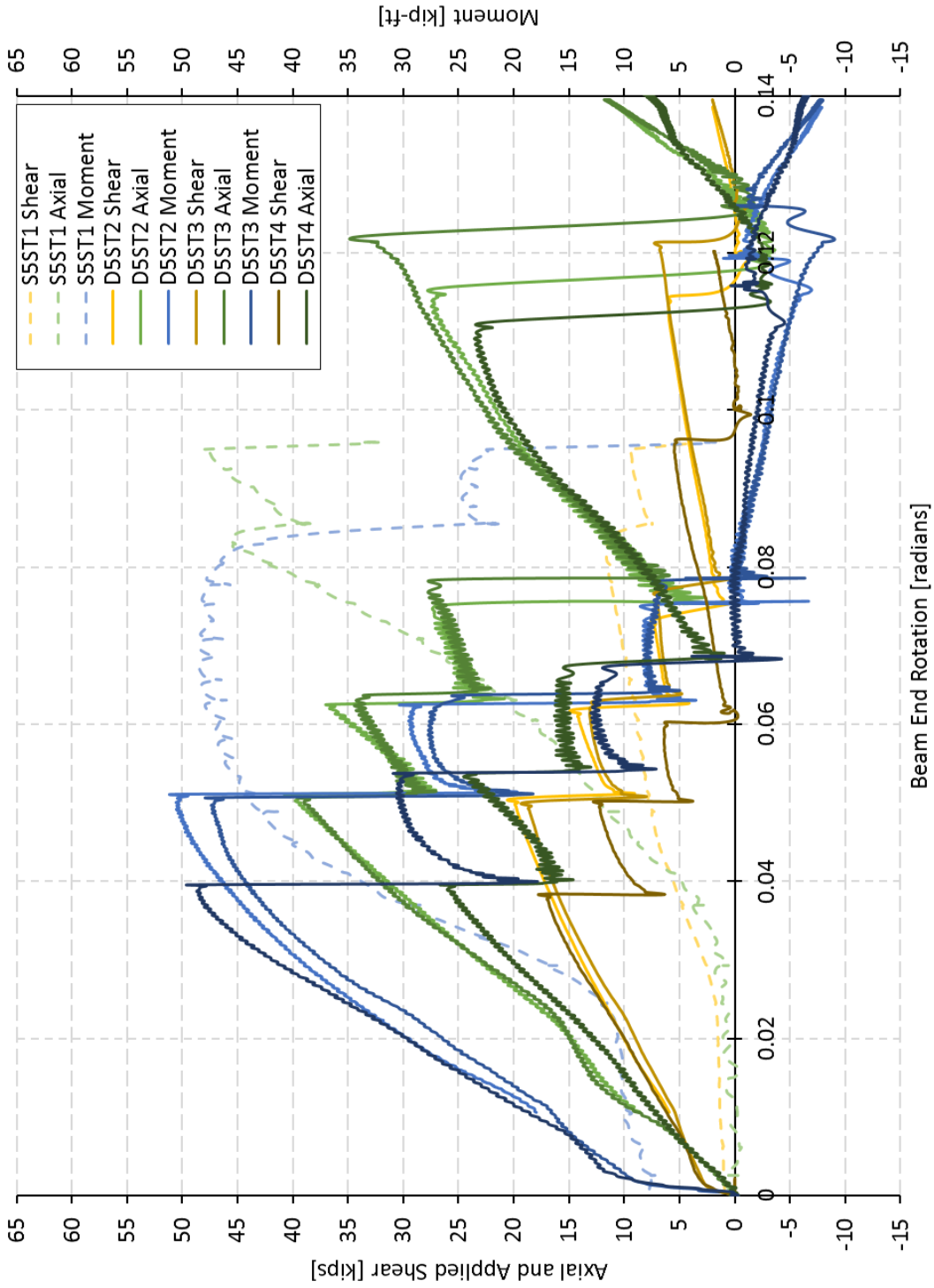

Figure 4.69: Five-Bolt Left Side Bolt Line Forces versus Beam End Rotation.

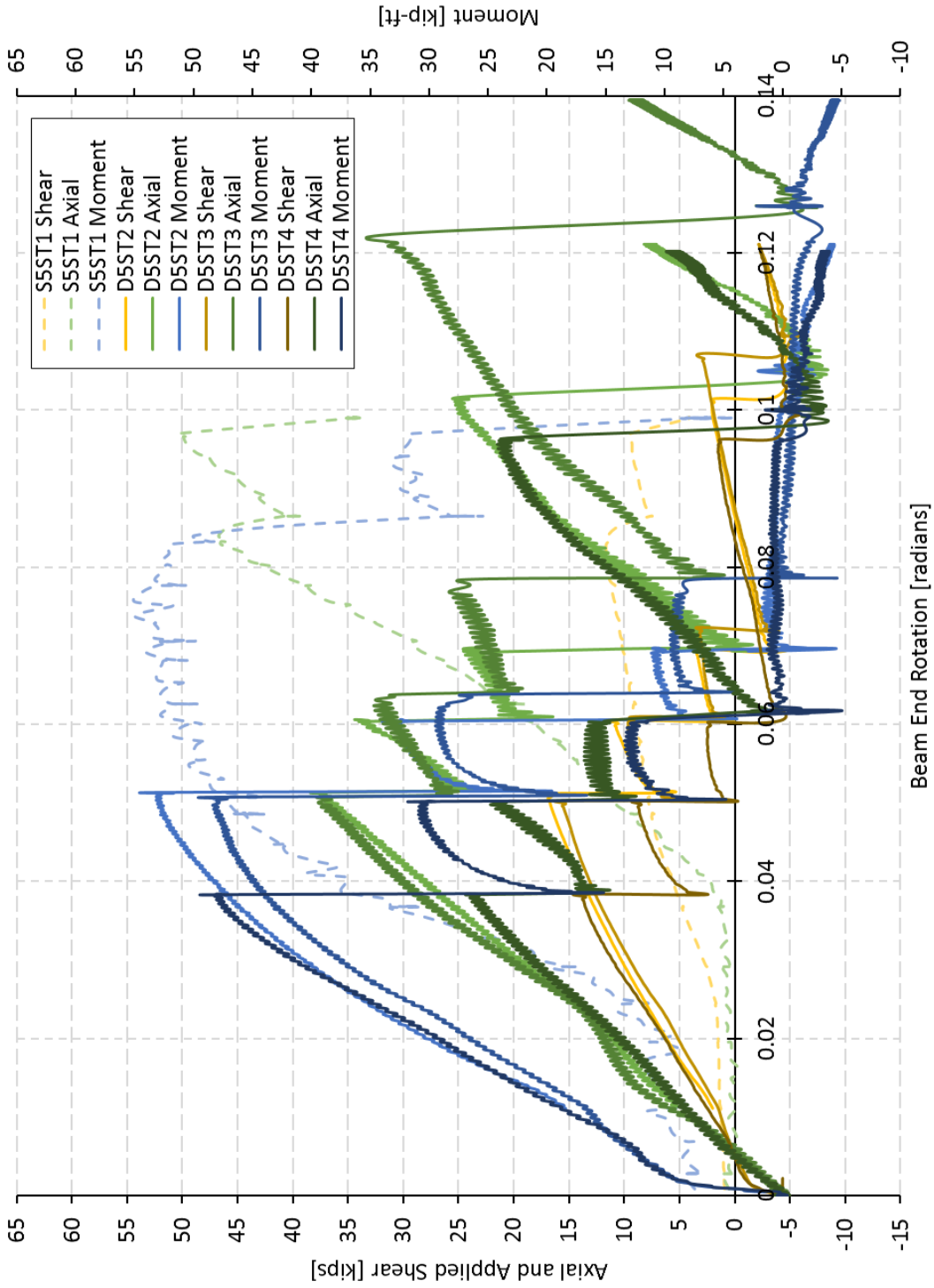

Figure 4.70: Five-Bolt Right Side Bolt Line Forces versus Beam End Rotation.

4.5.4 Summary

When comparing the static tests performed by Thompson [3] to the quasi-dynamic tests, it was found that every quasi-dynamic test experienced first-bolt failure at less rotation than the corresponding static test.

All configurations maintained similar moment capacities between both the static and dynamic tests. For all configurations, the shear capacity was lower in the static tests than the dynamic tests. As for axial forces, both the three- and four-bolt tests show final bolt rupture occurring at much higher axial forces in the static tests than in the dynamic tests. The five-bolt test did not show this drastic spike at final bolt failure; however, bolt failures occurred at loads higher than in the dynamic tests.

4.6 Statics Verification

A statics verification was performed to ensure that the data collected for each of the tests were reliable. The forces used in the statics verification were calculated at the same rotation between all of the tests, 0.02 to 0.04 radians. This rotation range was used because it occurred before initial bolt failure while the test remained in the linear-elastic range. This meant that the test beam was statically determinate and elastic, allowing

fundamental statics to be used in the analysis. Figure 4.71 shows a free body diagram of the test beam.

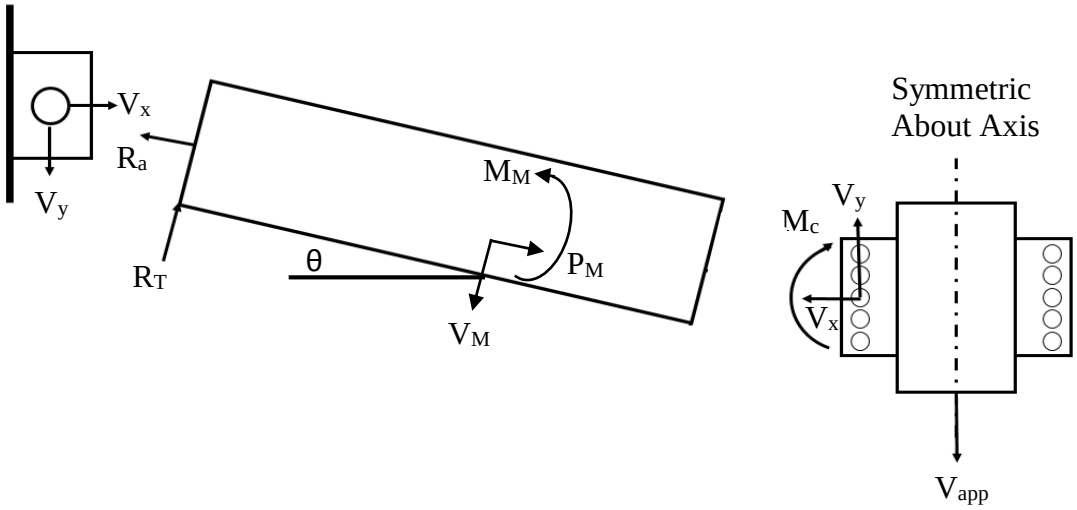

Figure 4.71: Free Body Diagram for Bolt Line Forces.

The longitudinal load R_A was set equal to that of P_M, the calculated axial load in the member. Transverse reactions in the member were calculated by summing the moment about the strain gauge location, shown as

$$R_T = \frac{M_M}{L_{SG}}, \quad (13)$$

where

R_T = Transverse reaction in the beam, kips,

M_M = Calculated moment at strain gauges solved using Equations (10), kip-in.,

L_{SG} = Distance from the true pin connection to the strain gage locations, equal to 36.125 in.

Vertical reaction, V_y, at the true pin was solved for by adding vertical components using trigonometry due to the rotation present in the system. Combining the vertical components of force from measured axial and moment, the total vertical reaction was computed as

$$V_y = R_A \sin\theta + R_T \cos\theta, \quad (14)$$

where

V_y = Vertical reaction at the true pin connection for one side, kips,

θ = Calculated beam end rotation, radians.

Reactions at the connection are equal and opposite of the reactions at the true pin. As discussed in Section 4.2, the moment at the connection, M_c, was found from linear extrapolation of the moment at the strain gauges, M_M.

A summary of the results from the statics verification for each test can be seen in Table 4.13. Test D4ST3 was not verified due to a data acquisition error within the data range under consideration. The data collected for points 0.02 to 0.04 radians of rotation were averaged and used in the calculations to find V_y in kips for each side. The results for the two sides were added together and compared to the full applied force, V_{app},. The percent error calculated for each test specimen ranged from 0.50% to 4.76%. Since the percent error in each experiment was relatively low, it proves that the input force measured effectively matches the internal forces and moments calculated through the strain measurements.

Table 4.13: Experimental Statics Verification.

Test Specimen	Side of Specimen	P_M [Kips]	M_M [Kip-In.]	Rotation [Radians]	V_y [Kips]	V_y Total [Kips]	V_{app} [Kips]	Error [%]
S3ST1	Right	1.24	36.60	0.0452	1.07	2.32	2.26	2.65
	Left	1.24	43.14		1.25			
D3ST2	Right	0.69	23.55	0.0429	0.68	1.391	1.34	3.81
	Left	0.91	24.12		0.71			
D3ST3	Right	1.73	37.84	0.0441	1.13	2.3	2.22	3.60
	Left	1.38	39.82		1.17			
S4ST1	Right	5.10	63.29	0.0176	1.85	3.78	3.88	2.58
	Left	4.95	66.50		1.93			
D4ST2	Right	7.83	94.44	0.0454	2.98	6.16	5.88	4.76
	Left	7.33	102.47		3.18			
D4ST3[a]	Right	---	---	---	---	---	---	---
	Left	---	---		---			
D4ST4	Right	9.91	95.47	0.0499	3.14	6.28	6.02	4.32
	Left	9.59	95.89		3.14			
S5ST1	Right	23.57	195.04	0.0451	6.47	12.75	12.24	4.17
	Left	22.95	189.11		6.28			
D5ST2	Right	23.04	226.61	0.0465	7.36	14.44	13.92	3.74
	Left	23.39	216.07		7.08			
D5ST3	Right	23.49	205.12	0.0473	6.80	13.53	13.07	3.52
	Left	23.31	202.72		6.73			
D5ST4	Right	13.90	161.25	0.0358	4.97	10.07	10.02	0.50
	Left	13.31	166.68		5.10			

[a] Statics Verification could not be performed due to error in data acquisition

4.7 Bolt Force Analysis

A basic bolt force analysis was conducted on each test specimen. This analysis was conducted using the forces and moment within the range where the moment was within the top one percent of maximum moment. The goal is to better understand how the interacting forces and moments act on the bolt. Kulak *et al.* [21] performed research on single bolts in shear to determine the ultimate bolt shear strength for ASTM A325 bolts. This value, in terms of stress, was found to be approximately 80.1 ksi. Thompson [3] used this as a benchmark to calculate that an ASTM A325 bolt with threads excluded could resist 35.4 kips.

Yang and Dewolf [22] performed research into the galvanization of plates used in connections with the use of 7/8 in. ASTM A325 bolts. This provides insight into how the galvanization process effects the capacity of a connection.

The galvanization process adds a coating of zinc to the outside of the steel, which affects the shear capacity of the bolts in the connection. In the research presented by Yang and Dewolf [22], it was found that the shear capacity of the connections with thick galvanized coatings was reduced due to the loss of clamping force. Yang and Dewolf found that there was a 30 kN, or 6.7 kip, difference in shear. This change in capacity is similar to that found in the current research for galvanized bolts.

To conduct the bolt force analysis, the axial forces measured within the range of the top one percent of maximum measured moment were divided into their component forces. The horizontal component of measured axial force was shown as

$$P_x = \frac{P_M * \cos\theta}{n}, \tag{15}$$

while the vertical component of the measured axial force was shown as

$$P_y = \frac{P_M * \sin\theta}{n}, \tag{16}$$

where P_M and θ are shown in Figure 4.71 and n is the number of bolts.

The Instantaneous Center of Rotation (ICOR) Method was used to analyze the applied shear, axial, and moment's effect on bolt forces. Unlike Thompson [3], elastic method for determining bolt forces wasn't used due to the inclusion of plastic deformations due to the quasi-dynamic load application.

As seen in Figure 4.72, the ICOR method specifies moment M_c shown in Figure 4.71 being transformed into a normalized unit shear force V_{norm} applied at an eccentricity,

e. Figure 4.73 presents the component bolt forces $F_{y,n}$ and $F_{x,n}$ at the identified rotation, θ, for each test with respect to the line of action.

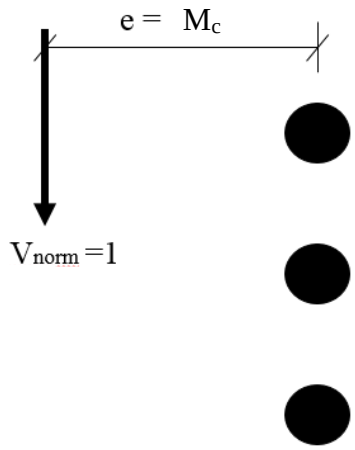

Figure 4.72: Moment ICOR Model.

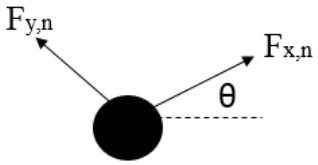

Figure 4.73: Moment ICOR Model Bolt Component Forces.

Trigonometric principles were used to transform the bolt component forces into one single force acting on the bolt. The horizontal force, $H_{mx,n}$, at each bolt was calculated as

$$H_{mx,n} = \left(F_{x,n} \cos\theta\right) + \left(F_{y,n} \sin\theta\right). \quad (17)$$

The vertical bolt force, $H_{my,n}$, was taken as

$$H_{my,n} = \left(F_{x,n} \sin\theta\right) + \left(F_{y,n} \sin\theta\right). \quad (18)$$

Due to the normalized shear value of one, vertical bolt forces due to measured moment were omitted resulting in simplified equations. The simplified equation for Equation (17) is shown as

$$H_{mx,n} = \left(F_{x,n} \cos\theta\right). \tag{19}$$

Equation (18) was simplified to

$$H_{my,n} = \left(F_{y,n} \sin\theta\right). \tag{20}$$

As previously mentioned, an ICOR method analysis was also conducted for eccentrically applied shear. The tests were conducted with an eccentricity of 3 1/2 in. due to dimensions of the connection. The ICOR method determined two forces, one in the horizontal direction $V_{mx,n}$, and one in the vertical direction, $V_{my,n}$. The bolt shear force $V_{bmax,n}$ was determined using a summation of the component forces. Thus,

$$V_{b\,max,n} = \sqrt{\left(P_x + H_{mx,n} + V_{mx,n}\right)^2 + \left(P_y + H_{my,n} + V_{my,n}\right)^2}. \tag{21}$$

The components of $V_{b\,max,n}$ can be seen in Figure 4.74 representing the analyzed bolt forces for each bolt. Table 4.14 shows these combined bolt forces. It can be seen that the bolt shear capacities for the three-bolt tests are relatively at similar bolt forces slightly lower than the benchmark set by Thompson [3]. As for the four- and five-bolt tests, the bolt forces calculated were consistently higher than the calculated benchmarks for both the carbon steel bolts and the galvanized bolts.

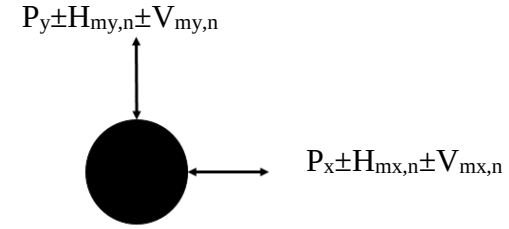

Figure 4.74: Bolt Force Analysis Components.

Table 4.14: Summary of Bolt Forces at Each Bolt.

Test Specimen	Side of Specimen	Maximum Bolt Forces (kips)				
		Bolt 1	Bolt 2	Bolt 3	Bolt 4	Bolt 5
S3ST1	RIGHT	29.34	3.90	22.18	---	---
	LEFT	28.89	3.84	21.84	---	---
D3ST2	RIGHT	30.10	4.31	22.13	---	---
	LEFT	30.64	4.24	22.85	---	---
D3ST3[a]	RIGHT	---	---	---	---	---
	LEFT	---	---	---	---	---
S4ST1	RIGHT	39.12	33.04	17.47	23.49	---
	LEFT	39.10	33.01	17.63	23.67	---
D4ST2	RIGHT	38.02	32.07	17.47	23.38	---
	LEFT	39.78	33.49	19.10	25.34	---
D4ST3	RIGHT	41.76	35.30	18.47	24.87	---
	LEFT	43.91	37.06	20.38	27.18	---
D4ST4	RIGHT	36.85	30.94	18.70	24.55	---
	LEFT	36.53	30.70	18.40	24.21	---
S5ST1	RIGHT	43.97	40.35	8.54	24.32	27.92
	LEFT	43.96	40.23	8.35	24.43	28.03
D5ST2	RIGHT	46.48	42.61	8.19	27.23	31.08
	LEFT	44.84	41.13	8.32	25.50	29.19
D5ST3	RIGHT	42.76	39.24	8.06	24.04	27.54
	LEFT	42.29	38.81	8.10	23.55	27.00
D5ST4	RIGHT	38.64	35.30	5.55	25.15	28.48
	LEFT	40.10	36.62	5.45	26.68	30.16

[a]Bolt force analysis for test D3ST3 was unable to be performed due to data acquisition errors

4.8 Work Analysis

It was hypothesized that the work done on the connection would be the same between a test which was statically loaded and one which was dynamically loaded. This was hypothesized due to the fact that a connection would see the same amount of work due to the forces and moments present in the system, regardless of how quickly the forces were introduced into the system. The work considered as part of the current research was evaluated within the linear-elastic range (i.e., prior to initial bolt fracture).

The work done due to a particular force can be found by calculating the area under the force versus displacement or moment versus rotation curve. To determine the work done on the connection each force needed to be integrated over its respective displacement: moment in the connection over rotation, axial force in the connection over beam elongation, and total applied force on the test specimen over vertical displacement. The first step in the process to calculate work was to filter the data using MATLAB. A copy of the MATLAB script can be found in Appendix F. Filtering removed any oscillation of data due to noise. A Butterworth Filter was used to reduce the frequency response in the data set by 80%. Figure 4.75 shows a typical data set (blue line) versus the filtered data (orange line). The shaded triangle included in Figure 4.75 shows an example of the area under the data that was calculated for applied load. This is equal to the amount of work done on the connection due to applied force. This same process was repeated for moment and shear.

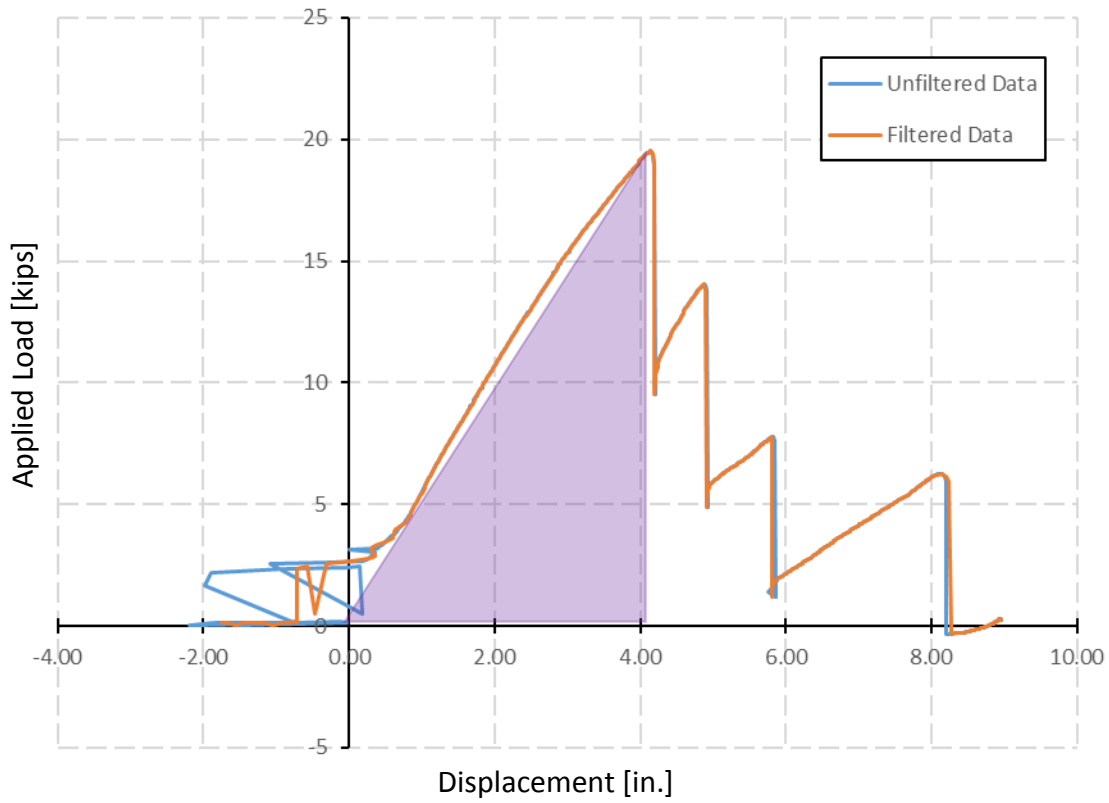

Figure 4.75: Test S5ST1 Filtered versus Unfiltered Data.

In order to calculate work done by axial force, beam elongation was calculated by

$$\Delta = \frac{\delta}{sin\theta} - x_f, \tag{22}$$

where

Δ= beam elongation, in.,

δ= actuator deflection in.,

θ= rotation of beam, radians,

x_f= horizontal distance from the true pin to the supported column flange face equal to 78.375 in.

After finding the amount of beam elongation in one time step, work was calculated through the summation of the trapezoidal area shown as

$$W = \sum[\frac{\Delta}{2} \times (P_{M1} - P_{M2})] , \quad (23)$$

where

W= work, in.-kips,

Δ= beam elongation at time step ‘n’, in.,

P_{Mn}= Axial force at time step ‘n’, kips.

Work done through moment was calculated by

$$W = \sum[\frac{(\theta_2 - \theta_1)}{2} \times (M_{M1} - M_{M2})] , \quad (24)$$

where

W= work, in.-kips,

θ_n= Rotation at time step ‘n’, radians,

M_{Mn}= Moment at time step ‘n’, kip-feet.

Work done by the shear force was then calculated as

$$W = \sum[\frac{(\delta)}{2} \times (V_{M1} - V_{M2})] , \quad (25)$$

where

W= work, in.-kips,

δ= actuator deflection at time step ‘n’, in.,

V_{Mn}= Applied load at time step ‘n’, kips.

After each of the elements of the work were calculated, the total work done was calculated through the summation of the elements of work. Table 4.15 shows the work done for the three-bolt tests is around 40 in.-kips, averaging to 39.46 in.-kips. After another bolt was added to the configuration, the work done by the system featured a much wider range, from 31.03 to 46.72 in.-kips. The average range of work done for the four-bolt configuration was 38.49 in.-kips. The five-bolt configuration was associated

with a higher level of work. The average for the five-bolt configuration was 47.83 in.-kips, ranging from 32.5 to 55.24 in.-kips. Axial work done on the system decreases as the number of bolts increases. Work done through applied load and moment decreases as the number of bolts increases. The data for the four- and five-bolt configurations were skewed slightly due to the addition of Tests D4ST4 and D5ST4, the tests using galvanized bolts.

Table 4.15: Summary of Work Done.

Test	Axial Work [inch-kips]	Applied Load Work [inch-kips]	Moment Work [inch-kips]	Work [inch-kips]	Percent Error [%]
S3ST1	9.80	30.22	0.75	40.77	--
D3ST2	9.63	28.74	0.79	39.16	3.95
D3ST3	7.51	30.14	0.78	38.43	5.74
S4ST1	8.71	36.80	1.22	46.72	--
D4ST2	5.41	32.91	1.10	39.42	15.62
D4ST3	6.05	29.79	.094	36.79	21.25
D4ST4	3.78	26.33	0.92	31.03	33.58
S5ST1	6.16	47.36	1.72	55.24	--
D5ST2	5.27	47.23	1.76	54.27	1.76
D5ST3	5.15	42.64	1.52	49.31	10.73
D5ST4	2.06	29.36	1.08	32.50	41.17

As seen in Table 4.15, the hypothesis that work done between the static test and quasi-dynamic tests would be the same in the connection was proven. Test D3ST2 differed from S3ST1 by 4% while test D3ST3 differed by 6%. When comparing the work performed in the four- and five-bolt tests, the galvanized bolt data were disregarded. The four-bolt range differed by 15% for D4ST2 and 21% for D4ST3. The five-bolt tests D5ST2 and D5ST3 compared with S5ST1 differed by 2% and 11%, respectively. Due to the data inconsistencies at the beginning of test D4ST3, the work done on the system was calculated through filtered data which effectively made a linear line from zero to the first

point of data. Other factors that resulted in error in the calculations of work include that during the four- and five-bolt tests, static tests increased and broke immediately while the dynamic tests increased and began letting off before bolt break occurred. An example of this tapering trend can be seen in Figure 4.61 between 0.063 and 0.065 radians. Another source of error is that due to catenary action in the dynamic tests, the forces increased at a much higher slope initiating earlier, not allowing for the slight accrual of load seen in the static tests. Inconsistencies such as these affected the calculation of work, thus affecting the comparison with the statically loaded test resulting in a higher percent error.

Chapter 5

CONCLUSIONS

5.1 Research Summary

The purpose of the research was to expand upon the testing program presented by Thompson [3]. The testing was performed to quantify the shear tab connection's behavior when subjected to a quasi-dynamic loading scenario.

5.1.1 Static Testing Comparisons

Eleven experimental tests were performed during the current research. Three of the tests were statically loaded, meaning the tests were loaded at a rate of one inch per minute. During the testing, it was found that the static tests performed by Thompson [3] compared well to the static tests performed in the current research. One can conclude from both sets of results that the connections have an innate robustness when subjected to extraordinary rotational demand that results in interactive shear, axial force and moment.

One main difference between the current research and the testing performed by Thompson [3] was his second failure mechanism. Thompson found that some of his shear tabs were "unzipping" from bolt hole to bolt hole. This phenomena was not seen during the current research and shows the differences in the data presented by Thompson as compared to the current research.

5.1.2 Quasi-Dynamic Effects

Out of the eleven tests performed, eight of the tests were conducted using a quasi-dynamic loading. These tests had an average loading rate of 2.7 in. per second. The quasi-dynamic tests sustained measurable moment resistance in each configuration of the shear plate tests. The resistance increased as the number of bolts in the connection

increased. This trend was also seen in the static tests. Axial forces were also present in the system, which became more dominant in the system as moment resistance reached its peak. The axial forces in the system show that catenary action is present under large deformations and that the connections are able to resist measurable magnitudes of axial force due to the catenary action.

It was hypothesized that the quasi-dynamic tests would follow similar trends as seen in statically loaded tests. This was followed by the hypothesis that the connection would follow the same trends but at lower rotation. Also, the work done by the system would not change regardless of the speed of the applied loading.

The three-bolt configuration showed flexural resistance at the start of each test. Catenary action began as moment plateaued. Initial bolt failure occurred as flexural resistance began to decline. The four-bolt configuration showed similar behavior; however, in the four-bolt tests, catenary action began under less rotation while moment and axial forces increased simultaneously. The five-bolt tests started with an immediate increase in catenary action along with flexural resistance. Bolt failure occurred as moment peaked. All of these results show how the connection can resist unanticipated forces and moments that accrue due to large rotational demands in the connection.

5.1.3 Utilization of Galvanized Bolts

The research showed the effects of using galvanized bolts in connections. Two tests, D4ST4 and D5ST4, used galvanized bolts. These tests showed significantly less axial and shear capacity, and the bolts failed under less rotation than tests that used carbon steel bolts. The shear capacity was approximately two kips lower than seen in the tests without galvanized bolts. The axial capacity was approximately ten kips less.

Moment resistance did not change significantly with the use of galvanized bolts. During the galvanization process, the bolt undergoes a physical change to the outside of the bolt. This physical change lowers the capacities of the bolts. This realization was unanticipated, as the original research plan did not include galvanized bolts. Further studies are warranted in the use of galvanized bolts in connections subjected to interactive loadings.

5.2 Needs for Future Research

The research presented has provided valuable insight into the behavior of single plate connections; however, further research needs to be done. Due to the disruption during data collection, a few tests provided inconclusive data. This was extremely prevalent in the three-bolt tests. It would be worthwhile to conduct a few additional three-bolt tests to confirm the results obtained in the current research.

As mentioned in the last section, the use of galvanized bolts should be researched further. It was found that the capacity of the galvanized bolts showed significant difference when compared to carbon steel bolts. Only two tests were conducted with galvanized bolts in the current research, but the results were compelling. Determining the difference of ASTM A325 carbon bolts and ASTM A325 galvanized was not a primary concern with this research, but it deserves further study as it is evident that there is significant difference between the bolts.

After Thompson [3] completed his research, others –Main and Sadek [4] and Daneshvar and Driver [9]-- conducted finite element modeling to compare to Thompson's experimental data. It would be beneficial to compare the results of the

current research to numerical models in an effort to fully understand the behavior of the connections under quasi-dynamic loading.

Lastly, a set of building design parameters would help efficiently design structures in accordance with this research. As long as these design parameters are met, the connections in a structure would effectively behave the same way, and provide the same robustness as the structures tested in this research. A future project could include a determination of the potential loading and framing geometry that could be supported using the capacities of the connections found herein. This could be done in conjunction with the finite element study discussed previously.

References

[1] Byfield, M., G.L. Kasim, C. Morison and E. Stoddart. 2014."A Review of Progressive Collapse Research and Regulations." United Kingdom. [Internet, www, PDF]. ADDRESS: https://www.semanticscholar.org/paper/A-Review-of-Progressive-Collapse-Research-and-Byfield-Beng/ad366acf20bddd20b73b03b422f490f731605173/pdf

[2] American Institute of Steel Construction (AISC). 2011. *Specification of Steel Construction 14th Edition.* Chicago, IL.

[3] Thompson, Scott. 2009. "Axial, Shear and Moment Interaction of Single Plate 'Shear Tab' Connections." Master's thesis, Milwaukee School of Engineering: Milwaukee, Wisconsin.

[4] Main, Joseph and Fahim Sadek. July 2012. *Robustness of Steel Gravity Frame Systems with Single-Plate Shear Connection.* Technical Note 1749. Engineering Laboratory, National Institute of Standards of Technology.

[5] Liu, Judy. 2000. "Experimental and Analytical Studies of the Cyclic Behavior of Simple Connections in Steel Frame Buildings." Doctoral Dissertation, University of California-Berkeley: Berkeley, California.

[6] Guravich, Susan J., and John L. Dawe. 2006. "Simple Beam Connections in Combined Shear and Tension." *Canadian Journal of Civil Engineering.* Vol. 33 (4), pp. 357-372.

[7] Girhammar, Ulf Arne. 1980. "Behavior of Bolted Beam-Column Connections under Catenary Action in Damaged Steel Structures: D12." *Swedish Council for Building Research.* University of Lulea: Lulea, Sweden.

[8] Sadek, Fahim, Sherif El-Tawil and H.S. Lew. 2008. "Robustness of Composite Floor Systems with Shear Connection: Modeling, Simulation, and Evaluation." *ASCE Journal of Structural Engineering*. Vol. 134 (11), pp. 1717-1725.

[9] Daneshvar, H. and R.G. Driver. "Application of Seismic Steel Connection Experiments to Column Removal Scenario." 2nd Specialty Conference on Disaster Mitigation. 9-12 June 2010.

[10] Alashker, Yasser, Sherif El-Tawil and Fahim Sadek. "Progressive Collapse Resistance of Steel-Concrete Composite Floor." *Journal of Structural Engineering*. October 2010. Pp.1187-1196.

[11] Livermore Software Technology Corporation. 2006. *LS-DYNA Keyword User's Manual*. Livermore, California: Livermore Software Technology Corporation.

[12] Foley, Christopher, Carl Schneeman and Kristine Barnes. "Quantifying and Enhancing the Robustness in Steel Structures: Part 1- Moment-Resisting Frames." *Engineering Journal.* Fourth Quarter, 2008, pp. 247-266.

[13] Computers & Structures, Inc. SAP2000 (Version 18). [Computer program]. Available: Computers & Structures, Inc., 1646 N. California Boulevard #600, Walnut Creek, CA 94596.

[14] Foley, Christopher, Carl Schneeman and Kristine Barnes. "Quantifying and Enhancing the Robustness in Steel Structures: Part 2- Moment-Resisting Frames." *Engineering Journal.* Fourth Quarter, 2008, pp. 247-266.

[15] Khandelwal, Kapil and Sherif El-Tawil. "Collapse Behavior of Steel Special Moment Resisting Frame Connections." *Journal of Structural Engineering.* May 2007, pp. 646-655.

[16] Gamaniouk, Taras. 2014. "Parametric Analysis of Progressive Collapse in High-Rise Buildings." Master's Thesis, Massachusetts Institute of Technology: Cambridge, Massachusetts.

[17] Song, Brian I., Halil Sezen and Kevin A. Giriunas. "Experimental and Analytical Assessment on Progressive Collapse Potential of Two Actual Steel Frame Buildings." Structures Congress, 2010, pp. 1171-1182.

[18] Oosterhof, Steven and Robert G. Driver. "An Approach to Testing the Performance of Steel Connections Subjected to Extreme Loading Scenarios." 2nd International Engineering Mechanics and Materials Specialty Conference. 14-17 June 2011.

[19] Hayes, Megan. 2016. "Robustness of WT Steel Connections during Quasi-Dynamic Loading." Master's Thesis, Milwaukee School of Engineering: Milwaukee, Wisconsin.

[20] Friedman, Adam. 2009. "Axial, Shear, and Moment Interaction of WT Connections." Master's Thesis, Milwaukee School of Engineering: Milwaukee, Wisconsin.

[21] Kulak, Geoffrey L., John W. Fisher, John H. A. Struik. 2001. *Guide to Design Criteria for Bolted and Riveted Joints*. 2nd ed. Chicago, Illinois: American Institute of Steel Construction.

[22] Yang, Jun and John T. Dewolf. 2000. "Relaxation in High-Strength Bolted Connections using Galvanized Steel." *Journal of Bridge Engineering.* May 2000. Pp. 99-106.

APPENDIX A:

"Conventional Configuration" Shear Tab Calculations

The following calculations outline the design procedure of a three-bolt shear tab configuration designed by the "Conventional Configuration" used in the AISC 14th Edition Specifications[1]. These calculations represent the expected capacities for the tested three, four, and five bolt shear tab connection subjected to vertical shear only. The calculations have been carried out without the use of the specified safety factors as the analytical ultimate connection capacities are pertinent to the current research. A summary of the ultimate shear connection capacities for the three-, four-, and five-bolt connections is shown in Table A-2.

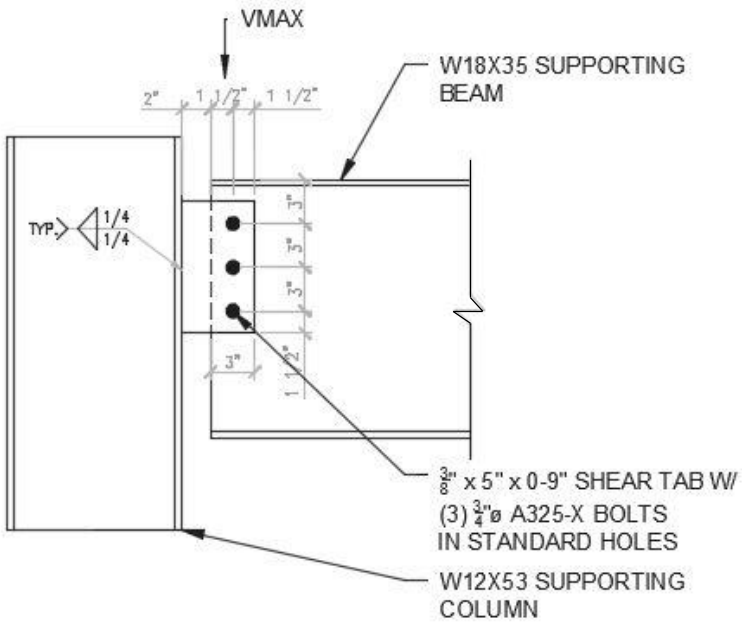

Figure A-1: Typical Three Bolt Shear Tab Connection "Conventional Configuration".

A.1 Connection Material Properties.

Table A-1: Material Properties.

	Yield Strength	Rupture Strength	t_{pl} / t_{web} / t_{flange}
Shear Plate	36 ksi	58 ksi	0.375 in
W18x35	50 ksi	65 ksi	0.300 in
W12x53	50 ksi	65 ksi	0.575 in

[1] American Institute of Steel Construction (AISC). 2011. *Specification of Steel Construction 14th Edition*. Chicago, IL.

A.2 "Conventional Configuration" Geometric Requirements (p.10-101).

a. The connection is limited to one column of bolts with the number of bolts, *n*, less than or equal to twelve bolts in the connection.

$$n = 3, 4, 5 \text{ bolts}$$

b. Distance from weld line to bolt line, *a*, less than or equal to 3 1/2 in.

$$a = 3\ 1/2\text{in.}$$

c. Standard Holes only.

d. The horizontal edge distance, $L_{eh,}$ from the center of the bolt hole to the edge of the connecting plate and beam web must be greater than twice the diameter of the bolt.

$$L_{eh} = 1\ 1/2\text{in.}$$

e. The vertical edge distance, L_{ev}, from the center of the bolt hole to the edge of the connecting plate must be equal to or greater than 1 1/4 in. for 3/4 in. diameter bolts.

$$L_{ev} = 1\ 1/2\text{in.}$$

f. Either the thickness of the connecting plate, t_{pl}, or beam web, t_w, must be thicker than one half the diameter of the bolt plus one-sixteenth of an inch.

$$t_{max} = 0.5(0.75\text{in.}) + 0\ .0625\text{in.} = 0.4375\text{in.}$$
$$t_{pl} = 0.375\text{in.} \quad t_w = 0.3\text{in.}$$

g. The minimum weld thickness, $t_{w,min}$, must be equal to or greater than 5/8 $t_{pl.}$

$$t_{w,min} = 0.625 * 0.375$$
$$t_{w,min} = 0.25\text{in.}$$

A.3 Bolt Shear Rupture Capacity (Eq. J3-1).

$$R_n = n * F_n * A_b \tag{A-1}$$
$$R_n = (3)*(54\text{ ksi})*\frac{\pi(0.75\text{ in})^2}{4}$$
$$R_n = 71.6\text{ kips}$$

A.4 Weld Shear Rupture Capacity (Eq. J2-4).

$$R_n = 0.6 * F_{exx} * \frac{\sqrt{2}}{2} * t_w * l_w * 2 \quad \text{(A-2)}$$

$R_n = 0.6*(70\text{ksi})*\frac{\sqrt{2}}{2}*(0.25\text{in})*(9\text{in}-0.25\text{in})*2$

$R_n = 129.9 \text{ kips}$

A.5 Connecting Plate Base Metal Shear Rupture (Eq. J4-4).

$$R_n = 0.6 * F_u * A_{nv} \quad \text{(A-3)}$$

$R_n = 0.6*(58 \text{ ksi})*(0.375\text{in})*(9\text{in}-0.25\text{in})$

$R_n = 114.2 \text{ kips}$

A.6 Supporting Column Flange Rupture Strength (p. 9-5).

$$t_{fl,\,min} = \frac{0.6*F_{exx}*\frac{\sqrt{2}}{2}*t_w*2}{06*F_u} \quad \text{(A-4)}$$

$t_{fl,\,min} = \frac{0.6*(70\text{ksi})*\frac{\sqrt{2}}{2}*(0.25\text{in})*2}{0.6*(65\text{ksi})}$

$t_{fl,\,min} = 0.381\text{in}.$

A.7 Connecting Plate Shear Yielding (Eq. J4-3).

$$R_n = 0.6 * F_y * A_g \quad \text{(A-5)}$$

$R_n = (0.6)*(36\text{ksi})*(9\text{in})*(0.375\text{in})$

$R_n = 72.9 \text{ kips}$

A.8 Connecting Plate Shear Rupture (Eq. J4-4).

$$R_n = 0.6 * F_u * A_{nv} \quad \text{(A-6)}$$

$$A_{nv} = t_{pl} * (l_{pl} - (n * (d_b + 0.125in)) \quad \text{(A-7)}$$

$A_{nv} = (0.375\text{in})*(9-(3*(0.75\text{in}+0.125\text{in}))$

$A_{nv} = 2.39\text{in}^2$

$R_n = (0.6)*(58\text{ksi})*(2.39\text{in}^2)$

$R_n = 83.2 \text{ kips}$

A.9 Connecting Plate Bolt Bearing (Eq. J3-6b).

$$r_n = 1.5 * L_c * t * F_u \leq 3.0 * d_b * t * F_u \quad \text{(A-8)}$$

$$L_c = L_{ev} - 0.5 * (d_b + 0.0625\text{in}) \quad \text{(A-9)}$$

$L_c = 1.5\text{in} - 0.5*(0.75 + 0.0625\text{in})$

$L_c = 1.094\ \text{in}$

$r_n = (1.5*(1.094\text{in})*(0.375\text{in})*(58\text{ksi}))$
$\leq (3.0*(0.75\text{in})*(0.375\text{in})*(58\text{ksi}))$

$r_n = 35.7\text{kips} \leq 48.9\text{kips}$

$R_n = 35.7\text{kips} + 2*(48.9\text{kips})$

$R_n = 133.6\ \text{kips}$

A.10 Supporting Beam Web Bolt Bearing (Eq. J3-6b).

$$r_n = 1.5 * L_c * t * F_u \leq 3.0 * d_b * t * F_u \quad \text{(A-10)}$$

$L_c = \text{N/A}$

$r_n = (3.0*(0.75\text{in})*(0.3\text{in})*(65\text{ksi}))$

$r_n = 43.9\text{kips}$

$R_n = 3*(43.9\text{kips})$

$R_n = 131.6\ \text{kips}$

A.11 Connecting Plate Block Shear Rupture (Eq. J4-5).

$$R_n = U_{bs} * F_u * A_{nt} + min(0.6 * F_y * A_{gv}, 0.6 * F_u * A_{nv}) \quad \text{(A-11)}$$

$$A_{gv} = t_{pl}*(L_{pl} - L_{ev}) \quad \text{(A-12)}$$

$A_{gv} = 0.375\text{in}*(9\text{in} - 1.5\text{in})$

$A_{gv} = 2.81\ \text{in}^2$

$$A_{nv} = t_{pl} * (L_{pl} - L_{ev} - ((n - .05) * (d_b + 0.125in))) \quad \text{(A-13)}$$

$A_{nv} = 0.375\text{in}*(9\text{in} - 1.5\text{in} - ((3 - 0.5)*(0.75\text{in} + 0.125\text{in})))$

$A_{nv} = 1.99\ \text{in}^2$

$$A_{nt} = t_{pl} * (L_{eh} - (0.5 * (d_b + 0.125in))) \quad \text{(A-14)}$$

$A_{nt} = 0.375\text{in}*(1.5\text{in} - (0.5*(0.75\text{in} + 0.125\text{in})))$

$A_{nt} = 0.398\ \text{in}^2$

$U_{bs} = 1.0$

$R_n = (1.0*58\text{ksi}*0.398\text{in}^2)$
$+\min((0.6*36\text{ksi}*2.81\text{in}^2), (0.6*58\text{ksi}*1.99\text{in}^2))$

$R_n = 83.9\ \text{kips}$

A.12 Supporting Beam Shear Yield (Eq. G2-1).

$$R_n = 0.6 * F_y * A_w * C_v \quad \text{(A-15)}$$

$R_n = (0.6)*(50\text{ksi})*(17.7\text{in})*(0.3\text{in})*(1.0)$

$R_n = 159.3\ \text{kips}$

Table A-2: "Conventional Configuration" Single Plate Un-Factored Shear Capacities per AISC 14th Edition Limit States.

Single Plate "Conventional Configuration" Ultimate Shear Capacity				
Connection Limit State	AISC 14th Equation	3-Bolt	4-Bolt	5-Bolt
Single Bolt Shear Rupture [kips/bolt]	J3-1	23.9	23.9	23.9
Shear Plate Single Bolt Tearout [kips/bolt]	J3-6b	35.7	35.7	35.7
Shear Plate Single Bolt Bearing [kips/bolt]	J3-6b	48.9	48.9	48.9
Beam Web Single Bolt Tearout [kips/bolt]	J3-6b	-	-	-
Beam Web Single Bolt Bearing [kips/bolt]	J3-6b	43.8	43.8	43.8
Bolt Shear Rupture [kips]	J3-1	71.6	95.4	119.3
Shear Plate Bolt Bearing [kips]	J3-6b	133.6	182.4	231.4
Beam Web Bolt Bearing [kips]	J3-6b	131.6	175.6	219.5
Weld Shear Rupture [kips]	J4-4	129.9	174.4	219.0
Base Metal Shear Rupture [kips]	J2-4	114.2	153.3	192.5
Shear Plate Shear Yield [kips]	J4-3	72.9	97.2	121.5
Shear Plate Shear Rupture [kips]	J4-4	83.2	110.9	138.7
Shear Plate Block Shear Rupture [kips]	J4-5	83.9	108.2	132.4
Beam Shear Yield [kips]	G2-1	159.3	159.3	159.3

APPENDIX B:

Single Plate “Hanger” Connection Calculations

The following calculations represent an idealized situation in which the shear tab connection designed per Appendix A is subjected to an unexpected tensile force. These calculations represent the expected capacities for the tested three-, four-, and five-bolt shear tab connections subjected to a perpendicular tensile force only to predict the expected catenary forces to define the failure mechanism during testing. The calculations and page number references shown throughout pertain to the 2011 AISC 14th Edition Specification[1] without the use of safety factors as the analytical ultimate connection capacities are applicable to the current research. Detailed calculations have been provided for the tested three-bolt shear tab connection. A summary of the ultimate shear connection capacities for the three, four, and five bolt connections is shown in Table B-1.

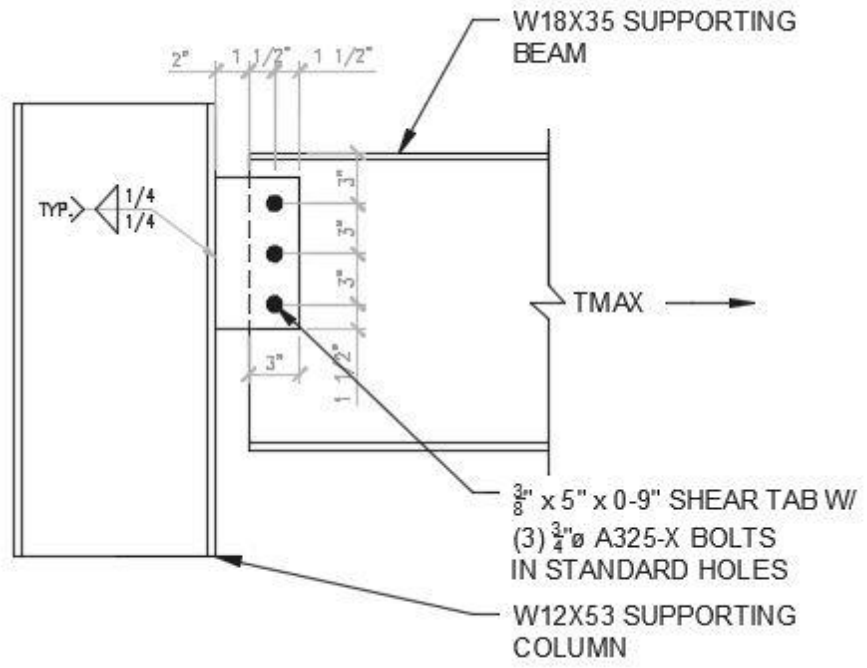

Figure B-1: Typical Three Bolt Shear Tab Connection Configuration – Tension Case.

[1] American Institute of Steel Construction (AISC). 2011. *Specification of Steel Construction 14th Edition*. Chicago, IL.

B.1 Connection Material Properties.

Table B-1: Connection Material Properties.

	Yield Strength	Rupture Strength	t_{pl} / t_{web} / t_{flange}
Shear Plate	36 ksi	58 ksi	0.375 in
W18x35	50 ksi	65 ksi	0.3 in
W12x53	50 ksi	65 ksi	0.575 in

B.2 Geometric Requirements.

Refer to the Appendix A Section A.2 for the geometric considerations required for the connection shown in Figure B-1.

B.3 Bolt Shear Rupture Capacity (Eq. J3-1).

$$R_n = n * F_n * A_b \quad \text{(B-1)}$$
$$R_n = (3)*(54\ \text{ksi})*\frac{\pi(0.75\ \text{in})^2}{4}$$
$$R_n = 71.5\ \text{kips}$$

B.4 Weld Tensile Rupture Capacity (Eq. J2-4 & J2-5).

$$R_n = F_w * A_w \quad \text{(B-2)}$$
$$F_w = 0.6*F_{EXX}*(1.0+0.5*\sin^{1.5}\theta) \quad \text{(B-3)}$$
$$F_w = 0.6*(70\text{ksi})*(1.0+0.5*\sin^{1.5}(90))$$
$$F_w = 63.0\text{ksi}$$
$$R_n = (63\text{ksi})*\frac{\sqrt{2}}{2}*(0.25\text{in})*(9\text{in-}0.25\text{in})*2$$
$$R_n = 194.9\ \text{kips}$$

B.5 Connecting Plate Base Metal Tensile Rupture (Eq. J4-2).

$$R_n = F_u * A_e \quad \text{(B-4)}$$
$$R_n = (58\ \text{ksi})*(0.375\text{in})*(9\text{in-}0.25\text{in})$$
$$R_n = 190.3\ \text{kips}$$

B.6 Connecting Plate Tensile Yielding (Eq. J4-1).

$$R_n = F_y * A_g \quad \text{(B-5)}$$
$$R_n = (36\text{ksi})*(9\text{in})*(0.375\text{in})$$
$$R_n = 121.5\ \text{kips}$$

B.7 Connecting Plate Tensile Rupture (Eq. J4-2).

$$R_n = F_u * A_e \quad \text{(B-6)}$$
$$A_e = A_e * U \quad \text{(B-7)}$$
$$A_e = (0.375\text{in})*(9-(3*(0.75\text{in}+0.125\text{in}))*(1.0)$$
$$A_e = 2.39\text{in}^2$$
$$R_n = (58\text{ksi})*(2.39\text{in}^2)$$
$$R_n = 138.7 \text{ kips}$$

B.8 Connecting Plate Bolt Bearing (Eq. J3-6b).

$$r_n = 1.5 * L_c * t_{pl} * F_u \leq 3.0 * d_b * t_{pl} * F_u \quad \text{(B-8)}$$
$$L_c = L_{ev} - 0.5 * (d_b + 0.0625\text{in}) \quad \text{(B-9)}$$
$$L_c = 1.5\text{in}-0.5*(0.75+0.0625\text{in})$$
$$L_c = 1.094 \text{ in}$$
$$r_n = (1.5*(1.094\text{in})*(0.375\text{in})*(58\text{ksi}))$$
$$\leq(3.0*(0.75\text{in})*(0.375\text{in})*(58\text{ksi}))$$
$$r_n = 35.7\text{kips}\leq 48.9\text{kips}$$
$$R_n = 3*(35.7\text{kips})$$
$$R_n = 107.1 \text{ kips}$$

B.9 Supporting Beam Web Bolt Bearing (Eq. J3-6b).

$$r_n = 1.5 * L_c * t_w * F_u \leq 3.0 * d_b * t_w * F_u \quad \text{(B-10)}$$
$$L_c = L_{ev} - 0.5 * (d_b + 0.0625\text{in}) \quad \text{(B-11)}$$
$$L_c = 1.5\text{in}-0.5*(0.75+0.0625\text{in})$$
$$L_c = 1.094 \text{ in}$$
$$r_n =(1.5*(1.094\text{in})*(0.3\text{in})*(65\text{ksi}))$$
$$\leq(3.0*(0.75\text{in})*(0.3\text{in})*(65\text{ksi}))$$
$$r_n = 32.0\text{kips}\leq 43.9\text{kips}$$
$$R_n = 3*(32.0\text{kips})$$
$$R_n = 96.0 \text{ kips}$$

B.10 Connecting Plate Block Shear Rupture (Eq. J4-5).

$$R_n = U_{bs} * F_u * A_{nt} + min(0.6 * F_y * A_{gv}, 0.6 * F_u * A_{nv}) \quad \text{(B-12)}$$

$$A_{gv} = 2 * t_{pl} * L_{ev} \quad \text{(B-13)}$$

$$A_{gv} = 2*(0.375\text{in})*(1.5\text{in})$$

$$A_{gv} = 1.13\text{in}^2$$

$$A_{nv} = 2 * t_{pl} * (L_{ev} - (0.5) * (d_b + 0.125in)) \quad \text{(B-14)}$$

$$A_{nv} = 2*\ 0.375\text{in}*(1.5\text{in}-(0.5)*(0.75\text{in}+0.125\text{in}))$$

$$A_{nv} = 0.8\ \text{in}^2$$

$$A_{nt} = t_{pl} * (L_{pl} - (n-1) * (d_b + 0.125in) - 2 * L_{ev}) \quad \text{(B-15)}$$

$$A_{nt} = 0.375\text{in}*(9\text{in}-(3-1)*(0.75\text{in}+0.125\text{in})-2*(1.5\text{in}))$$

$$A_{nt} = 1.59\ \text{in}^2$$

$$U_{bs} = 1.0$$

$$R_n = (1.0*58\text{ksi}*1.59\text{in}^2) + \min((0.6*36\text{ksi}*1.13\text{in}^2), (0.6*58\text{ksi}*0.8\text{in}^2))$$

$$R_n = 116.52\ \text{kips}$$

B.11 Supporting Beam Web Block Shear Rupture (Eq. J4-5).

$$R_n = U_{bs} * F_u * A_{nt} + min(0.6 * F_y * A_{gv}, 0.6 * F_u * A_{nv}) \quad \text{(B-16)}$$

$$A_{gv} = 2 * t_w * L_{ev} \quad \text{(B-17)}$$

$$A_{gv} = 2*(0.3\text{in})*(1.5\text{in})$$

$$A_{gv} = 0.9\text{in}^2$$

$$A_{nv} = 2 * t_w * (L_{ev} - (0.5) * (d_b + 0.125in)) \quad \text{(B-18)}$$

$$A_{nv} = 2*\ 0.3\text{in}*(1.5\text{in}-(0.5)*(0.75\text{in}+0.125\text{in}))$$

$$A_{nv} = 0.64\ \text{in}^2$$

$$A_{nt} = t_w * ((n-1) * s) - (n-1) * (d_b + 0.125in) \quad \text{(B-19)}$$

$$A_{nt} = 0.3\text{in}*((3-1)*3\text{in})-(3-1)*(0.75\text{in}+0.125\text{in}))$$

$$A_{nt} = 1.28\ \text{in}^2$$

$$U_{bs} = 1.0$$

$$R_n = (1.0*65\text{ksi}*1.28\text{in}^2) + \min((0.6*50\text{ksi}*0.9\text{in}^2), (0.6*65\text{ksi}*0.64\text{in}^2))$$

$$R_n = 107.8\ \text{kips}$$

Table B-2: Single Plate Un-Factored Tensile Capacities per AISC 14th Edition Limit States.

Single Plate Ultimate Tensile Capacity				
Connection Limit State	AISC 14th Equation	3-Bolt	4-Bolt	5-Bolt
Single Bolt Shear Rupture [kips/bolt]	J3-1	23.9	23.9	23.9
Shear Plate Single Bolt Tearout [kips/bolt]	J3-6b	35.7	35.7	35.7
Shear Plate Single Bolt Bearing [kips/bolt]	J3-6b	48.9	48.9	48.9
Beam Web Single Bolt Tearout [kips/bolt]	J3-6b	32.0	32.0	32.0
Beam Web Single Bolt Bearing [kips/bolt]	J3-6b	43.9	43.9	43.9
Bolt Shear Rupture [kips]	J3-1	71.6	95.4	119.3
Shear Plate Bolt Bearing [kips]	J3-6b	107.1	142.8	132.5
Beam Web Bolt Bearing [kips]	J3-6b	96.0	128.0	160.0
Weld Shear Rupture [kips]	J2-4	194.9	261.7	328.5
Base Metal Tensile Rupture [kips]	J4-4	190.3	255.6	320.8
Shear Plate Tensile Yield [kips]	J4-3	121.5	162.0	202.5
Shear Plate Tensile Rupture [kips]	J4-4	138.7	184.9	231.1
Shear Plate Block Shear Rupture [kips]	J4-5	116.5	163.1	209.3
Beam Web Block Shear Rupture [kips]	J4-5	107.8	149.3	190.7

APPENDIX C:

Shop Drawings

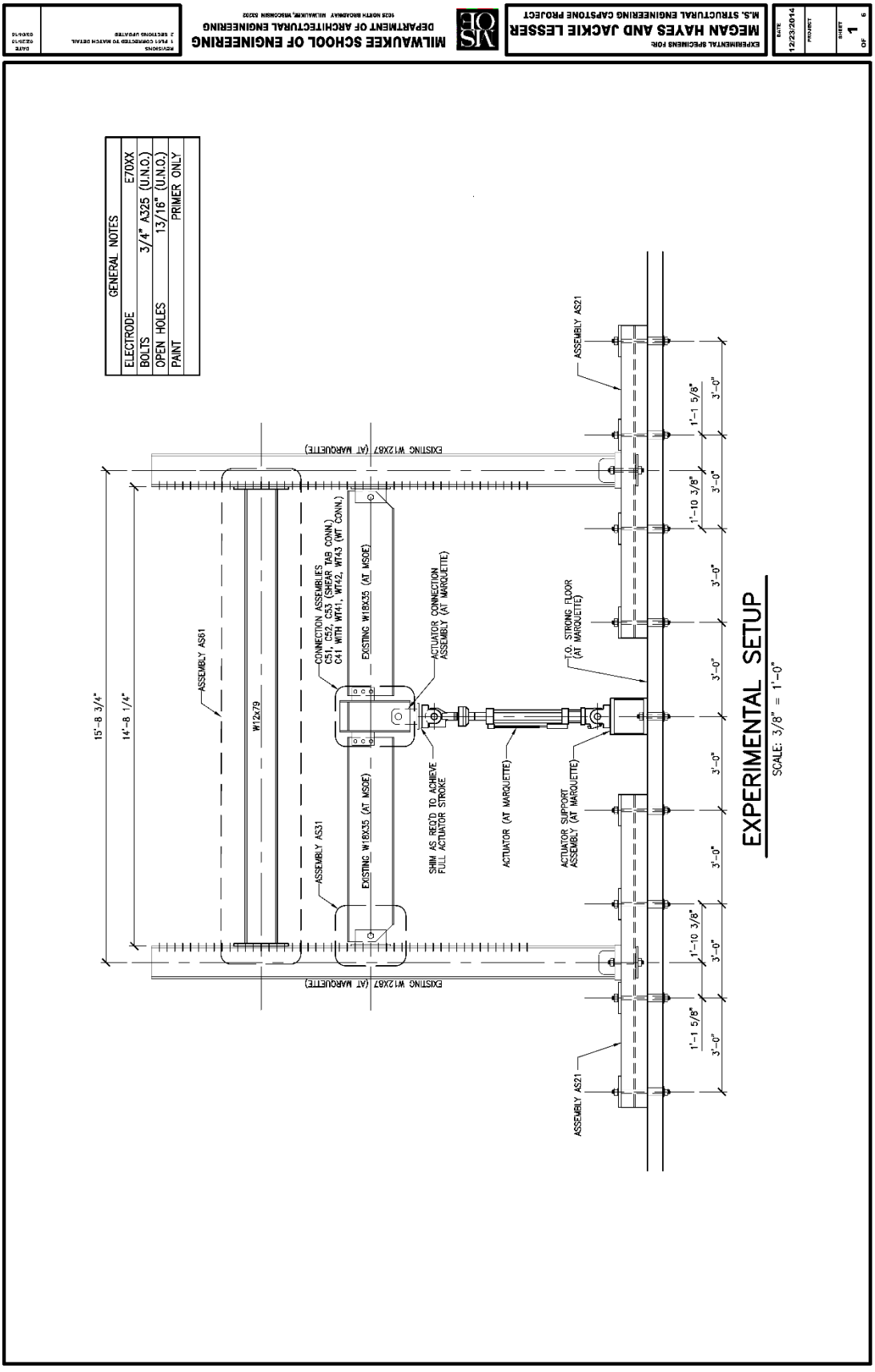

Figure C-1: Experimental Setup.

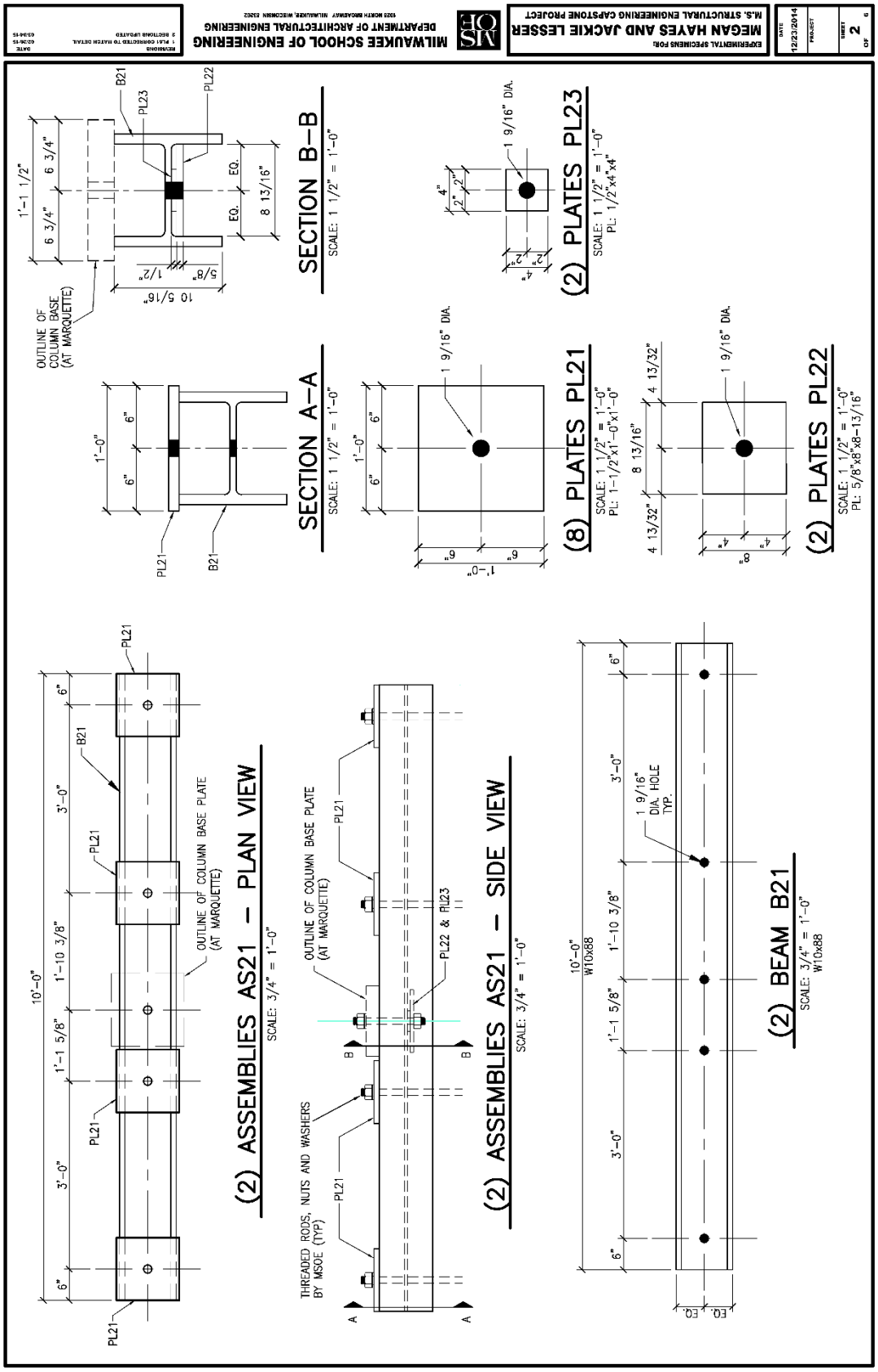

Figure C-2: Test Frame Parts.

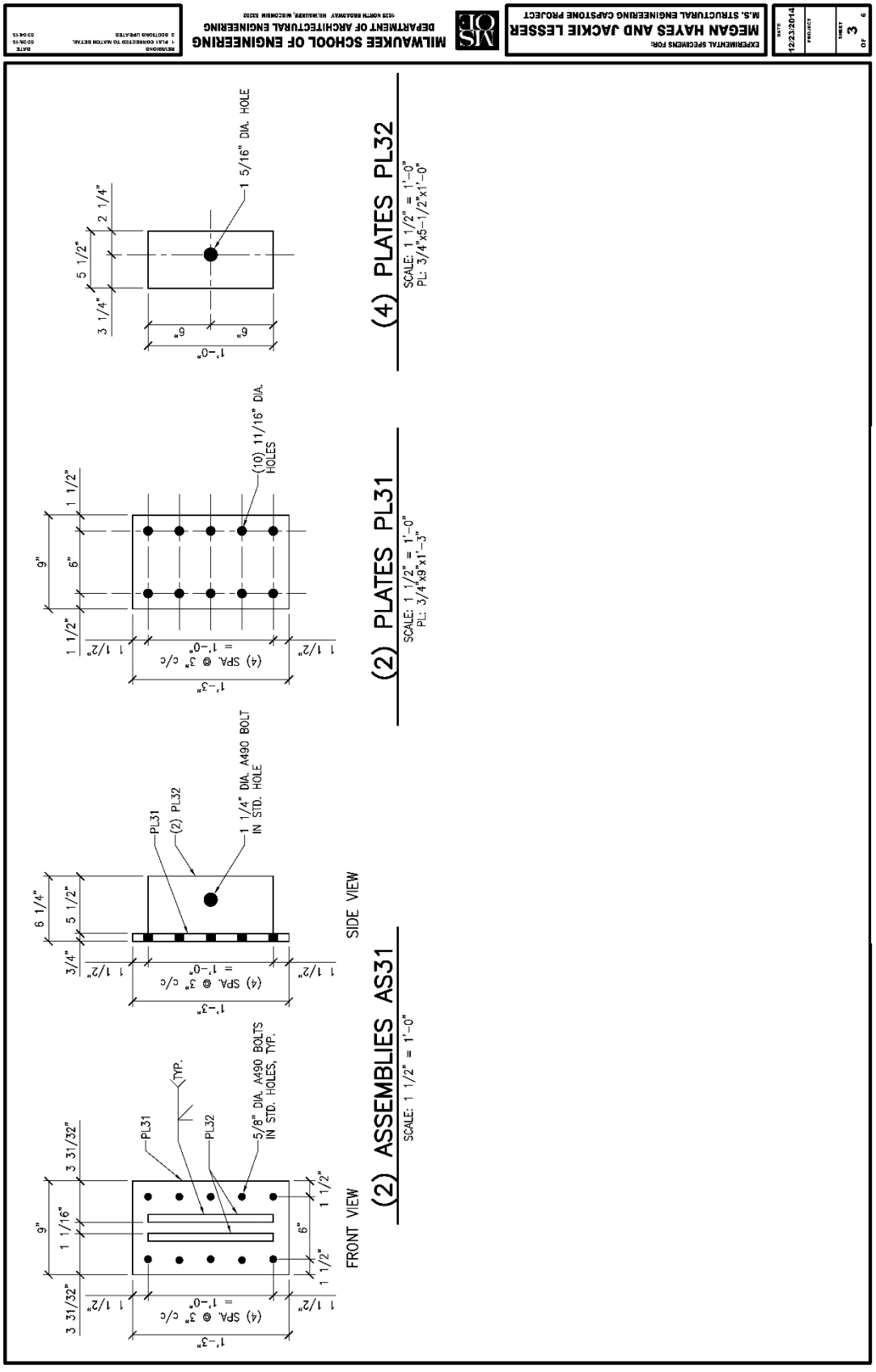

Figure C-3: Test Frame Parts.

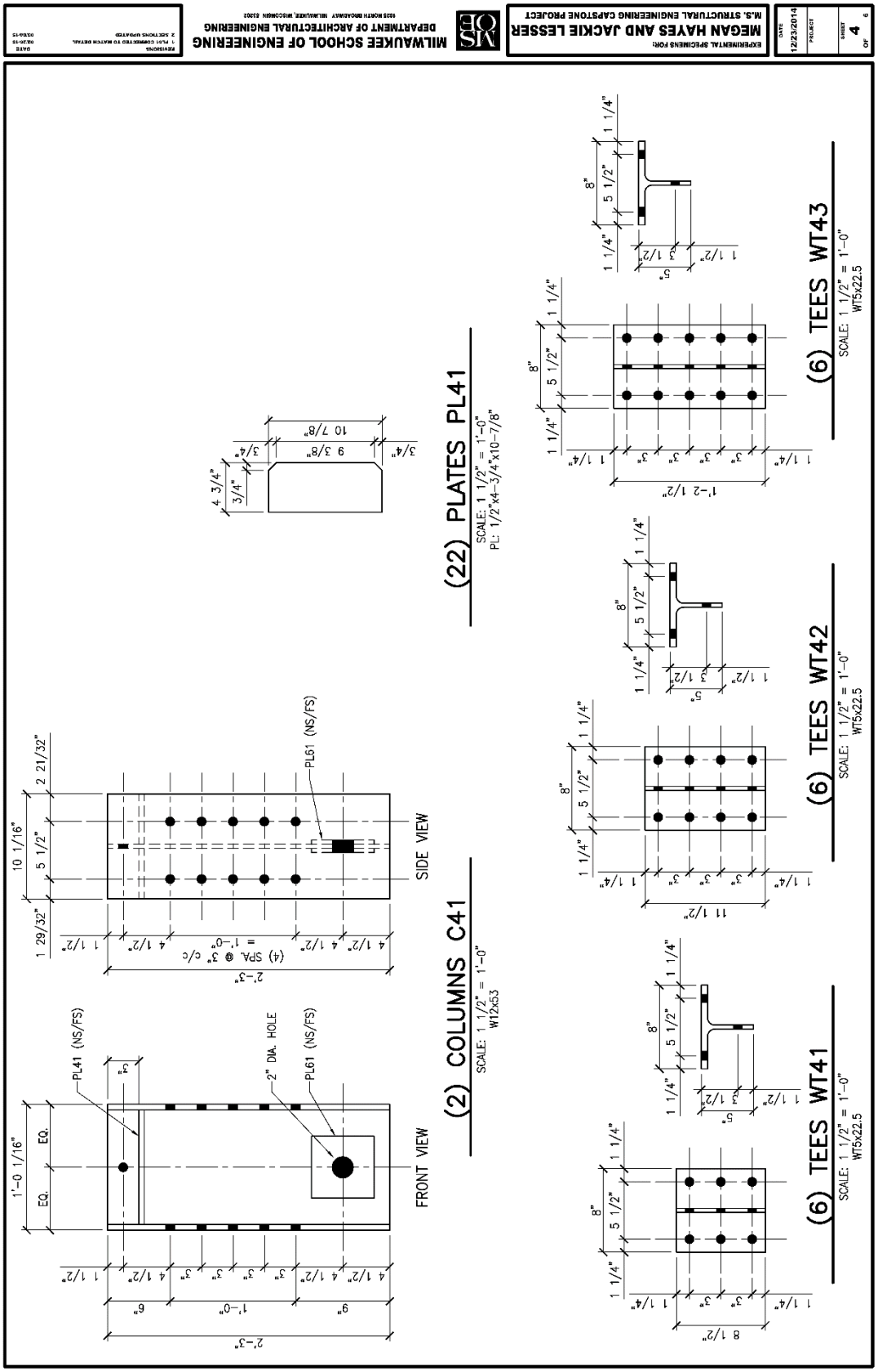

Figure C-4: Columns and WTs.

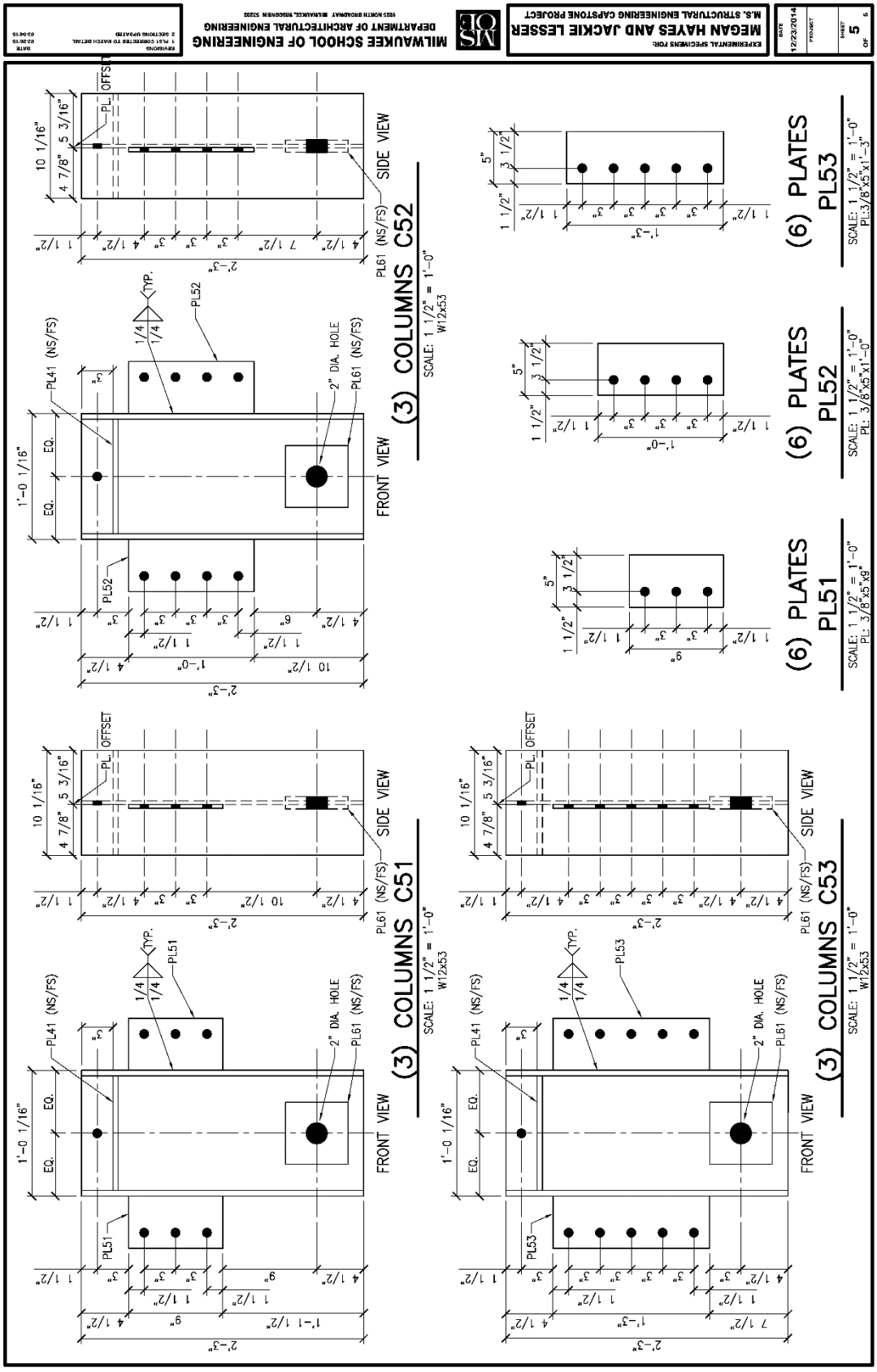

Figure C-5: Columns and Shear Tabs.

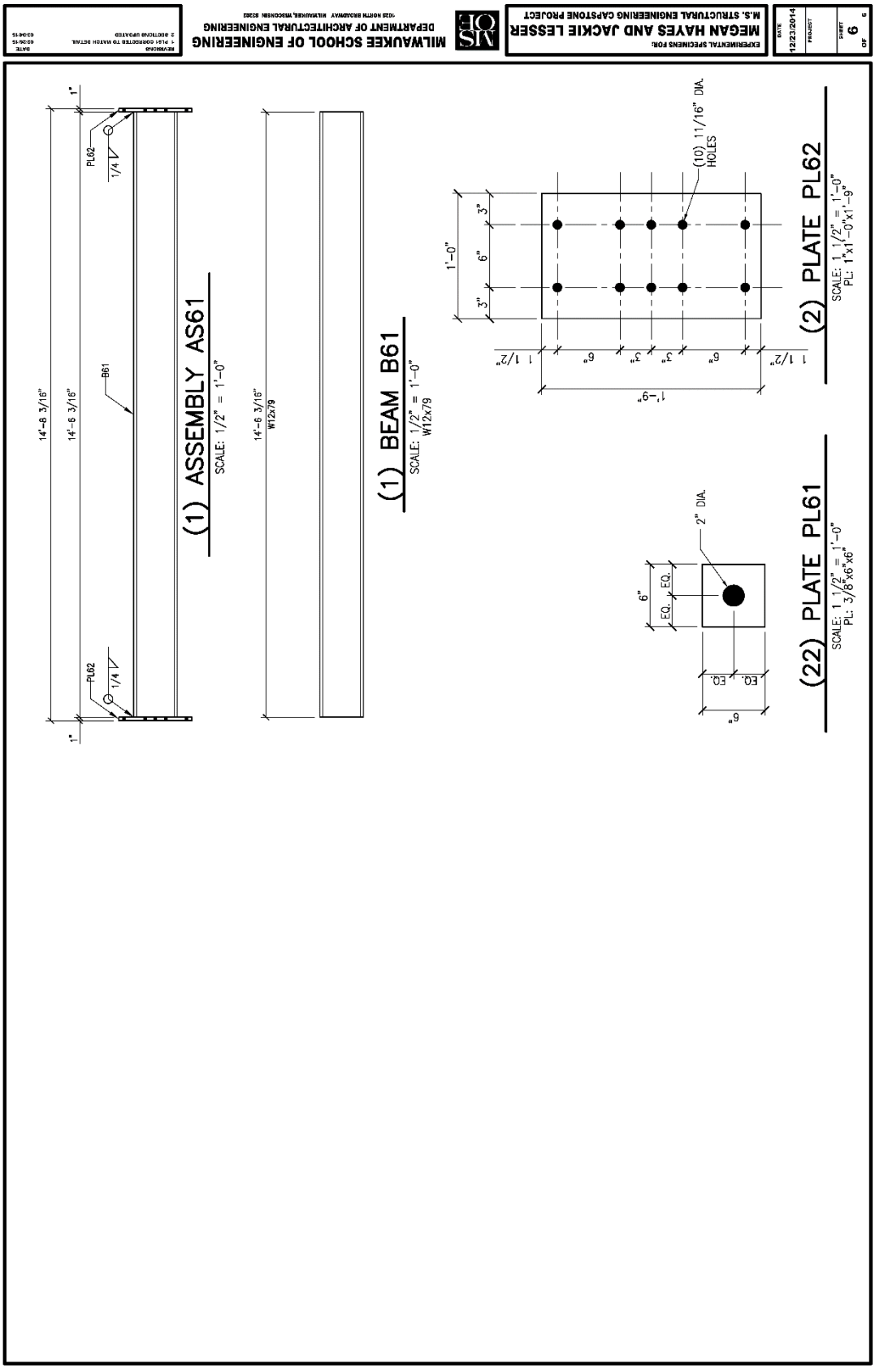

Figure C-6: Test Framing Beam and Parts.

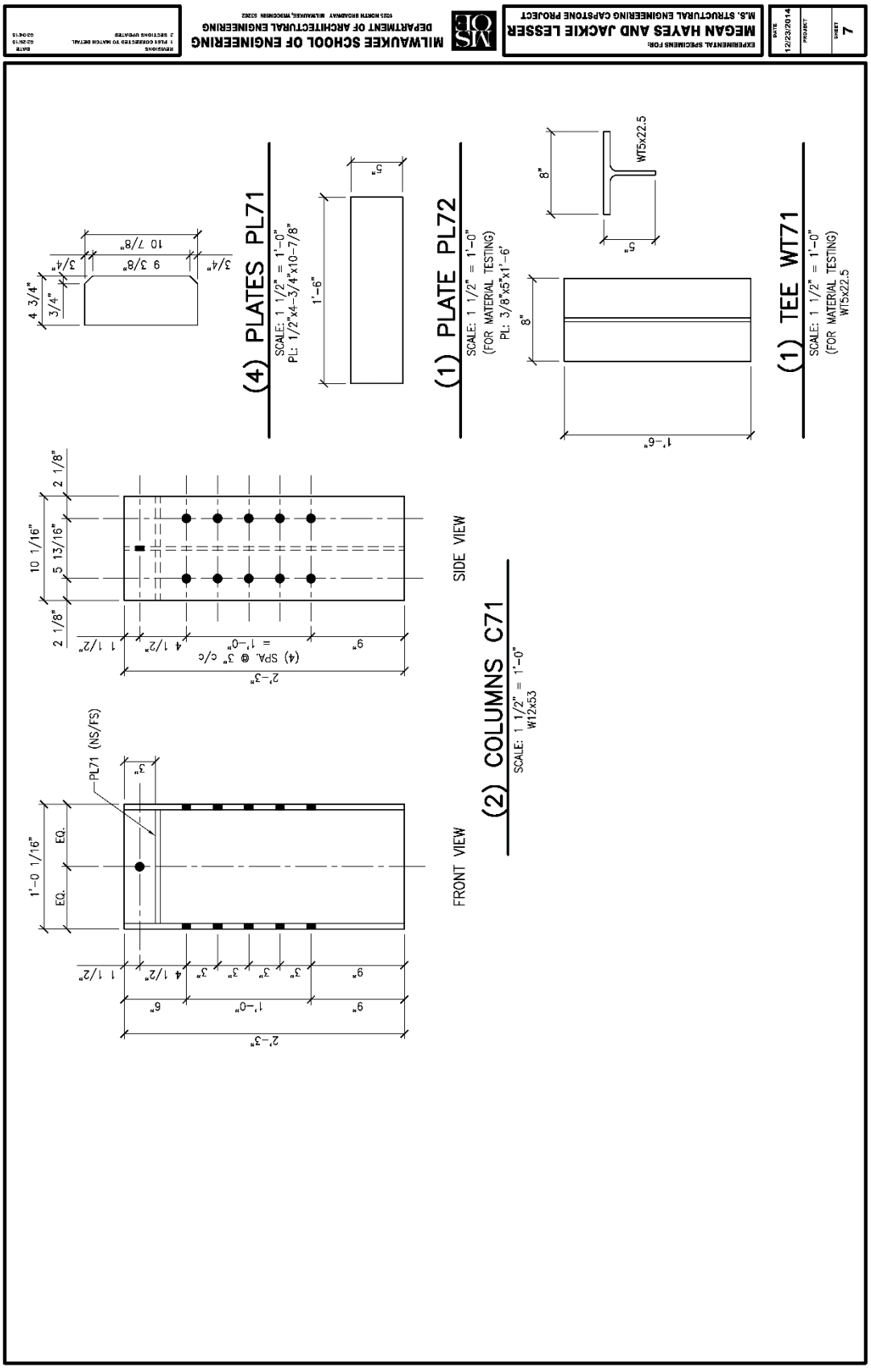

Figure C-7: Extra Specimen for Material Test.

APPENDIX D:

Materials Test Results

11/20/2015

Sample ID: MSOE plate 1.mss
Specimen Number: 2
Tagged: False

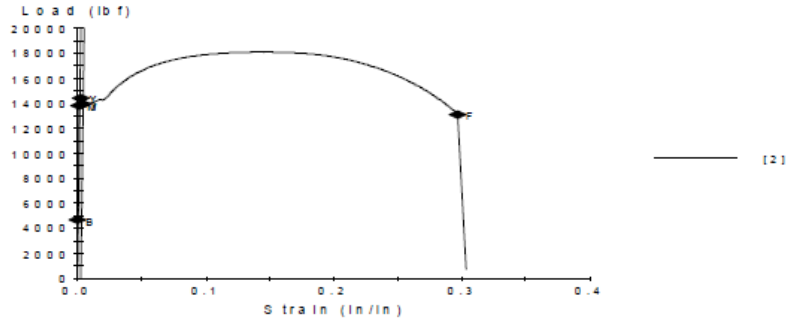

Specimen Results:

Name	Value	Units
Thickness	0.37500	in
Width	0.62385	in
Area	0.23394	in^2
Modulus	30532500.74841	psi
Load At Offset Yield	13906.57548	lbf
Stress At Offset Yield	59443.91181	psi
Load At Yield	14440.33241	lbf
Stress At Yield	61725.46557	psi
Peak Load	18116.55573	lbf
Peak Stress	77439.54954	psi
Break Load	13065.07062	lbf
Break Stress	55846.88387	psi
Strain At Break	0.29731	in/in

Specimen Comment:

11/20/2015

Sample ID: MSOE plate 2.mss
Specimen Number: 3
Tagged: False

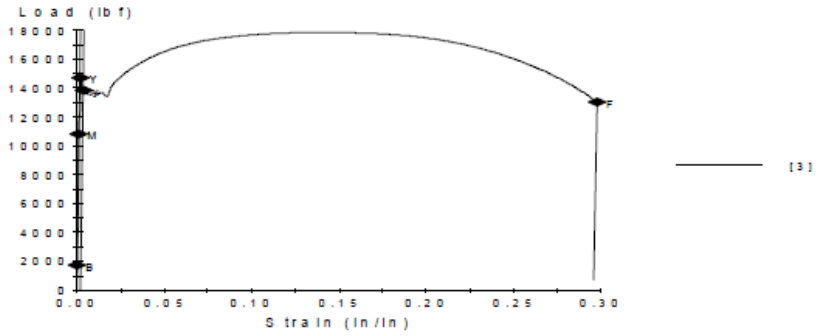

Specimen Results:

Name	Value	Units
Thickness	0.37000	in
Width	0.62240	in
Area	0.23029	in^2
Modulus	33795444.17849	psi
Load At Offset Yield	13841.00306	lbf
Stress At Offset Yield	60102.82529	psi
Load At Yield	14686.40399	lbf
Stress At Yield	63773.87311	psi
Peak Load	17842.59485	lbf
Peak Stress	77479.23732	psi
Break Load	13007.28384	lbf
Break Stress	56482.50380	psi
Strain At Break	0.29811	in/in

Specimen Comment:

11/20/2015

Sample ID: MSOE plate 3.mss
Specimen Number: 4
Tagged: False

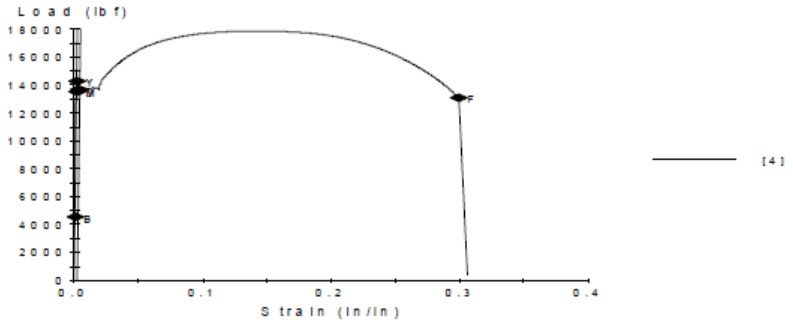

Specimen Results:

Name	Value	Units
Thickness	0.37100	in
Width	0.62735	in
Area	0.23275	in^2
Modulus	28607173.27293	psi
Load At Offset Yield	13658.87244	lbf
Stress At Offset Yield	58685.34582	psi
Load At Yield	14272.61472	lbf
Stress At Yield	61322.28956	psi
Peak Load	17862.56094	lbf
Peak Stress	76746.49359	psi
Break Load	13069.16317	lbf
Break Stress	56151.65994	psi
Strain At Break	0.29930	in/in

Specimen Comment:

11/20/2015

Sample ID: MSOE plate 4.mss
Specimen Number: 5
Tagged: False

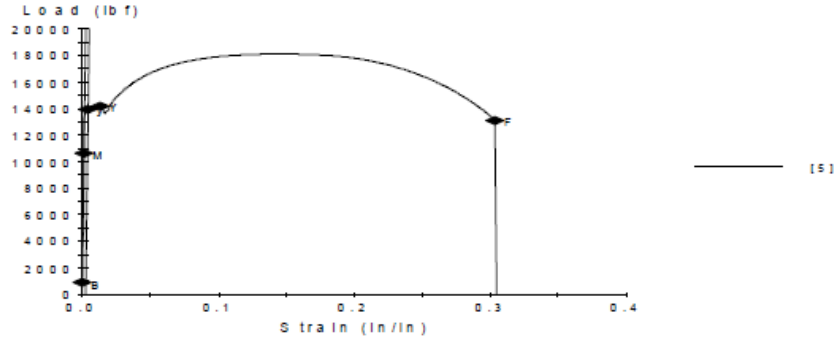

Specimen Results:

Name	Value	Units
Thickness	0.38400	in
Width	0.62325	in
Area	0.23933	in^2
Modulus	28643457.98745	psi
Load At Offset Yield	13956.24986	lbf
Stress At Offset Yield	58314.13735	psi
Load At Yield	14150.92978	lbf
Stress At Yield	59127.57877	psi
Peak Load	18126.12947	lbf
Peak Stress	75737.36602	psi
Break Load	13093.36726	lbf
Break Stress	54708.70933	psi
Strain At Break	0.30350	in/in

Specimen Comment:

APPENDIX E:

Metallurgy Test Results

The following metallurgical test results have been included only to specify the results pertaining to carbon ASTM A325 bolts made in the USA. All test information pertaining to Chinese bolts was performed for Hayes[1].

[1] Hayes, Megan. 2016. "Robustness of WT Steel Connections during Quasi-Dynamic Loading." Master's Thesis, Milwaukee School of Engineering. Milwaukee, Wisconsin.

Analysis

of

Hayes MSST

3/4 Inch Diameter ASTM A325 Bolts

for

Mr. David Newman
Milwaukee, WI

by

Raymond A. Fournelle, Ph.D., P.E.
Metallurgical Consultant
1029 North Jackson Street, #509A
Milwaukee, WI 53202

January 7, 2016

_____
Raymond A. Fournelle, Ph.D., P.E.
Metallurgical Consultant

Summary

The Rockwell C hardness, microstructure and chemical composition of three different ¾ inch ASTM A325 heavy hex bolts were evaluated and compared to ASTM A325 specifications. The bolts were given the following designations: HS Bolt, Chinese JDF Bolt and "n" Bolt. The Rockwell C hardness of all three bolts met the ASTM A325 specification that the hardness be less than HRC 34. All three bolts exhibited quenched and tempered microstructure; however, the microstructure at the center of the shanks of the "n" bolts was different from that in the center of the shanks of the HS bolts and the Chinese JDF bolts. Both the Chinese JDF and HS bolts exhibited uniform tempered martensitic microstructures across the cross section of the shanks, while the "n" bolts exhibited a tempered martensitic microstructure near the outer edge of the cross section and a microstructure consisting of a mixture of tempered martensite, ferrite, pearlite and bainite in the center. As such, the hardness of the "n" bolts was slightly lower in the center. Energy dispersive spectroscopy of the bolt materials shows that the HS bolts and the Chinese JDF bolts are made of alloy steels containing small amounts of chromium, while the "n" bolts are made of carbon steel. This probably explains why the "n" bolts were softer at the center. They did not have enough alloy elements to through harden. Regardless of the differences in the hardness, microstructure and composition, all three bolts meet the requirements of ASTM A325.

Background

Sectioned ¾-10 x 2 ¼ A325 heavy hex bolts from three different manufacturers (HS Bolt, Chinese JDF Bolt and "n" Bolt) were provided by Mr. David Newman for determination of their hardness, microstructure and chemistry. Four cross sections about ¼ inch thick had been cut from the shanks of the bolts with a water cooled band saw. The markings on the heads of the bolts were consistent with them being ASTM A325 Type 1 bolts. According to the specification these can be made of either carbon steel or alloy steel. While the chemical composition specification for carbon steel bolts is straight forward, that for alloy steel bolts allows for a variety of combinations of alloy elements like Mn, Cr, Ni, Mo and Si.

Hardness Testing

The cross section surfaces on one section from each bolt were first ground through 120 grit SiC. Five Rockwell C hardness measurements were then performed on one side of these specimens in the pattern shown in Figure 1 using a Wilson Rockwell Model B523T hardness tester, which was checked against Yamamoto Test Block #437-669 (HRC 31.6) for calibration.

As can be seen in Table 1 the average hardness of each bolt was below HRC 34, which is a requirement of ASTM A325 for ¾ inch x 2 ¼ inch bolts. It can also be seen that the hardness values for the HS and Chinese JDF bolts were uniform over the entire cross section, while the hardness of the "n" bolt was lower in the center. As shown below this is related to the "n" bolt being made of carbon steel and not having enough hardenability to transform to martensite at its center on quenching during heat treatment. Both the HS and Chinese JDF bolts were made of alloy steel and through hardened to 100% martensite at their center on quenching. This difference between the "n" bolt and the HS and Chinese JDF bolts notwithstanding, the "n" bolts still meet ASTM A325 specifications.

Metallography

A second cross section specimen from each bolt was mounted in LECOSET 100 acrylic mounting compound for examination of its microstructure. A third specimen from each bolt was cut in half with an abrasive cut off wheel, and half of it was mounted in LECOSET 100 for examination of the microstructure of the longitudinal section. These metallographic specimens were then ground through 600 grit SiC, polished through 1.0 μm Al_2O_3 and etched for 5 seconds with 3% Nital. They were examined and photographed with an Olympus PME3 metallograph using bright field illumination.

As can be seen in Figures 2 and 3 the HS bolts and the Chinese JDF bolts have uniform tempered martensitic microstructures over their entire cross sections. This is what one would expect in through hardened bolts. As can be seen in Figure 4 the microstructure at

the center of the "n" bolt consisted of a complex mixture of tempered martensite, ferrite, pearlite and bainite, while that ¼ inch from the center consists of tempered martensite. As such, it is not through hardended. This is what one would expect from a carbon steel bolt of this size. Note that, while this bolt is not through hardened, it does meet the hardness, heat treatment and chemistry specified in ASTM A325.

Energy Dispersive X-ray (EDS) Analysis

Energy dispersive analysis of the bolt materials was performed on the center of one of the cross sections of each of the bolts after the cross section had been ground through 240 grit SiC. The EDS was performed using a JEOL JSM 6510LV Scanning Electron Microscope equipped with a NORAN System 7 Spectral Imaging System. The microscope was operated at 20kV and a working distance of 19 mm. A 100 second acquisition time was used to acquire each spectrum, and a standardless filter with a φ-ρ-z correction was used to quantify it.

As can be seen in Figures 5 and 6 and Table 2 both the HS bolts and the Chinese JDF bolts contain a small amount of Cr in combination with a small amount of Mn, which indicates that they are made of alloy steel according to the definition of alloy steel in ASTM A325. This is why these bolts have been through hardened. The Cr and Mn give them sufficient hardenability to through harden. As can be seen in Figure 7 and Table 2 the "n" bolts do not contain any Cr. This means that they are made of carbon steel, which has less hardenability that the alloy steels used for the HS bolts and the Chinese JDF bolts. This is why the "n" bolts did not through harden.

Conclusion

Even though there are differences in hardness, microstructure and chemistry for the three different bolts, they all meet the hardness, heat treatment and chemical requirements of ASTM A325.

Table 1. Rockwell C Hardness Values

Bolt Designation	Measurement Number					Avg.	Std. Dev.
	1	2	3	4	Center		
IIS Bolts	32.2	32.0	32.1	32.9	31.1	32.1	0.6
Chinese JDF Bolts	29.4	29.8	29.5	28.2	27.9	29.0	0.8
"n" Bolts	27.9	27.0	27.3	24.8	25.2	26.4	1.4

Table 2. Bolt Compositions in Comparison to ASTM A325 Specifications (wt.%)

Bolt Designation	Fe	C	Mn	Si	P	S	Cr
ASTM 325 Type 1 Carbon Steel	Bal.	0.30-0.52	0.60 min	0.15-0.30	0.040 max	0.050 max	
ASTM 325 Type 1 Alloy Steel	Bal.	0.30-0.52	0.60 min	0.15-0.35	0.035 max	0.040 max	
IIS Bolts	Bal.	0.37	1.49	0.30			0.27
Chinese JDF Bolts	Bal.	0.38	1.17	0.30			1.10
"n" Bolts	Bal.	0.53	1.50	0.40			

Table 1. Rockwell C Hardness Values

Bolt Designation	Measurement Number					Avg.	Std. Dev.
	1	2	3	4	Center		
IIS Bolts	32.2	32.0	32.1	32.9	31.1	32.1	0.6
Chinese JDF Bolts	29.4	29.8	29.5	28.2	27.9	29.0	0.8
"n" Bolts	27.9	27.0	27.3	24.8	25.2	26.4	1.4

Table 2. Bolt Compositions in Comparison to ASTM A325 Specifications (wt.%)

Bolt Designation	Fe	C	Mn	Si	P	S	Cr
ASTM 325 Type 1 Carbon Steel	Bal.	0.30-0.52	0.60 min	0.15-0.30	0.040 max	0.050 max	
ASTM 325 Type 1 Alloy Steel	Bal.	0.30-0.52	0.60 min	0.15-0.35	0.035 max	0.040 max	
IIS Bolts	Bal.	0.37	1.49	0.30			0.27
Chinese JDF Bolts	Bal.	0.38	1.17	0.30			1.10
"n" Bolts	Bal.	0.53	1.50	0.40			

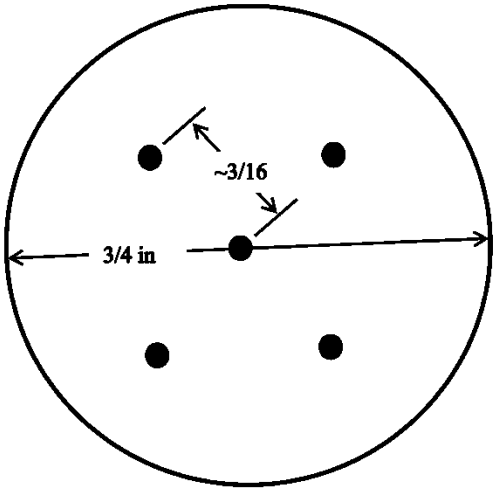

Figure 1. Location of Rockwell C hardness measurements.

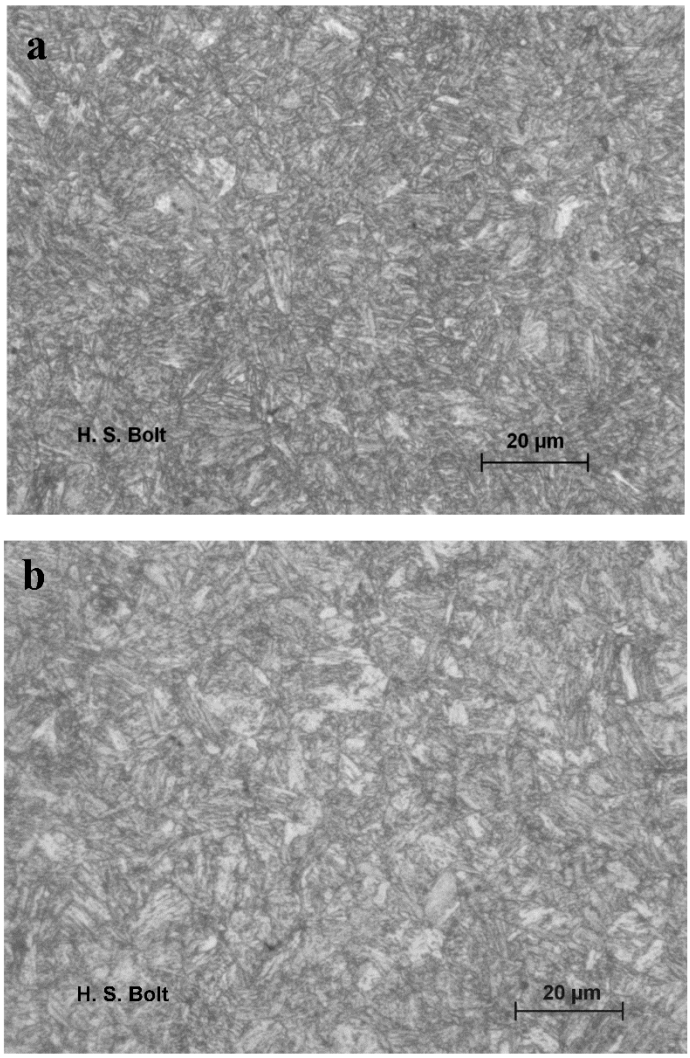

Figure 2. Microstructure of HS bolts. (a) Center. (b) ¼ inch from center. Both microstructures consist of tempered martensite.

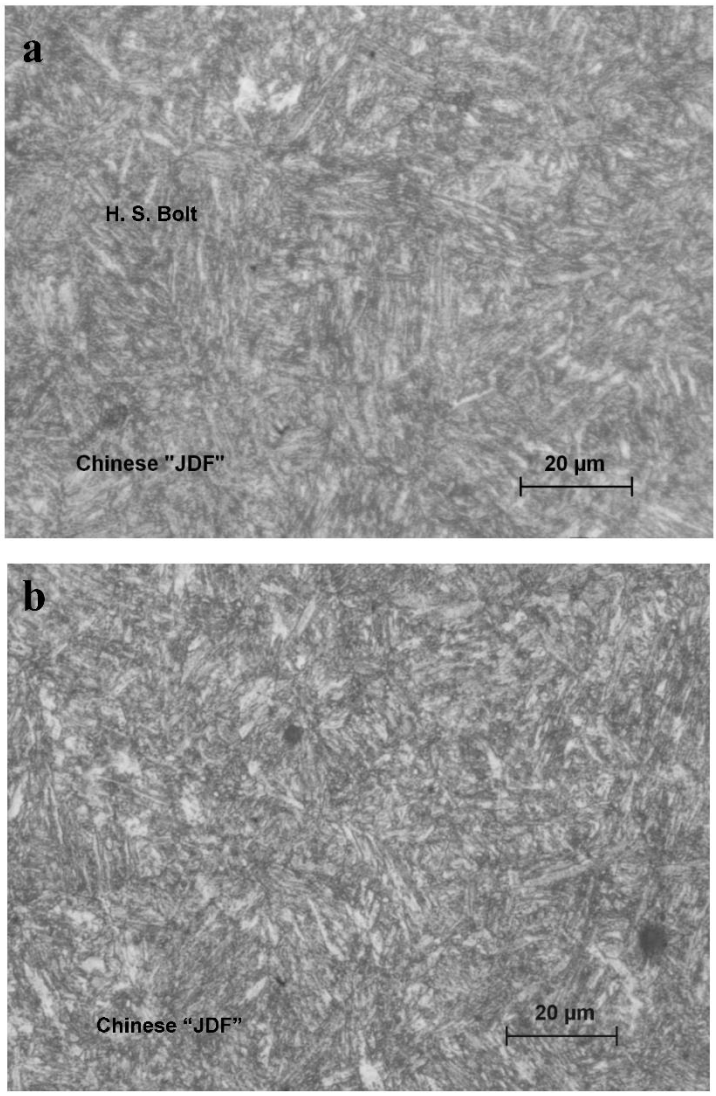

Figure 3. Microstructure of Chinese JDF bolts. (a) Center. (b) ¼ inch from center. Both microstructures consist of tempered martensite.

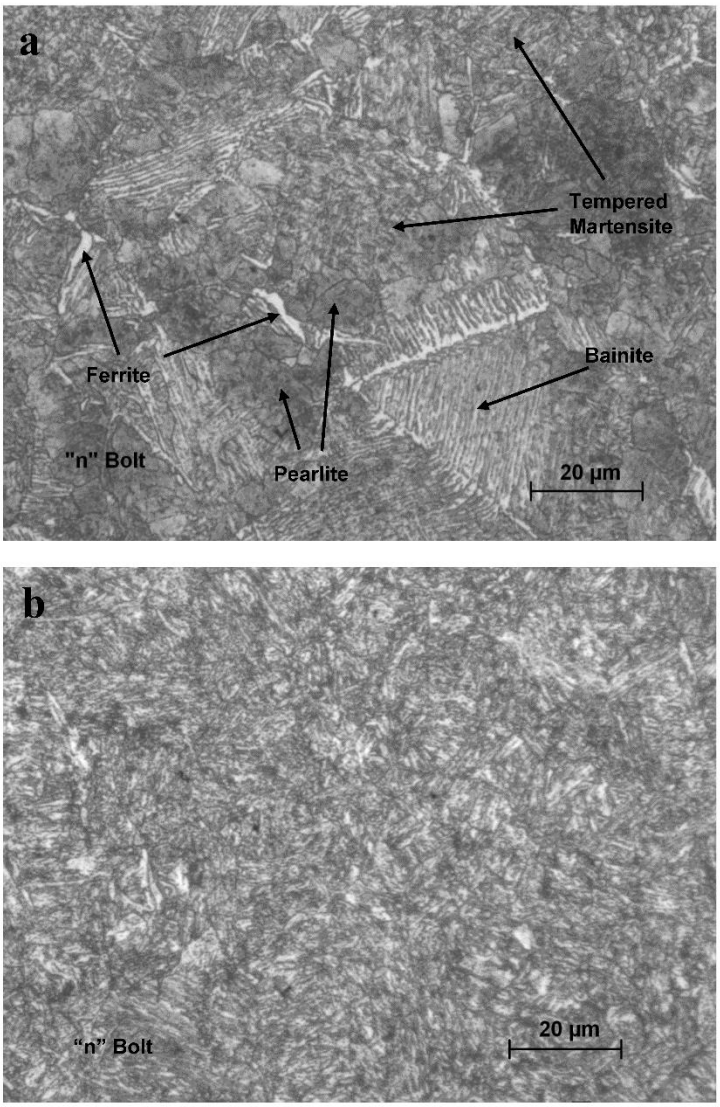

Figure 4. Microstructure of "n" bolts. (a) Center. (b) ¼ inch from center. The microstructure at the center is a complicated mixture of martensite, ferrite, pearlite and bainite. At ¼ inch from the center it is tempered martiensite.

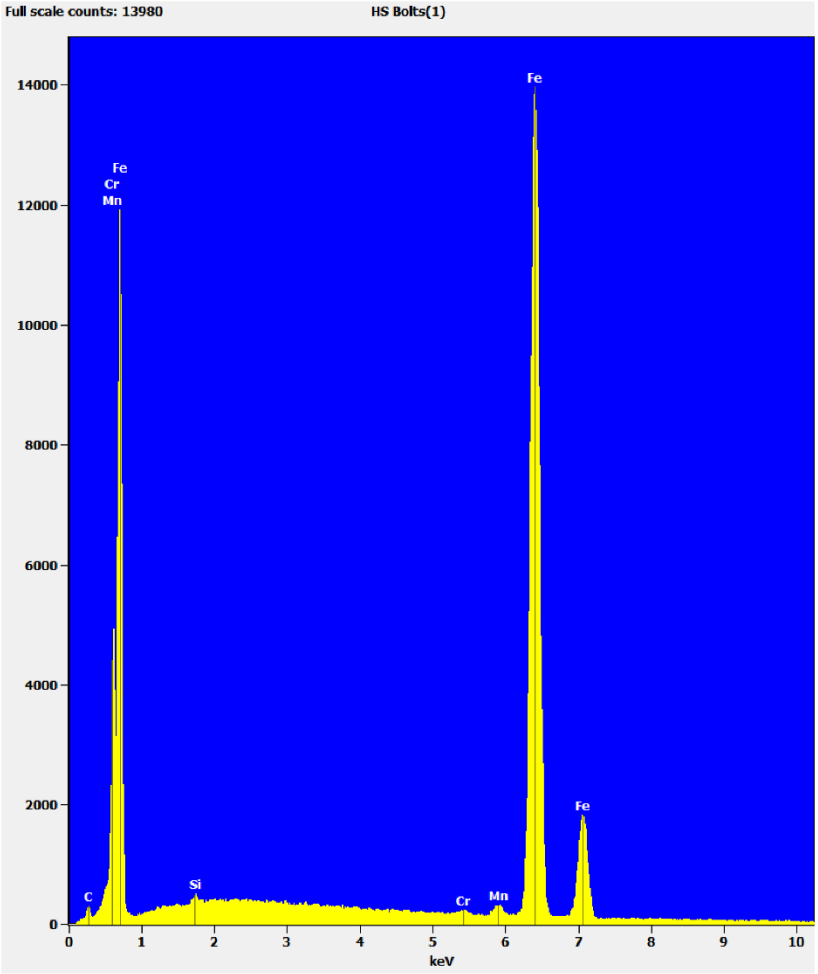

Figure 5. EDS spectrum from HS bolt showing small amounts of Mn and Cr indicating an alloy steel.

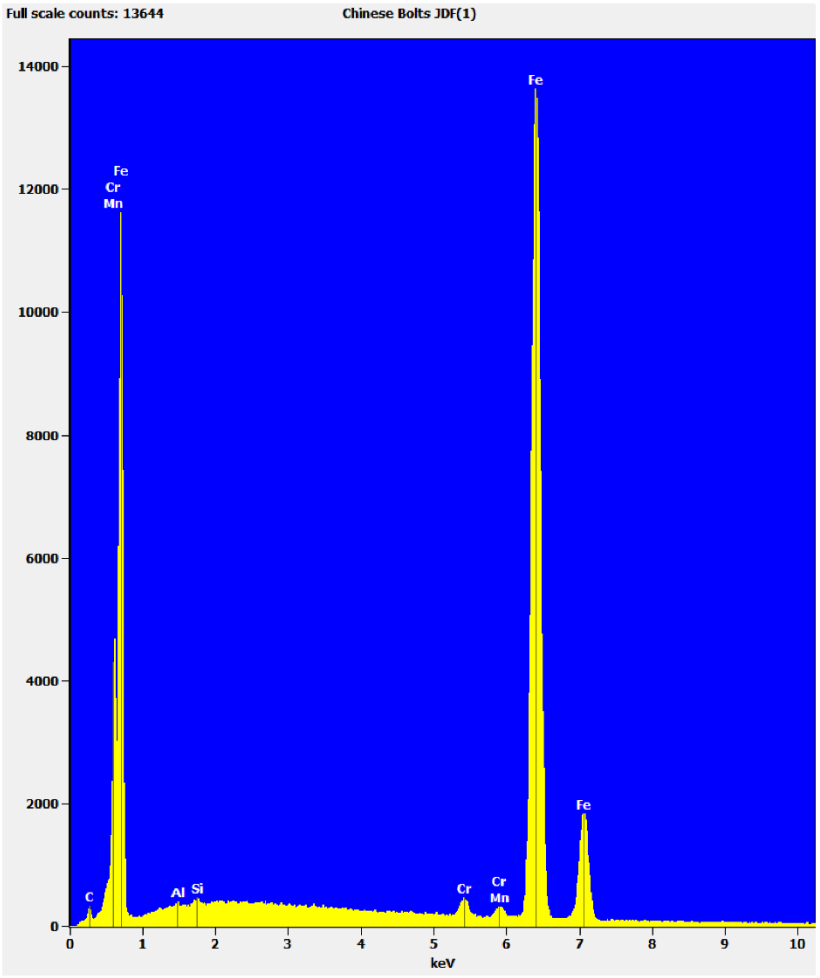

Figure 6. EDS spectrum from Chinese JDF bolt showing small amounts of Mn and Cr indicating an alloy steel.

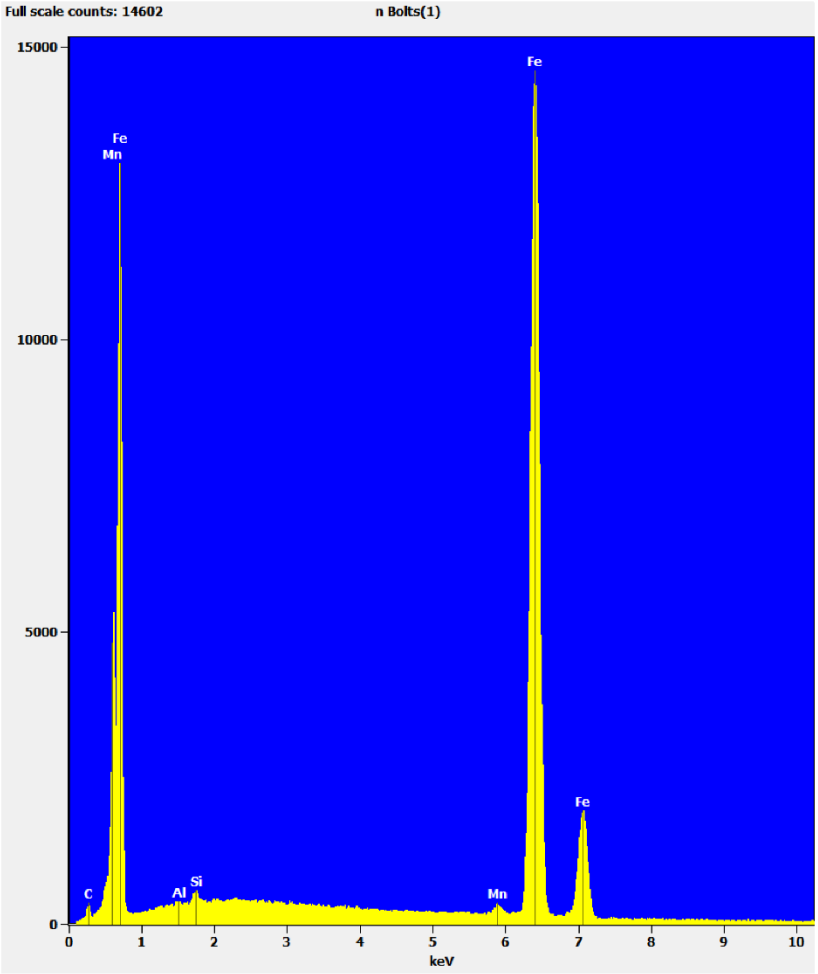

Figure 7. EDS spectrum from "n" bolt showing no Cr indicating a carbon steel.

APPENDIX F:

MATLAB Filter Information

```
% Implemention of a Low pass Butterworth filter using the

filtfilt command

%% change the data, sampling frequency, cutoff frequency
and order of the filter based on your requirements
% File written by Avinash Parnandi.
%xx = [1:100];
%data = sin(188*xx)+rand(1,100);  % noisy data; change it
to whatever is your data
clear all
clc

xx=xlsread('H:\Masters\Analysis Needed\3
bolt\energy\3st3.2.xlsx'); %inside the quotes put your file
name
a=length(xx(1,:));

A(1:length(xx),1)=xx(:,1);
%%
for i=2:a;
    horiz=xx(:,1); %isolate horizontal axis (independent
variable)
    data=xx(:,i); %isolate which column you would like to
filter

    f=10;%  sampling frequency --> more or less leave this
alone
    f_cutoff = 0.8; % cutoff frequency

    fnorm =f_cutoff/(f/2); % normalized cut off freq, you
can change it to any value depending on your requirements

    [b1,a1] = butter(10,fnorm,'low'); % Low pass
Butterworth filter of order 10
    low_data = filtfilt(b1,a1,data); % filtering

    freqz(b1,a1,128,f), title('low pass filter
characteristics')
    figure
    subplot(2,1,1), plot(horiz,data), title('Actual data')
    grid on
    subplot(2,1,2), plot(horiz,low_data), title('Filtered
data')
    grid on

    close all
```

```
    A(:,i)=low_data;
end

cd ('H:\Masters\Analysis Needed\3 bolt\energy')
xlswrite('3st3analysis.xlsx',A)
cd ('H:\Masters\Analysis Needed\3 bolt\energy')
```

Appendix G:

Test Data Output

The experimental data recorded for this research is available upon request. Contact the Milwaukee School of Engineering campus library for further information on how to obtain access to the experimental data.

Structural Engineering

Capstone Report Approval Form

Master of Science in Structural Engineering – MSST

Milwaukee School of Engineering

This capstone report, entitled "Robustness of Shear Plate Connections under Quasi-Dynamic Loading," submitted by the student Jacklyn E. Lesser, has been approved by the following committee:

Faculty Advisor: _____ Date: _____

Dr. Christopher Raebel

Faculty Member: _____ Date: _____

Dr. Richard DeVries

Faculty Member: _____ Date: _____

Dr. Hans-Peter Huttelmaier

Faculty Member: _____ Date: _____

Dr. Christopher Foley